Temperature changes in the environment around ground source heating and cooling systems:

thermal plume modelling and literature review

Chief Scientist's Group report

September 2024

Version: SC220017/R1

We are the Environment Agency. We protect and improve the environment.

We help people and wildlife adapt to climate change and reduce its impacts, including flooding, drought, sea level rise and coastal erosion.

We improve the quality of our water, land and air by tackling pollution. We work with businesses to help them comply with environmental regulations. A healthy and diverse environment enhances people's lives and contributes to economic growth.

We can't do this alone. We work as part of the Defra group (Department for Environment, Food & Rural Affairs), with the rest of government, local councils, businesses, civil society groups and local communities to create a better place for people and wildlife.

Published by:

Environment Agency
Horizon House, Deanery Road,
Bristol BS1 5AH

www.gov.uk/environment-agency

Further copies of this report are available from our publications catalogue: www.gov.uk/government/publications or our National Customer Contact Centre: 03708 506 506

Email: research@environment-agency.gov.uk

Author(s):
Paolo Bertolini; Aidan E. Foley;
with inputs from David Banks (Senior Research Fellow, University of Glasgow)

Keywords:
Ground source heating and cooling, geothermal, environmental impact, thermal plume, modelling.

Research contractor:
Mott MacDonald Ltd, 8-10 Sydenham Road, Croydon CR0 2EE.

Environment Agency's Project Manager:
Sian Loveless

Project number:
SC220017/R1

Citation:
Environment Agency (2024) Temperature changes in the environment around Ground Source Heating and Cooling (GSHC) systems: Thermal plume modelling and literature review. Environment Agency, Bristol.

Research at the Environment Agency

Scientific research and analysis underpins everything the Environment Agency does. It helps us to understand and manage the environment effectively. Our own experts work with leading scientific organisations, universities and other parts of the Defra group to bring the best knowledge to bear on the environmental problems that we face now and in the future. Our scientific work is published as summaries and reports, freely available to all.

This report is the result of research commissioned by the Environment Agency's Chief Scientist's Group.

You can find out more about our current science programmes at https://www.gov.uk/government/organisations/environment-agency/about/research

If you have any comments or questions about this report or the Environment Agency's other scientific work, please contact research@environment-agency.gov.uk.

Dr Robert Bradburne
Chief Scientist

Contents

List of Figures

List of Tables

Executive Summary

The work described in this report follows from 2 other reports examining potential environmental receptors to ground source heating and cooling (GSHC) systems (Environment Agency, 2024a), and a review of the current state of the GSHC market (Environment Agency, 2024b). That work is built upon here with I) a literature review summarising temperature changes and extent of temperature changes in the ground (or "thermal plumes") around a 'closed-loop' borehole heat exchanger (BHE) GSHC system, and II) a modelling study to simulate the evolution of thermal plumes from arrays of BHE through a series of 3-D numerical computer simulations using FEFLOW® software.

The modelled BHE systems were chosen to represent typical ground source cooling systems, which extract cool water and inject heat into the ground. A baseline scenario represented a saturated sandstone aquifer with properties similar to those found for Permo-Triassic sandstones in England. Thermal plume boundaries were defined as the 1°C temperature change isocontour within the plume.

The baseline scenario was used for a sensitivity analysis of (hydro)geological and BHE characteristics to understand which parameters influenced thermal plume migration. The parameters tested included thermal conductivity, volumetric heat capacity, effective porosity, Darcy flux[1], dispersivity, GSHC system power capacity and system cyclicity.

The sensitivity analysis indicates that thermal plume lengths for the BHE systems modelled are generally less than 50m. This distance is exceeded in a few cases where either Darcy flux is low (below 0.002 m/d with a thermal load of ~100 MWh/year) and/or the applied thermal load is high (above 200 MWh/year[2]).

The model was then adapted or altered to model a series of scenarios representative of other hydrogeological conditions commonly found in England. These scenarios included; a heat abstraction, alternate heating and cooling (partially balanced), a partially saturated aquifer, a typical London Basin setting, mudrock, fluvial sand and gravel, and a worst case scenario (to understand the maximum possible thermal plume temperature and migration).

Changes in temperatures were found to be small across most modelled scenarios, with plume temperatures at 25 m from BHE arrays only exceeding 1°C in the London Basin and mudrock scenarios, although reaching 10°C in the worst-case scenario. Temperature changes for both sensitivity analysis and scenario modelling are provided in tables in the

---

[1] Groundwater flow per unit area of aquifer (metres cubed per second per metre squared of aquifer perpendicular to direction of flow under a given hydraulic gradient).

[2] A system of this size could heat approximately 20 average UK homes assuming an average heating demand of ~10 MWh/year.

summaries of the sensitivity analysis and scenario modelling sections of the report respectively.

The findings from the modelling studies are broadly in-line with findings from the literature, both in terms of the sensitivity of plume transport to specific parameters (notably, Darcy flux, thermal conductivity and dispersivity), and the dimensions of plumes reported in other modelling studies and in field studies that collected longer longer-term data. Although this study did not model a series of BHEs in a downgradient sequence, such scenarios were identified in the literature where multiple BHEs/BHE arrays are aligned along a groundwater flowpath, leading to cumulative effects exceeding the impacts identified in this study.

An additional conclusion from the literature review is that other anthropogenic sources of ground heat (for example from landfills, sewers, underground car parks etc.) commonly exceed background ground/groundwater temperatures by several degrees, and may present sources of ground heating or cooling of the same order of magnitude or greater than closed-loop BHE arrays.

Glossary

Baseline	Starting environmental conditions established at the outset of a study and against which impacts of a specific scheme may be assessed. A baseline may or may not be a natural condition – i.e. anthropogenic impacts may already be present and still form part of a baseline against which subsequent impacts are assessed.
Background	The generally prevailing conditions in the wider environment. May serve as a baseline for specific impact studies.
BHE	Borehole heat exchanger
Boundary conditions (BC)	The temperature, flux or hydraulic conditions specified at the boundaries of a model.
Closed-loop GSHC systems	“Systems that extract heat or cold from the ground by circulating a heat carrier fluid around an array of closed pipe loops (borehole heat exchanger)” (POST, 2022).
Dispersivity	A parameter used to describe the multitude of heterogeneities within the ground that contribute to the dispersion of thermal and contaminant plumes as they migrate through the ground.
Evapotranspiration	The combination of evaporative losses of water from surfaces and transpirative losses of water from plants (i.e. water that is taken up by a plant’s roots and lost through its leaves and stem.)
Exfiltrate	To discharge from an aquifer (for example, at a spring)
FLEQ	Full load equivalent hours
GCHE	Ground coupled heat exchanger (synonymous with GSHC)
GSHE	Ground source heat exchanger (synonymous with GSHC)
Ground source heating and cooling (GSHC)	The use of the ground as a source (heating) or sink (cooling) of heat.
Head boundary conditions	A hydraulic-head boundary condition applies a predefined hydraulic head to a model node. This can lead to an inflow into the model when neighbouring nodes have a lower potential, or

	to an outflow from the model when there is a gradient from the neighbouring nodes towards the boundary.
Heat flux boundary conditions	A heat flux boundary condition applies a predefined heat flux to nodes along a line (2D model) or to nodes enclosing faces of elements (3D).
Hydraulic conductivity	The capacity of a porous/fractured media to transmit water.
Infiltrate	In hydrological sciences, referring to rainwater or surface waters infiltrating the ground. This may be either diffusely, at a landscape scale (for example by rainfall sinking into soils) or at point sources such as sinkholes receiving concentrated surface runoff (typically streams, sometimes rivers).
m AOD	Meters above Ordnance Datum
Matrix bypass fissure flow	Where groundwater flow within a soil or aquifer is rapidly transported along fissures and either not taken up, or taken up in only limited proportions, by pores within the soil or rock matrix.
Microgeneration certification scheme (MCS)	“A standards body that certifies, quality assures and provides consumer protection for microgeneration installations and installers” (POST, 2022).
Open-loop GSHC systems	(for heating) “A geothermal system that typically pumps warm groundwater directly from an aquifer or flooded mine system via a production borehole and, after heat extraction, returns the cooled water to the system via an injection” (POST, 2022).
Receptor	People, animals, property, and anything else that could be affected by a hazard.
Sinking streams	Concentrated surface water runoff entering the ground at sinkholes.
Subsurface urban heat islands (SUHI)	The subsurface expression of the Urban Heat Island effect.
Surface air temperatures (SAT)	The temperature of the air at just above ground level at a location.
Surface sealing	The phenomenon of sealing natural ground surfaces (usually soils) with concrete and tarmac, thereby preventing infiltration of rainwater and significantly reducing evapotranspiration.

Temperature boundary conditions	A temperature boundary condition applies a predefined temperature to a node. This can lead to an inflow of energy into the model when neighbouring nodes have a lower temperature or to an outflow from the model when there is a temperature gradient from the neighbouring nodes towards the boundary condition.
Thermal plumes	Defined within this report as anything within the 1°C isocontour of a temperature change propagating through the ground.
Urban heat island (UHI)	The widespread phenomenon of elevated air temperatures within the urban environment in comparison to surrounding rural areas. Arising due to high thermal mass, surface sealing and energy usage within urban compared to rural environments.

1 Introduction

1.1 Background and objectives

Ground source heating and cooling (GSHC) systems that use borehole heat exchangers (BHE) are increasingly used to heat or cool buildings. Their installation is at present partly subsidised by the UK government under the boiler upgrade scheme (BUS)[3]. In addition to the availability of funding via the BUS, in October 2023, heat was recognised as a pollutant in groundwater in amendments to the Environmental Permitting Regulations (EPR)[4]. The Environment Agency will therefore regulate heat as a pollutant in groundwater systems, and therefore need to understand the possible direct and indirect temperature-related environmental risks from GSHC systems.

The work described in this report follows on from 2 other reports examining potential environmental receptors to GSHC systems, and a review of the current state of the GSHC market:

- Environment Agency (2024a) Identifying potential receptors to ground source heating and cooling (GSHC) systems.
- Environment Agency (2024b) Ground source heating and cooling (GSHC): Status, policy, and market review.

GSHC systems are a low-carbon form of energy relative to purely fossil fuel heating/cooling systems. However, they can potentially cause environmental impacts, such as increasing or decreasing temperatures at sensitive ecological or other receptors within the ground or connected environments, for example springs (see Environment Agency 2024a). The Environment Agency seeks to achieve a balance between facilitating the development of low-carbon energy sources with protecting potential temperature-sensitive receptors from harm.

The purpose of this work is to better understand how thermal plumes develop around closed-loop BHE in the subsurface and which factors have the greatest influence on thermal plume development. The work described in this report builds on the previous 2 reports with:

[3] https://www.gov.uk/apply-boiler-upgrade-scheme

[4] See https://www.legislation.gov.uk/uksi/2016/1154/contents/ for the 2016 EPRs and https://www.legislation.gov.uk/uksi/2023/651/regulation/5/ for 2023 EPR amendments (accessed 19/03/2024).

- A literature review summarising temperature changes and extent of temperature changes in the ground (or “thermal plumes”) around ‘closed-loop’ GSHC sources; and,
- A thermo-hydrogeological modelling study to investigate the evolution of thermal plumes from arrays of ‘closed-loop’ BHE, through a series of 3-D numerical computer simulations using FEFLOW ® software (DHI-WASY, 2023). This included sensitivity analyses and scenario modelling.

The focus of this report is on ‘closed-loop’ BHE systems as ‘open-loop’ systems were comprehensively modelled in an earlier report for the Environment Agency conducted by Carbon Zero Consulting and Holymoor Consultancy Ltd (2010). The difference between the 2 types of GSHC system is explained in the following section (Section 1.2).

This knowledge will help the Environment Agency identify settings and GSHC characteristics in which thermal impacts could be higher or lower so that they can be regulated appropriately.

1.2 GSHC and closed-loop BHEs

GSHC systems are an efficient and low-carbon alternative to traditional gas- or oil-fired boilers for space and water heating. They can capture heat from the ground (using buried pipes, vertical boreholes or groundwater pumped from aquifers), raise it to a higher temperature, and transfer it to a building to provide water or space heating. Ground-source heat pumps can also be used for cooling by reversing the configuration, that is, capturing heat from inside the building and transferring it to the ground. They can be used for heating and cooling buildings from single homes to large public buildings such as hospitals or schools[5], as well as for heating and cooling networks, which distribute heat between a variety of customers in a region.

GSHC using the shallow ground or groundwater resources is feasible almost anywhere in the UK, across different geological and hydrogeological settings.

There are two main types of GSHC system: closed-loop and open-loop.

- Closed-loop systems abstract heat using a heat carrier fluid that is circulated through pipes in the ground (a BHE) (Figure 1-1); and,
- Open-loop systems extract heat from groundwater that is pumped from and (usually) returned to an aquifer.

[5] An average UK home has a heating demand of ~10 MWh/y

A closed-loop system comprises a sealed pipe network, buried within the ground, through which a heat carrier fluid is continuously circulated. Closed-loop systems can use either shallow (generally less than 2 m depth) horizontal pipes installed in trenches, or deep vertical pipes installed in boreholes, depending on the site conditions.

Closed-loop ground heat exchangers are alternatively termed as ground coupled heat exchanger (GCHE) and ground source heat exchanger (GSHE). Vertical closed-loops also are known as borehole heat exchangers (BHE) and are the focus of the modelling in this report. Most BHE consist of U-pipes, with a single pipe forming a 'U' within a borehole to create a single loop; or a double U-pipe when two U-pipes are inserted in the borehole. Another, less common, type includes coaxial pipes or concentric heat exchangers (i.e. where one pipe is nested within another pipe). A circulating fluid or heat transfer fluid, usually a water-antifreeze mixture (for example, glycol), is pumped through the pipe and used to exchange heat with the ground and transport it in the heat pump system.

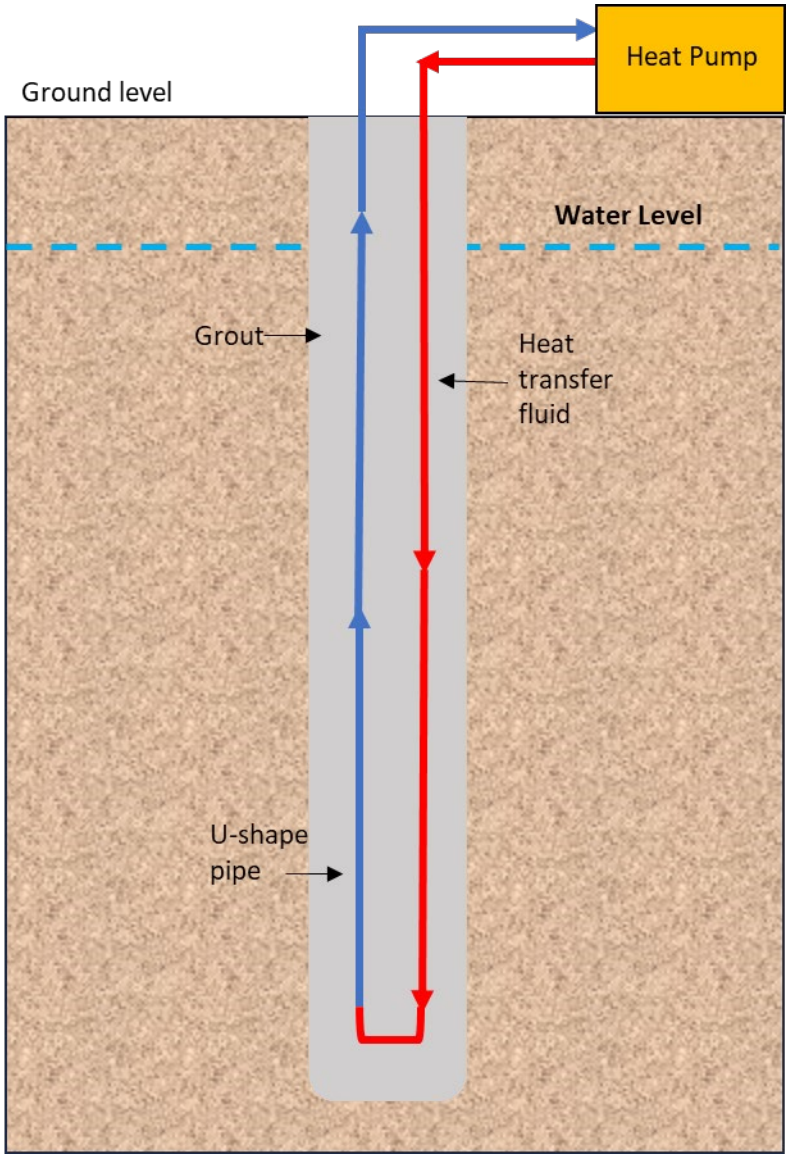

Figure 1-1: Schematic diagram of a closed-loop borehole heat exchanger (in cooling mode), blue arrows show cooled fluid returning to the heat pump and red arrows show warm fluid returning to the ground.

1.3 Literature review

A review was undertaken to identify and summarise existing literature describing subsurface temperature changes, and the extent of those changes (thermal 'plumes') around closed-loop GSHC sources.

The literature review addressed the following principal question:

a. What are typical thermal plume distances and temperatures associated with closed-loop BHEs / BHE arrays as reported in the literature?

To answer the principal research question, a number of subsidiary questions were first identified and addressed, and these are detailed in Section 2. The main findings of the literature review were used to inform the numerical modelling study and are also presented in Section 2.

The literature review sought to identify suitable case study datasets of monitored temperatures around closed-loop GSHC systems that could be used to analyse and verify findings from the modelling. These are presented in Section 3.

The literature review also helped to identify typical hydrogeological and thermogeological properties of rocks used in the modelling study, to ensure the values used represented typical bedrock and superficial deposits settings found in England. These are reported with the modelling study in Section 3.

Please note that throughout this report the terms 'ground temperature' and 'groundwater temperature' are treated synonymously. The reasons for this are given in more detail in Section 2.3.2.

1.4 Numerical modelling study

The major thermo-hydrogeological parameters influencing the 3-D spatial and temporal thermal impacts of BHE were identified through:

1) A comprehensive sensitivity analysis, performed with numerical simulations using the finite element code FEFLOW® 8.1 (DHI-WASY, 2023). This assessed how the

size of the thermal plume[6] is influenced by thermal and hydrogeological subsurface properties and BHE setup.

2) Assessment of thermal plume development in thermo-hydrogeological settings, or scenarios, typical for England.

The sensitivity analysis examined the impact of varying the major hydrogeological, system and geothermal factors of:

- groundwater flux;
- subsurface thermal conductivity;
- subsurface volumetric heat capacity;
- subsurface thermal dispersity;
- effective porosity;
- borehole depth; and,
- BHE system energy demand.

This sensitivity analysis was conducted from a baseline scenario representative of a saturated sandstone bedrock aquifer, such as the Permo-Triassic.

The evolution of the thermal plumes from closed-loop GSHC schemes were simulated with a series of further scenarios. These were chosen as representative of ranges of a) alternative operational requirements for the closed-loop system and b) different aquifer and non-aquifer conditions representative of common English geological settings. The scenarios simulated are listed below:

i. Baseline scenario with closed-loop system for heat extraction;
ii. Baseline scenario with unsaturated aquifer;
iii. Baseline scenario with closed-loop system alternating heat extraction and injection phases;
iv. London Basin aquifer;
v. Mudrock aquitard (i.e. Mercia Mudstone Group);
vi. Fluvial sand and gravels aquifer; and
vii. Conservative / worst case scenario.

Model simulations for these scenarios were conducted for a period of 50 years to represent long-term impacts over the operational lifetime of a GSHC system.

Details of the modelling study are given in Sections 3 and 4 and summarised in Section 5.

[6] Defines in this report as the 1°C isocontour of thermal alteration within the ground (see also Section 2.3.3).

2 Literature review

2.1 Introduction and main research questions

This literature review summarises existing literature describing subsurface temperature changes, and the extent of those changes (typically in the form of thermal 'plumes') around GSHC sources. Specifically, it addresses thermal plumes associated with closed-loop borehole heat exchangers (BHE). The literature review forms a part of, and fed into, the modelling study of thermal plume geometry, and sensitivity analysis of the variables controlling propagation of thermal plumes arising from closed-loop BHEs in the subsurface (Sections 3 and 4).

The literature review addresses the following principal question:

a. What are typical thermal plume distances and temperatures associated with closed-loop BHEs / BHE arrays as reported in the literature?

The purpose of answering this question is to better understand the potential scale and distribution of thermal plumes in the subsurface. This can be used to identified receptors that could be impacted by those plumes. Please note:

- Closed-loop BHEs are typically located in the relatively shallow subsurface (defined here as within 150m of the surface), and this review focuses primarily on such shallow BHE systems.
- The term 'thermal plumes' covers both the addition of heat to the ground, resulting in plumes of elevated temperature, as well as the extraction of heat from the ground, resulting in plumes of reduced temperature.

To answer the principal research question, a number of subsidiary questions were addressed:

b. What are typical baseline groundwater temperatures and variability in the UK, and the main factors that affect these?

c. What temperature change, in comparison to background, might reasonably define the limits of a thermal plume?

d. What are the confounding[7] factors and considerations for temperature changes in groundwater, and what are the magnitude of these changes (where empirical data are readily available)?

[7] i.e. those factors also influencing temperature changes in the subsurface not related to BHE systems, e.g. urban heat island effects.

e. What are the environmental limits for thermal plume migration?

In addition to the above questions, the literature review sought to identify suitable case study datasets from monitored closed-loop GSHC systems to compare with the numerical modelling.

2.2 Methodology

Information for the literature review included:

- Both peer reviewed literature and reports;
- International examples where directly relevant; and,
- Findings from case studies and modelling work.

Available literature and reports were identified in four ways:

- Broad search-engine internet search using Google;
- Google Scholar database search;
- Review of literature gathered for the systems mapping of environmental receptors to temperature changes arising from GSHC (Environment Agency, 2024a); and,
- Personal recommendations of literature by steering and project group members.

Internet search terms targeting the principal question included the phrases:

- Thermal plume groundwater;
- Closed-loop thermal plume;
- Borehole heat exchanger thermal plume;
- Environmental impact thermal plume; and
- Ground source thermal plume.

For each of these search terms, the first 150 published references returned on Google and Google Scholar were initially screened by title for relevance to either the principal or subsidiary questions. These were then screened by abstract, bearing in mind the requirement to study closed-loop rather than open-loop GSHC[8].

In addition to using internet searches, personal recommendations by steering and project team members were examined, and key references from the literature reviewed in the

[8] A number of these search terms returned results regarding open-loop systems. However, where these were deemed relevant to one or more of the questions they were retained (screened in). Where reviewed literature relates specifically to open-loop systems (but the findings still deemed relevant) it is noted in the literature review text.

production of Environment Agency (2024a) and (2024b) were identified for relevance to the above research questions, and citations within them also screened.

At this stage, where not already held, references were then obtained if they were freely publicly available, or in some cases obtained via direct requests to authors via email.

On the basis of an initial screening of the Abstract and, where available, additional content, references were placed into one of four categories:

1. Primary references: Of direct relevance in answering either the main or subsidiary questions, either by directly addressing the same questions, or providing data, analysis, case studies etc. relevant to assessment of those questions.

2. Secondary references: Of minor or tangential relevance in answering either the main or subsidiary questions.

3. Other background references or open-loop: References not directly relevant to answering either the main or subsidiary questions, but useful for wider background context of the study.

Of these:

- ‘Other background references or open-loop’ were not screened beyond Title and Abstract, and only retained in the spreadsheet database (Appendix A) to record that they had been screened.

- All ‘Secondary references’ were reviewed at Abstract level and, if seemingly relevant, further reviewed by screening Introductions and for any useful headings or diagrams. Any Secondary references that appeared more relevant than they had done initially were re-categorised as Primary references. Similarly, any that appeared less relevant at this stage were re-categorised as ‘Other background references’.

- All ‘Primary references’ were then reviewed in further detail for relevance and synthesis under the main questions to be answered by the literature review. Where primary references were deemed less relevant at this stage they were moved to ‘Secondary’ or ‘Other...’ references.

The literature surveyed is international and many non-England-focused references were retained where they offer insights into processes and identify magnitudes of impacts associated with thermal plumes in groundwater. Non-English language references were automatically screened out of the review, except for regulatory standards, guidance or legislation where relevant.

2.3 Results and Discussion

2.3.1 Number of references screened and categorised.

Overall, the literature review screened in excess of 500 article, book, report and thesis titles. Of these,193 were categorised as either ‘Primary Importance’, ‘Secondary Importance’ or ‘Other background or Open Loop’. These 193 references are tabulated in Appendix A, which provides information on:

- Title
- Year of publication
- Author/s
- Web link
- Category (‘Primary Importance’, ‘Secondary Importance’ or ‘Other background or Open Loop’)
- Whether or not it was possible to obtain the reference (recorded as ‘held’ or ‘not held’).

Of the 193 references screened in more detail 56 of them were categorised as ‘Primary references’ and are of particular use in answering the research questions. Please see Appendix A for an overview of the wider literature available.

2.3.2 What are typical baseline groundwater temperatures and variability in the UK, and the main factors that affect these?

This question is relevant to the overall research topic as it is important to first define what typical background (ground/groundwater) temperatures may be expected in the UK (and more specifically, England). This information is necessary in order to define a benchmark against which anthropogenic thermal impacts may be measured.

This aspect of the literature review examines existing natural, historical background temperature variations. Anthropogenic impacts, such as subsurface urban heat islands (SUHI) and climate change-related temperature impacts, whether anthropogenically derived or not, are also discussed in Section 2.3.4.

In answering this question (and throughout this report), please note the following:

- The terms ‘Ground temperature’ and ‘Groundwater temperature’ are treated synonymously.
    - Temperature measurements reported in the literature are a mixture of groundwater temperature measurements, measurements made in dedicated grout-filled temperature monitoring boreholes (i.e. the probe is not in contact with groundwater), and monitoring of BHE heat exchanger fluid temperature.

- For the majority of groundwaters ‘ground temperature’ may be taken as a proxy for ‘groundwater temperature’ (and vice versa), due primarily to rapid equilibration between ground and groundwater temperatures[9].
- However, this may not hold true for groundwater systems with significant fracture or fissure flow, such as karst limestones, in which surface waters may infiltrate and exfiltrate before than thermal equilibration is reached (for example, Ford & Williams 1989; Kresic & Stevanovic, 2010).
- Additionally, the geothermal/ground source heating literature often refers to temperature in degrees Kelvin (°K), whereas the hydrogeological literature typically refers to temperature in degrees centigrade or Celsius (°C). As 1°K = 1°C, Celsius are used throughout this report for the sake of simplicity (with the exception of reporting some standard units in the modelling section of the report where Kelvin is referred to in a number of equations (Section 3)).

- Different parts of England (and the UK) exhibit different background temperatures and temperature variability, and hence definition of baseline in particular instances (for example, for a local hydrogeological risk assessment of a scheme) should be based on local data acquired from either the literature or direct field monitoring.

Findings

Typical UK ground/groundwater temperatures

Busby (2015) presents a detailed study of shallow ground temperatures in the UK at 1 m depth using soil temperature data from 106 Met Office weather stations. He found that mean annual ground temperatures varied from 12.7°C in southern England to 8.8°C in northern Scotland. In a European-wide study, Rybach and Sanner (2000) report that seasonal temperature effects are essentially reduced to zero at a depth of 15 m and hence, at any locality, the ground at that depth reflects the annual average air temperature. This finding is corroborated for the UK by Bloomfield and others (2013). For the UK, Perry and Hollis (2005) report annual average air temperatures varying from 12°C in southern England to 8°C in northern Scotland, and so these temperatures are likely to be reflected in groundwater temperatures at 15 m depth.

The overall climate of the British Isles is strongly controlled by oceanic temperatures, but within this context the main control on temperature, besides latitude, is altitude[10]. Busby (2015) reports that the decrease of temperature with altitude is on average 0.65°C per 100 m across Britain (after International Civil Aviation Organization, 1993).

---

[9] This assumption is made in the modelling aspects of this study.

[10] In addition to altitude and latitude, continental climates are also controlled by their distance from the nearest oceans.

Stuart and others (2010) analysed groundwater temperature data from 3,700 boreholes with a median depth of 91 m across England and Wales. They found that the average groundwater temperature for this dataset was 11.35°C with one standard deviation of 1.76°C (although some potential data quality issues associated with the dataset are raised, including the possibility of numerous measurements having been impacted by ambient air temperature during sampling). The same dataset is also discussed by Bloomfield and others (2013).

There are strong additional heating (and in some instances, cooling) factors associated with towns and cities, and this is discussed in Section 2.3.4).

Geothermal gradients and thermal waters

At depths greater than ~15 m, ground temperatures in the UK are affected by geothermal gradients (Bloomfield and others, 2013; Busby, 2015). The UK average geothermal gradient is 2.6°C per 100 m depth (Busby, 2015), which varies depending on groundwater flow and geological heterogeneity, and can be as high as 3.5°C per 100 m (Darling, 2019) in some localities.

Meinzer (1923) first proposed a definition of thermal waters as those "...whose water has a temperature appreciably above the mean annual temperature of the atmosphere in the vicinity of the spring." Abesser and Smedley (2008) define thermal waters as groundwater at more than 5°C above the local mean annual temperature and suggests groundwater with a temperature of more than 2°C above the annual average contains at least a thermal component. Other authors have presented similar definitions, as discussed in Environment Agency (2020). Darling (2019) proposes a more conservative threshold of 20°C and the National Geological Screening (for example, Hough and others, 2018) used a value of 15°C.

Naturally occurring thermal waters exist in various places in the UK and must be considered when defining a natural background range of groundwater temperature. Environment Agency (2020) present a table which is reproduced below (Table 2-1) to demonstrate the highest naturally occurring temperatures observed in English groundwater.

Table 2-1: Thermal springs in England (after Table 5.1 from Environment Agency, 2020).

Location	Spring	Temperature
Bath, Somerset	Unspecified	40°C
	Cross Bath	41°C
	The Hetling Spring	47°C
	The King's Bath	45°C
Bristol	Hotwells	24°C
Bakewell, Derbyshire	British Legion	11.6°C
	Recreation Ground	13.3°C
Bradwell, Derbyshire	Bradwell Spring	12.4°C
Buxton, Derbyshire	St. Anne's Well	27°C
Crich, Derbyshire	Meerbook Sough[3], Leashaw Farm	17°C
	Ridgeway Sough, Whatstandwell	14.1°C
Dove Valley, Derbyshire	Beresford Dale	13.8°C
Dimin Dale, Derbyshire	Lower Dimindale	11.5°C
Matlock, Derbyshire	-	20°C
Stoney Middleton, Derbyshire	Stoke Sough, Grindleford	14°C
	Stoney Middleton Spring	18°C

Table 2.1 indicates natural temperatures of groundwater in England of up to 47°C at Bath, and 27°C in Derbyshire. Whilst these values are local to these areas, a geothermal gradient is present in all localities throughout England, such that probable changes in baseline temperature with depth are on the order of one to several degrees over the length of closed-loop BHEs, which typically range between a few tens up to 200-300 metres.

Other factors influencing ground/groundwater temperature

Other natural influences on groundwater temperature, especially in the near surface, include infiltration and bank storage of river waters, especially under high water conditions and across meanders. Winter floods may significantly reduce the temperature of groundwater in alluvial aquifers, especially where the rivers are large, and vice versa, may raise the temperature of alluvial groundwater (Garcia-Gil and others, 2014; Navarro and Mateo-Lazaro, 2014).

Similarly, as mentioned briefly above with regards karst limestones, there can be significant natural annual fluctuations in groundwater temperatures associated with sinking streams or matrix-bypass fissure flow. In such settings the groundwater may locally be at significantly different temperature to the surrounding rock mass as, due to the velocity of groundwater flow, non-temperature-equilibrated water may penetrate an aquifer for many kilometres, and even exit the aquifer prior to achieving thermal equilibrium with it. There are many examples of this from Carboniferous limestones in the UK (for example Gunn, 2014; Gunn and others, 2015) and the phenomenon has also been demonstrated in the English chalk (for example Worthington & Foley, 2021). Indeed, temperature acts in many ways as an ideal tracer as it is essentially a property of the water alone, rather than an additional chemical constituent. There is a large literature dealing with the use of temperature as a tracer in groundwater, which is beyond the scope of this review, but Anderson (2005) provides a broad overview of the subject.

Other potential influences on groundwater temperature include urban environments, coastal influences, temperature inversions in lakes, and rapid ice/snow thaw and associated rapid recharge, all of which may result in significant temperature changes.

Summary

Natural temperature variations in English groundwater are driven by numerous processes. Without external influences such as significant surface water interaction or unusual geological/hydrogeological settings, groundwater temperatures in the UK at a depth beyond that influenced by seasonal variations (15 m) range between 8°C and 12°C, with strong controls relating to latitude and altitude. The average groundwater temperature for England and Wales was found by Stuart and others (2010) to be 11.35°C with a one standard deviation of 1.76°C, although these authors considered this figure to be biased to the high side due to data quality issues.

Elsewhere natural groundwater temperatures reach 47°C at the hot springs at Bath in Somerset, and over 20°C at numerous other locations in Somerset, Bristol and Derbyshire. At all locations in England a geothermal gradient is present, and the average is 2.6°C/100 m depth.

2.3.3 What temperature change, in comparison to background, might define the limits of a thermal plume?

This question is important in answering the principal question as it addresses how we might define a thermal plume such that it is distinguishable from baseline temperature and variations in baseline temperature.

Findings

Definitions of thermal waters were provided in the previous section, with Abesser and Smedley (2008) suggesting a threshold of 2°C above local baseline as representing the presence of 'at least a component' of thermal water. They do not provide a justification for this number, although it is just above the one standard deviation (SD) of groundwater temperature identified across the England/Wales dataset (1.76°C) and hence is expected to capture ~70% of variability.

Elsewhere in the literature a 1°C change in temperature from baseline is widely reported as defining a thermal impact or plume (for example Abesser and others, 2023; Gizzi and others, 2020; Daemi and Krol, 2019; Pophillat and others, 2019, 2020; Piga and others, 2017; Lo Russo and others, 2012; 2014), and this offers a pragmatic and easily understood definition of a thermal plume.

Other definitions of a thermal plume used in the literature include:

- Garcia-Gil & Moreno (2019) note that Spanish legislation defines thermal waters as 4°C above mean annual surface temperature at the site.
- Epting and others. (2013) delineated zones of 3°C and 5°C above baseline on the basis of Swiss legislation permitting 3°C temperature changes down-gradient of thermal groundwater use.
- Carbon Zero Consulting and Holymoor Consultancy Ltd (2010) (in an open-loop study) used 50% of the temperature difference between the abstracted and reinjected water, which in their study was a difference of 10°C, hence a plume boundary definition comprising the 5°C isocontour.

However, much of the literature that discusses heat impacts on groundwater systems does not provide any definition as to the boundaries of thermal plumes, simply reporting changes against baseline. This is particularly the case for numerous modelling studies which tend to rely on visualisation of the scale of thermal impact along a continuum, such as shown in Figure 2-1.

Thus, many modelling studies define a baseline temperature as an initial boundary condition and judge thermal impacts against that single defined baseline. In such cases, isocontours defining different parts of thermal plumes can be constructed to any number of decimal places. This degree of precision can delimit the full extent of a plume but might imply a greater degree of certainty than (necessarily) simplified models can represent.

Measurement accuracy of in-situ ground/groundwater temperatures is typically reported to be 0.1°C (for example Abesser and others, 2023), and across the surveyed literature temperature changes in field studies are usually reported to this degree of precision. However, such small changes in temperature might in reality be masked by other influences and environmental impacts associated with these small changes would likely be minimal.

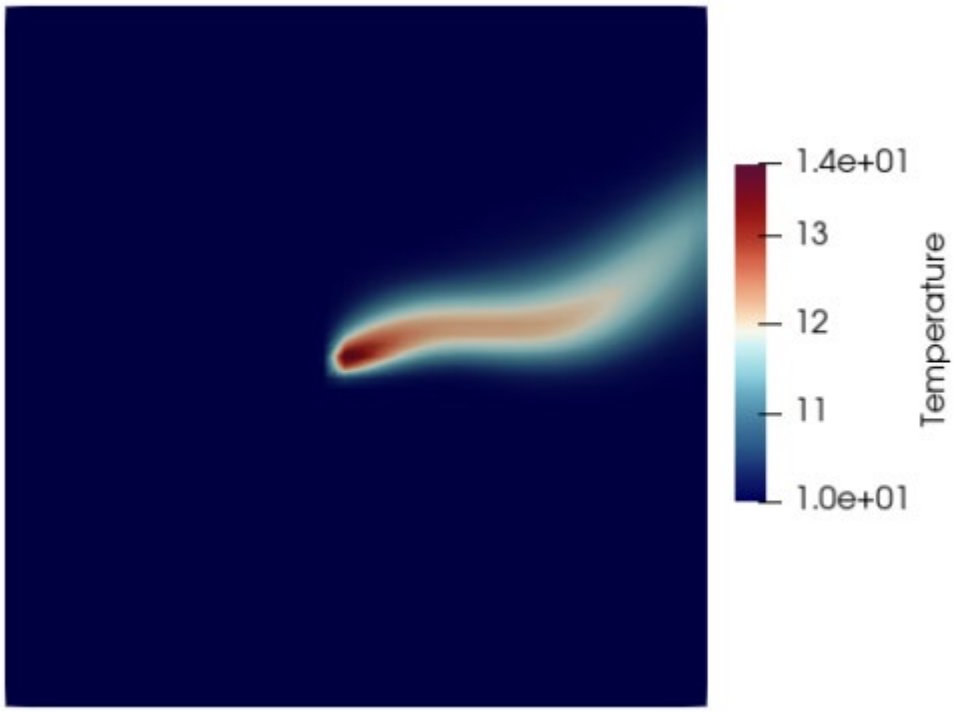

Figure 2-1: Groundwater temperature map showing a modelled example of a BHE thermal plume (after Leiteritz and others, 2022[11]).

[11] Reproduced under Creative Commons License CC By 4.0 Deed (https://creativecommons.org/licenses/by/4.0/)

Summary and recommendation

For the purposes of this study, a 1°C definition of a thermal plume boundary[12] has been used. This has wide precedence across a variety of studies within the literature, and benefits from being simple to use and easy to understand. It is also an order of magnitude greater than typical temperature probe precision and most of the studies reviewed here report ground/groundwater temperature data to one decimal place. Whilst 1°C is less than one SD of the national (England and Wales) dataset (Stuart and others, 2010), it should be recognised that that dataset covers a very large area with significant altitudinal and latitudinal variation, as well as potentially some data quality issues.

A 1°C definition of a thermal plume boundary is adopted for presentation of modelling results in Section 3.

2.3.4 What are the confounding factors and considerations for temperature changes in groundwater, and what are the magnitude of these changes (where empirical data are readily available)?

Section 2.3.2 reported literature review findings for naturally occurring, historical baseline temperatures, excluding anthropogenic impacts and climate change-related temperature impacts (whether anthropogenically derived or not). These are discussed here and cover a wide range of sources of temperature-related impacts to the subsurface.

Findings

Climate change

The main reference analysing historical groundwater data temperature trends for the UK is Bloomfield and others (2013), who state that there is some evidence for an increase in average groundwater temperatures in the UK of between 0.01 and 0.02°C/year between 1990 and 2008. However, separating a small climate change signal from other confounding factors (described in more detail below) remains challenging (Bloomfield and others, 2013). Beyond the UK, Epting and Huggenberger (2013), Bayer and others (2016), and Epting (2017) found that subsurface heating associated with climate change is secondary to local and regional anthropogenic factors, such as urbanisation.

[12] For the purposes of environmental impact assessment, this term may be more accurately described as a “thermal plume of interest” – that is, a useful arbitrary boundary needs to be defined in order to categorise what is and isn’t affected by a temperature change, and real changes less than 1°C are challenging to discern in the environment against background noise and may, therefore, also have limited impact.

More broadly, climate change is widely assessed as likely to result in increased surface air temperatures and rainfall temperatures across the British Isles. The Intergovernmental Panel on Climate Change (2021) report that an approximately 1°C increase in average global surface temperature was observed between approximately 1970 and 2020 (with reference to an 1850 – 1900 baseline). Such changes will of course impact ground/groundwater temperatures, and Egidio and others (2024) have undertaken a systematic review of the international literature on how groundwater temperature is affected by climate change. Additional detail is beyond the scope of this report, but the reader is recommended to consult Egidio and others (2024) for further information.

Primary anthropogenic causes of temperature change in groundwater, and subsurface urban heat islands (SUHI)

There are numerous potential anthropogenic causes of changes to subsurface temperatures. The primary sources identified in the literature include the following (not listed in any particular order):

i. Surface sealing, whereby evapotranspiration as a ground surface cooling process is largely prevented by hard surfaces (tarmac, concrete, paving etc);
ii. Buildings and building foundations;
iii. Road and subway tunnels;
iv. Ring mains for water supply, including both conductive heating and temperature impacts of leakage;
v. Buried district heat networks;
vi. Underground car parks;
vii. Sewer networks;
viii. Open and closed-loop GSHC systems; and,
ix. Landfills.

Whilst these impacts may occur anywhere, they are often highly concentrated in urban areas, and consequently anthropogenic impacts to subsurface temperatures tend to be greatest in urban areas and hence are discussed in this context below.

Urban heat islands (UHI) were widely reported on since first documented in the 1950s (for example Landsberg, 1956) and relate to the higher atmospheric temperatures found in urban environments compared to surrounding countryside. Less studied were SUHI, with literature reporting this phenomenon appearing in the late 1990s and early 2000s but growing rapidly thereafter.

For example, Changnon (1999) identified positive temperature bias of approximately 0.6°C in urban compared to rural ground temperature datasets. Taniguchi and Uemura (2005) and Taniguchi and others (2007; 2009) demonstrated that a longer history of urbanisation was associated with greater temperature increases in the subsurface, identifying and discussing SUHI in several Asian cities. In North America, Ferguson and Woodbury (2004, 2007) identified SUHI of up to 5°C in the city of Winnipeg, and in Europe, studies of SUHI were undertaken for the cities of Cologne (Zhu and others, 2010; Menberg and others, 2013), Berlin, Munich, Frankfurt, Karlsruhe and Darmstadt (Menberg and others, 2013),

finding temperature increases between 3 and 7°C. Epting and others (2013, 2017), and Epting and Huggenberger (2013) also report SUHI effects of up to 9°C above background, and in Zaragoza (Garcia-Gil and others, 2014, 2020a, 2000b) report localised temperature changes of up to 13.7°C. Blum and others (2021) consider more widely whether or not thermal use of groundwater constitutes a form of pollution, looking at many of the processes listed above, and presenting a sustainable policy framework in this regard.

In the UK, the majority of studies relating to SUHI focus on London. Fry (2009) identifies potential increases in groundwater temperatures associated with (open-loop) GSHC systems in London, and Headon and others (2009), and Pike and others (2011) present groundwater temperature profiles for London to be used as a benchmark for the development of future groundwater cooling schemes. They identify a number of possible natural and anthropogenic mechanisms for increases in fluid temperature logs with depth. Banks and others (2009) identify similar increases in Tyneside, finding that "…historical downward conductive heat 'leakage' from the …urban environment has modified subsurface temperatures to a depth of at least 55m" (Banks and others, 2009). Luo and Asproudi (2015) identified a SUHI effect for London of up to 3.5°C, as well as a general soil-warming trend across the UK of 0.17°C per decade, whereas elsewhere in London, Abesser and others (2023) identify local increases of up to 20°C at depths up to 20 m, and over 1°C at depths up to 75 m, resulting from the influence of near-surface infrastructure. More widely, Busby (2015) provides shallow soil temperature estimates for all UK cities and many major towns, including estimated differences between urban and rural Surface Air Temperatures (SAT) for each location. This is relevant as both Menberg and others (2013) and Taniguchi and others (2007) both identified strong positive correlations between SAT and groundwater temperature.

The list of anthropogenic temperature change sources presented above may be classified into two sorts (after Rotta Loria and others, 2022), namely I) large-scale surface drivers of subsurface heat, such as surface sealing, buildings and other urban infrastructure that maintain an atmosphere UHI which then diffuses into the subsurface (items i and ii from the list), and II) local or point-source drivers of heat flux (items iii to ix).

To understand the magnitude of thermal fluxes in an urban environment arising from a combination of such sources, Epting and others 2013 calculated the thermal flux in an approximately 5.5 km^2 area of the city of Basel, Switzerland, before and after development of infrastructure. They found that the baseline (pre-development) thermal flux calculated for rainfall recharge, groundwater flux and river-aquifer interactions amounted to 44 MW/yr. By contrast, the post-development thermal flux for the same area nearly doubled to 85 MW/yr, with the city adding 41 MW/yr to the ground energy balance from a combination of buildings/infrastructure and groundwater users (i.e. open and closed-loop GSHC systems). This resulted in measured urban ground temperatures of up to 17°C, against a baseline groundwater temperature of 10°C, i.e. a net increase of 7°C. They noted that subsurface urban heat temperature distribution is dependent upon three factors in addition to the natural thermo/hydrogeological setting:

- Historical duration of heat loading;

- Distance between source of heat (building) and a given measurement point; and,
- Density of buildings in a given area.

Abesser and others (2023) present a useful visualisation (Figure 2-2) of the influence of infrastructure on ground temperature for a Canadian university campus. They use a model developed from historical maps and aerial photography showing how the campus developed over the latter half of the 20th Century. This model is calibrated against measured temperature depth profiles. They demonstrate changes in subsurface temperature of up to 10°C on the basis of buildings, sewage systems[13], car parks and road infrastructure alone (i.e. without any GSHC systems present). The changes resulting from this infrastructure development are illustrated in Figure 2-2.

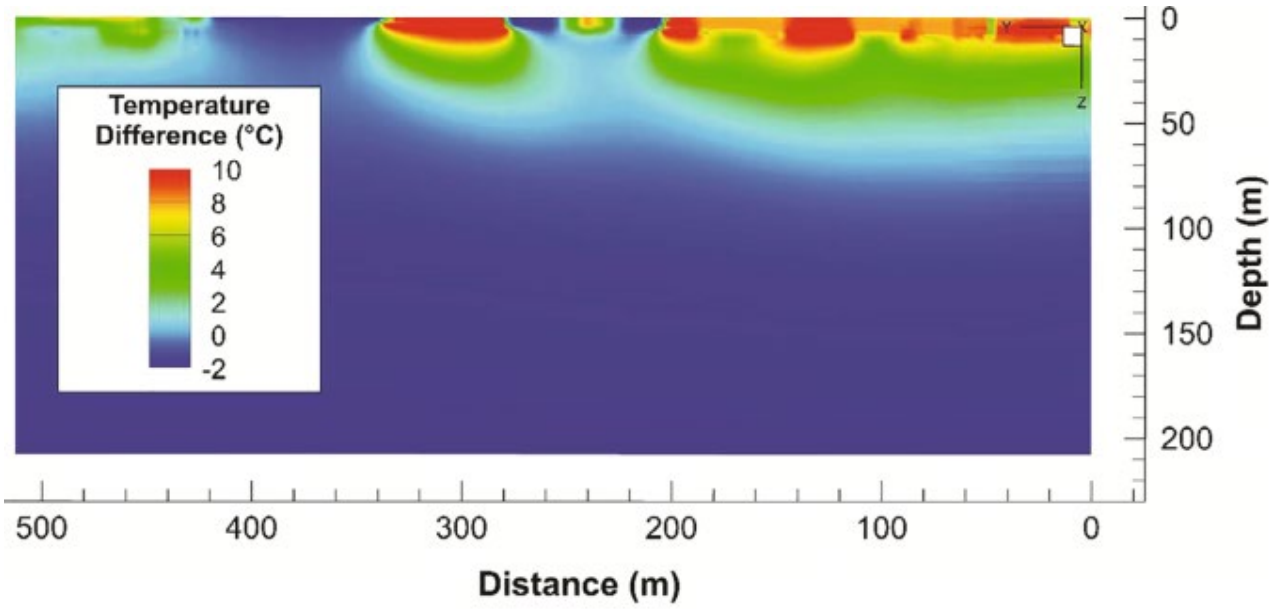

Figure 2-2: Difference in subsurface temperature with and without infrastructure prior to BHE activation for a town in Canada, after Abesser and others 2023[14].

Of the anthropogenic causes of increased subsurface heat listed above, there is a small but significant body of work on the temperature impact of underground car parks (UCP) on urban subsurface heat (Zhu, 2015; Rotta Loria and others, 2022; Noethen and others,

[13] Menberg and others (2013) use sewage pipe temperatures of 18.5 degrees in their modelling of heat flux in German cities, and this value is used in the modelling by Abesser and others (2023) (Figure 2.2).

[14] Reproduced under Creative Commons License CC By 4.0 Deed (https://creativecommons.org/licenses/by/4.0/)

2023). UCP dissipate heat generated from car engines from the UCP atmosphere to the ground. These structures can be a significant point-source of heat input to the subsurface. For example, Noethen and others (2023) analysed monitored temperature data from 31 UCPs across Germany and Switzerland, and followed this with analysis of an additional 5,040 UCPs in Berlin alone. They found the mean temperature within the UCPs was 18.8 ± 4.9°C.

Other anthropogenic sources of localised temperature changes noted in the literature are from sewer infrastructure, reported by Abesser and others (2023), and Menberg and others (2013) as suitably modelled at a constant temperature of 18.5°C, and similarly, Tissen and others (2019) summarise literature showing that landfills are typically responsible for thermal plumes 3°C – 10°C higher than background.

Summary and recommendations

There are a wide variety of temperature confounding factors that can impact subsurface temperatures and should be considered when trying to understand temperature changes in groundwater that may arise from GSHC. These are often concentrated in urban environments, and in such a setting may be classified into two broad groups; I) large-scale surface drivers of subsurface heat, such as surface sealing and buildings and other urban infrastructure that maintain an atmospheric UHI which then diffuses into the subsurface, and II) local or point-source drivers of heat flux, such as sewer systems, underground car parks and existing building cooling or heating systems. Most literature is concerned with the impacts of heating rather than cooling the ground, and typical SUHI temperatures range from 3 to 9°C higher than adjacent rural ground temperatures. Locally, temperature changes are reported as reaching over 25°C above baseline.

2.3.5 What are the environmental limits for thermal plume migration?

Natural limits on thermal plume propagation within the ground result from equilibrium between injected/extracted heat and the capacity of ground/groundwater systems to absorb or counteract temperature changes. Thermal plumes in the ground dissipate via mechanisms including advection, dispersion and conduction, and may also be truncated by intersection with natural groundwater system boundaries such as the atmosphere/ground surface, rivers and the sea. There are numerous physical properties of both rocks and water that exert controls on thermal plume migration, of which the most influential are the Darcy flux (volume of flow per unit cross sectional area of aquifer for a given hydraulic gradient), the thermal conductivity of the rock mass (see Section 2.3.6 for a detailed discussion) and the dispersivity. However, interactions between these can be complex. For example, Banks (2015) states:

“Increasing the groundwater flow velocity decreases the size of the steady-state plume (as judged by a specific temperature contour) as heat is advected away from the borehole more efficiently. This is slightly counter intuitive and is due to the fact that, with a faster groundwater flow, a steady state is approached far more rapidly. With a slow groundwater flow, steady state takes longer to achieve, by which time the thermal plume is bigger.”

“Increasing the thermal conductivity decreases the plume in the x direction. In other words, the plume becomes more circular, as conductive heat transfer becomes increasingly important relative to advection.”

Effective porosity is another parameter with complex effects, as, for a given hydraulic gradient, an increase in effective porosity reduces groundwater velocity and changes the void ratio of the ground, meaning a different distribution of bulk thermal properties between rock matrix and interstitial water. These have, for example, significantly different specific heat capacities and can therefore absorb differing amounts of heat energy before changing temperature.

Such technicalities as mentioned above are beyond the scope of this literature review but are discussed in greater detail in Section 3 of this report. However, in general, the size and temperature of anthropogenic thermal plumes are limited primarily by the size of the heat source and by the boundary conditions of the geological/hydrogeological system in which they are situated. Rivers, the sea, and the ground surface, are all major boundaries responsible for controlling the extent of anthropogenic thermal plumes.

2.3.6 What are typical thermal plume distances and temperatures associated with closed-loop BHEs / BHE arrays as reported in the literature? Are case study data available?

There are very few studies of thermal plumes associated with closed-loop/BHE systems that contain monitored data extending beyond the short term of days to weeks. Many studies use short-duration thermal response tests at these timescales of days/weeks to determine thermo- /hydrogeological parameters and conduct long-term studies via modelling using data from these tests. For the most part, those models remain uncalibrated against longer time series data, although there is a broad consensus across modelling studies regarding the physical thermo- / hydrogeological processes controlling heat transport how to model them. Some studies use measured ground heat profiles together with historical mapping of urban development to model the historical development of heat distribution in the subsurface (for example, Abesser and others 2023).

Below, a selection of results from modelling studies are summarised to give an indication of the typical scales and distances of thermal plume development that have been reported, followed by a short synopsis of two studies that do provide some longer term data.

Modelling studies with short term data

- Epting & Huggenberger (2013) present some limited data for the city of Basel in Switzerland and a modelling study of the alluvial aquifer. The model accounts for GSHC systems as well as numerous other SUHI type sources of ground heat, in particular buildings constructed below the water table. Their modelling demonstrates several thermal plumes extending for distances of up to a few hundreds of metres, some of which terminate at the River Rhine. They note that

superposition of multiple thermal processes lead to temperatures up to 9°C above background.

- Abesser and others (2023), Case study #1: Modelled plumes at ~1°C change from background at a distance of ~150 m after 20 years in a limestone/dolostone aquifer resulting from a BHE array consisting of 18 BHEs exchanging ~400 MWh/year.
- Abesser and others (2023), Case study #2: This study modelled the 25 year evolution of a cold thermal plume arising from a BHE array of 58 BHEs in a chalk aquifer with an energy exchange of up to ~586 MWh/year. They found:
    - Reductions in temperature increased locally with lower groundwater flow, with an extreme scenario case (no-flow, high heat extraction) resulting in a 17°C reduction in temperature within the array itself;
    - Under a higher flow scenario with the same heat exchange, temperature reductions within the ground were as high as 5.5°C within the array, and up to 2.6°C at a distance of ~100m at the downstream boundary of the system (aquifer discharging to river); and,
    - Thermal equilibrium was achieved within ~10 years for the scenario with groundwater flow, but without such flow did not reach steady state within 25 years.
- Abesser and others (2023), Case study #3: Thermal plume modelling of a 290 MWh/year BHE array of 50 BHEs (for building heating) in an interbedded shale/sandstone/limestone aquifer, over a period of 20 years, showed that:
    - BHE array temps dropped by up to 6°C over 20 years;
    - A 1°C change from background was modelled at a distance of ~150 m after 20 years.
- Daemi & Krol (2019) modelled a building cooling system of up to 531 MWh/year calculating a 1°C temperature change at a distance of up to ~65m after ten years of operation (18 BHEs situated in a unform sand aquifer).
- Schelenz and others (2017) in a study of a 24 MWh/year system identified, in their worst case scenario of a rhyolite aquifer overlain by a glacial till, that the maximum temperature change (cooling) within the ground amounted to 6.7°C within the BHE array, falling to 4 – 5°C at a distance of 10m, and a 1°C at a distance of 130 m.

Closed-loop GSHC studies with longer-term data

The literature review did identify two studies reporting longer-term impacts and backed by data extending over at least some years (Rivera and others, 2015; Meng and others, 2018). These are discussed in more detail below.

- Rivera and others (2015) present a dataset from a 13 year study of a single BHE in an interbedded conglomerate/marl/sandstone formation supplying a domestic residence at a seasonal (October to April) operational heat extraction rate of 70W m^{-1} over a depth of 105m. Monitoring boreholes were installed at 0.5m and 1m distance from the BHE. The monitoring borehole at 1m distance showed maximum temperature changes after 13 years of less than 2°C at a depth of about 35m, indicating a limited plume extent over this time.

- Meng and others (2018; 2019) and Viencken and others (2019) describe findings from a detailed case study of a neighbourhood in Cologne, Germany. This site has 51 GSHC (of which 47 are closed-loop and 4 are open-loop) installed to depths of up to 40m over an area of 500m x 300m within an alluvial sand and gravel aquifer. The system was installed in 2008 and approximately 5 years of field temperature data were collected between 2013 and 2018. As 90% of GSHC operational capacity was used solely for building heating (i.e. heat extraction from the ground), the thermal plumes were colder than the background groundwater temperature. The studies concluded that:
    - Temperature differences between monitoring wells upgradient (background) and ~75 m downgradient of the neighbourhood exhibited maximum differences of 1.2°C over 5 years.
    - Temperature changes at individual wells were recorded as up to 0.8°C over 5 years.
    - At monitoring points 75m downstream of the neighbourhood, temperature changes of up to 0.4°C were recorded over 3 years (between 2013 and 2016).
- Further to the above, Meng and others (2018) also calibrated a model against 3 years' of field data (2013-2016) and ran it for a 25 year model simulation. Their main findings were as follows (see also Figure 2-3):
    - Boreholes aligned along individual flowpaths produce the greatest overall temperature impacts;
    - In the most affected places within the study area, ground temperatures dropped to 3.2°C, although this was in only ~1% of the total study area. This represented an ~8°C reduction in temperature against background;
    - BHE arrays of the same polarity (either cooling or heating the ground) should be situated at least tangentially to the direction of groundwater flow, as cooling (or heating) impacts are additive;
    - Conversely, a closed-loop BHE array can be highly beneficial to another of opposite polarity immediately downgradient of it[15];
    - Temperature impacts are higher where groundwater velocity is lower, as temperature differences dissipate less rapidly[16];
    - Lower groundwater velocity also results in longer times to achieve thermal equilibrium[167];
    - Most individual BHE systems had come into thermal equilibrium after 20 years, however;

[15] Arguments are presented in numerous places in the literature for regulating heating and cooling schemes so that either multiple schemes are in balance within an area, or individual schemes are run in as close to a balanced operation as possible (i.e. summer cooling, winter heating)

[16] As found in the modelling study described in Section 3 of this report.

- The designated receptor at B (Figure 2-3) had not reached equilibrium after 25 years. (Point B is at the end of a flowpath that has multiple contributory schemes removing heat form the ground);
- At point B, the combined GSHC schemes had breached the 6°C German regulatory limit[17] for temperature change after 25 years.

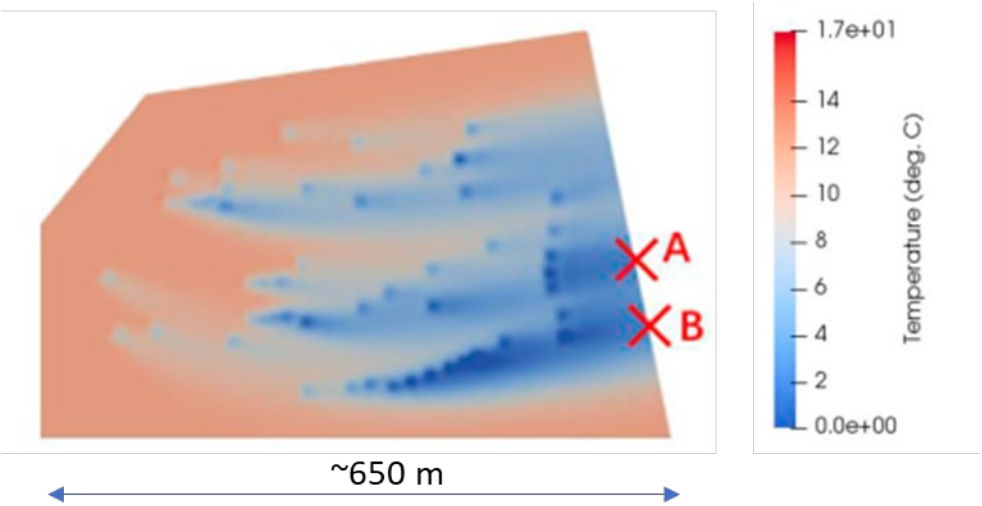

Figure 2-3: Modelled cold temperature plumes associated with multiple closed-loop ground source heating schemes in a district of Cologne, Germany (adapted from Meng and others, 2018[18]). Red crosses marked A and B represent defined compliance points for temperature changes.

2.3.7 Evidence gaps

Growth in the use of GSHC systems since the 1990s has led to many research studies, although the majority of these reported in the literature are aimed at improving and optimising GSHC system design and operation, for both closed and open loop systems.

The main evidence gap identified in this literature review is the absence of medium and long-term field studies of thermal plume propagation from closed-loop BHE systems. With a couple of exceptions, studies predominantly rely on modelling thermal plumes based on short-term (days to weeks) thermal response tests or literature values of thermo-hydrogeological parameters.

---

[17] VDI 4640 Blatt 1: 2000-12: Thermische Nutzung des Untergrundes. Bauphysik 2001;23:115-115.

[18] Reproduced under Creative Commons License CC By 4.0 Deed (https://creativecommons.org/licenses/by/4.0/)

However, modelling studies do form a broad consensus on how thermal plumes should be modelled and are typically in agreement with regards the influence of key parameters (Darcy flux, thermal conductivity, effective porosity etc.) on subsurface heat transport.

Another evidence gap lies in environmental impact assessment of thermal plumes, with only a few studies citing these concerns as a factor in motivating the research. The bulk of studies are concerned with optimising BHE and BHE array performance, assessing and avoiding thermal feedback between systems, determining system sustainability, and conditions for thermal equilibrium. This is reflected in the variation between, and in many instances missing or incomplete, national and international (for example EU) legislation of the impacts of heating or cooling the subsurface (Haehnlein and others, 2010; Tsagarakis and others, 2018; Garcia-Gil and others, 2020a).

2.3.8 Literature review summary and conclusions

The literature review examined evidence for thermal plume distances and temperatures associated with closed-loop BHEs/BHE arrays. Only two studies were identified with monitoring data more than a few weeks in duration, and most studies reported in the literature have modelled particular sites in detail. Alongside the main research question, a number of subsidiary questions have also been addressed, and the principal findings are as follows:

- Typical UK baseline ground/groundwater temperatures vary between 12.7°C in southern England to 8.8°C in the north of Scotland. An average groundwater temperature of 11.35°C, with a one standard deviation of 1.76°C was identified for England and Wales, although this is potentially skewed to the high side.

- Natural groundwater temperatures reach 47°C at the hot springs at Bath, Somerset, and over 20°C at numerous other locations in Somerset and Derbyshire. At all locations in England a geothermal gradient is present, and the average is 2.6°C/100 m depth.

- A 1°C temperature change, in comparison to background, provides a pragmatic definition of the limits of a thermal plume. This value is easy to understand, exceeds typical instrument precision by approximately 1 order of magnitude, and is used in numerous places within the literature.

- Numerous confounding factors influencing ground temperature are identified. Where ground temperature regulations exist (internationally), ground temperatures exceeding threshold values are often affected by anthropogenic heat sources that are not regulated. Such sources and processes may be divided into two sorts:

    - Large-scale surface drivers of subsurface heat, such as surface sealing, buildings and other urban infrastructure that maintain an

atmosphere UHI which then diffuses into the subsurface (for example surface sealing, buildings and building foundations); and,
    - Local or point-source drivers of heat flux (for example underground car parks, sewer networks and landfills).

- Environmental limits for subsurface thermal plume migration are governed by physical boundary conditions, of which the main ones are the atmosphere (ground surface), rivers and the sea.

The main evidence gaps identified in this literature review is the absence of medium and long-term field studies of thermal plume propagation from closed-loop BHE systems. With a couple of exceptions, studies predominantly rely on modelling thermal plumes on the basis of short-term (days to weeks) thermal response tests or literature values of thermo-hydrogeological parameters.

However, modelling studies do form a broad consensus on how thermal plumes should be modelled and are typically in agreement with regards the influence of key parameters (Darcy flux, thermal conductivity, effective porosity etc.) on subsurface heat transport. Overall the literature provides a sufficiently wide range of case studies to underpin an informed understanding of temperature migration in commonly encountered settings. However, there are few studies specifically addressing environmental impact assessment of thermal plumes, with only a few studies citing these concerns as a factor in motivating the research. The bulk of studies are concerned with optimising BHE and BHE array performance, assessing and avoiding thermal feedback between systems, determining system sustainability, and conditions for thermal equilibrium.

3 Numerical model development

3.1 Choice of simulator

Numerical modelling of thermal plumes was performed in FEFLOW®, a density-dependent, fully coupled groundwater flow and heat transport code for both saturated and unsaturated conditions (DHI-WASY 2023).

FEFLOW® offers different approaches for simulating heat transport around borehole heat exchangers (BHE) (Diersch and others 2010; 2011a,b) that are coupled to a heat source or sink (often via a heat pump). The BHEs are represented as 1 dimensional (1D) elements embedded in a 3 dimensional (3D) finite-element model. BHE boundary conditions are calculated using a simplified analytic approach for the heat transfer in the X and Y directions, assuming a local thermal equilibrium between the elements of the heat exchanger.

3.2 Theoretical background

As the theoretical background for heat transport is well established, the following theoretical description, as implemented in FEFLOW®, is taken directly from Piga and others (2017):

> "Flow and heat-transport in saturated porous media occurs by conduction (driven by temperature gradient), advection (due to the flow of the fluid phase), and dispersion (induced by the heterogeneity of the groundwater velocity field). These mechanisms are described by the heat conservation equation in a two-phase (solid and liquid) medium, with the assumption of a groundwater flow aligned with the x-axis:

$$\rho c\frac{\partial T}{\partial t}+\rho_w c_w v_D\frac{\partial T}{\partial x}+(\lambda+\rho_w c_w v_D\alpha_L)\frac{\partial^2 T}{\partial x^2}+(\lambda+\rho_w c_w v_D\alpha_T)\left(\frac{\partial^2 T}{\partial y^2}+\frac{\partial^2 T}{\partial z^2}\right)=H \quad (1)$$

> where ρc and $\rho_w c_w$ are the thermal capacities (J/m^3/K) of the porous medium and of the liquid phase, respectively; T is the temperature (K (i.e. degrees Kelvin, where 1K = 1°C)), considered equal for the solid and the liquid phases (i.e., the thermal equilibrium is considered instantaneous); v_D is the Darcy velocity (m/s); α_L and α_T are, respectively, the longitudinal and transverse dispersivities (m) relative to the groundwater flow direction; λ is the thermal conductivity of the porous medium (W/m/K); and H is the heat source/sink (W/m^3).
>
> The first term of Equation (1) is the temperature variation over time, which depends on the volume-averaged (bulk) heat capacity of the porous saturated medium (ρc):

$$\rho c = n_e \rho_w c_w + (1 - n_e)\rho_s c_s \quad (2)$$

where $\rho_s c_s$ is the thermal capacity ($J/m^3/K$) of the solid phase.

The second term describes the advection, which is a function of the Darcy flux (vD):

$$v_D = -K\frac{\partial h}{\partial x} = -Ki \quad (3)$$

where K is the hydraulic conductivity[19] (m/s), h is the hydraulic head (m), and i is the hydraulic gradient along the x direction (dimensionless).

Conduction depends on the bulk thermal conductivity[20] in the third term of Equation (1):

$$\lambda = (1 - n_e)\lambda_s + n_e\lambda_w \quad (4)$$

where λ_s and λ_w are the thermal conductivities ($W \cdot m/K$) of, respectively, the solid matrix and the groundwater, and n_e is the effective porosity (dimensionless). Thermal dispersion is described in Equation (1) by the corresponding coefficients αL and αT.

Dividing Equation (1) by ρ_c, we get:

$$\frac{\partial T}{\partial t} + \frac{v_e}{R_{th}}\frac{\partial T}{\partial x} + D_x\frac{\partial^2 T}{\partial x^2} + D_y\frac{\partial^2 T}{\partial y^2} + D_z\frac{\partial^2 T}{\partial z^2} = \frac{H}{\rho c} \quad (5)$$

where v_e is the effective velocity of groundwater through the pores, calculated as:

---

[19] Here K is the descriptor of the parameter hydraulic conductivity, with units m/s, rather than the unit of temperature, namely Kelvin. Where temperature appears in an equation the descriptor is ‘T’.

[20] Piga and others (2017) thus assume that the bulk thermal conductivity of a saturated porous medium is the weighted arithmetic mean of the mineral and water components. In our modelling, we have made the assumptions that the bulk thermal conductivity is better estimated as the weighted geometric mean.

$$v_e = \frac{v_D}{n_e} \quad (6)$$

Since heat is exchanged between the fluid and the solid phase, the advective velocity of the thermal plume is lower than the groundwater flow velocity. This phenomenon is similar to solute sorption in porous media with linear kinetics. By analogy, it is therefore possible to define the thermal retardation coefficient of Equation (5) as the ratio between the effective velocity of groundwater (v_e) and heat front (v_{th}):

$$R_{th} = \frac{v_e}{v_{th}} = \frac{(1-n_e)\rho_s c_s + n_e \rho_w c_w}{n_e \rho_w c_w} = \frac{\rho c}{n_e \rho_w c_w} \quad (7)$$

D_x, D_y, and D_z are the longitudinal, transversal and vertical thermal dispersion coefficients (m^2/s):

$$D_x = \frac{\lambda}{\rho c} + \frac{v_e}{R_{th}} \alpha_L$$

$$D_y = D_z = \frac{\lambda}{\rho c} + \frac{v_e}{R_{th}} \alpha_T \quad (8, 9)"$$

This theoretical framework is applied to the baseline, sensitivity and scenario modelling for this project as set up within FEFLOW® and described further below.

3.3 Baseline scenario – model setup

The objective of the first part of this work is to evaluate and compare the influence of thermal and hydrogeological subsurface properties, as well as GSHC system parameters, on the evolution and spatial distribution of the thermal plume originating from a GSHC system, i.e. a sensitivity analysis.

A baseline scenario was used to conduct the sensitivity analysis. This was a generic but typical GSHC system setup simulating a BHE array within a saturated sandstone aquifer. Baseline model parameters are summarised in Table 3-1. Descriptions and the rationale for applying these parameters are explained in Sections 3.3.1 to 3.3.6.

Table 3-1: Summary of baseline model settings and parameters applied (AOD is elevation in metres above Ordnance Datum).

Parameters	Value
Model size	9000m x 4000m x 300m (Figure 3-3)
Elevation of top and base of model	+50m AOD and -250mAOD
Vertical model domain discretisation	13 layers (14 slices)
Model discretisation (element number)	464,620
Total simulation time	50 years
Time steps maximum duration	10 days
Closed-loop BHE system power capacity and BHE array details	45kW total system capacity 14 BHEs, 120m deep (27W/m) 15m between BHE
Closed-loop BHE system operational cyclicity	3 months cooling at 1.08MWh/d and 9 months off Total 97.2 MWh/year for cooling (heat rejection to ground)
Fluid flow boundary conditions	Fixed head BC for groundwater inflow (southern edge of model) (Layer 1 to 14) = +80m AOD Fixed head BC for groundwater outflow (northern edge of model) (Layer 1 to 14) = +50m AOD All other boundaries “no flow”
Heat transport boundary conditions	Fixed Temperature Boundary (top of Layer1) =10.5°C Heat Flux BC (base of Layer 14) =0.06W/m^2

	Fixed temperature BC for lateral model edges (Layer 1 to 14) set equal to temperature starting conditions for each layer, as calculated in steady state run.
Matrix thermal conductivity (λ_s) which yields target bulk saturated thermal conductivity (calculated by weighted geometric mean)	2.93W/m/K Layer 2 to Layer 13 2.55W/m/K Layer 1
Water thermal conductivity (λ_w)	0.6W/m/K
Target bulk saturated thermal conductivity (λ)	2.5W/m/K
Matrix volumetric heat capacity ($\rho_s c_s$) which yields target saturated volumetric heat capacity (calculated by weighted arithmetic mean)	1.98MJ/m^3/K Layer 2 to Layer 13 2.18MJ/m^3/K Layer 1
Water volumetric heat capacity ($\rho_w c_w$)	4.19MJ/m^3/K
Target bulk saturated volumetric Heat Capacity (ρc)	2.2MJ/m^3/K
Hydraulic conductivity ($K_{x,y,z}$) in the x, y, z directions	$K_{x,y}$=5m/d Layer 2 to 13 K_z=0.5m/d Layer 1 $K_z=K_{x,y}/10$
Hydraulic gradient (i)	0.0033 (30 m head decline over 9000 m)
Darcy flux (v_D)	0.017m/d
Effective porosity (n_e)	10% Layer 2 to 13 1% Layer 1

Longitudinal thermal dispersity (αL) and transversal thermal dispersivity (αT)	20m 2m

3.3.1 Model dimensions and discretisation

The finite element model is comprised of nodes that form a mesh. Numerical values that simulate heat and flow transport are computed for each of the nodes (Figure 3-1).

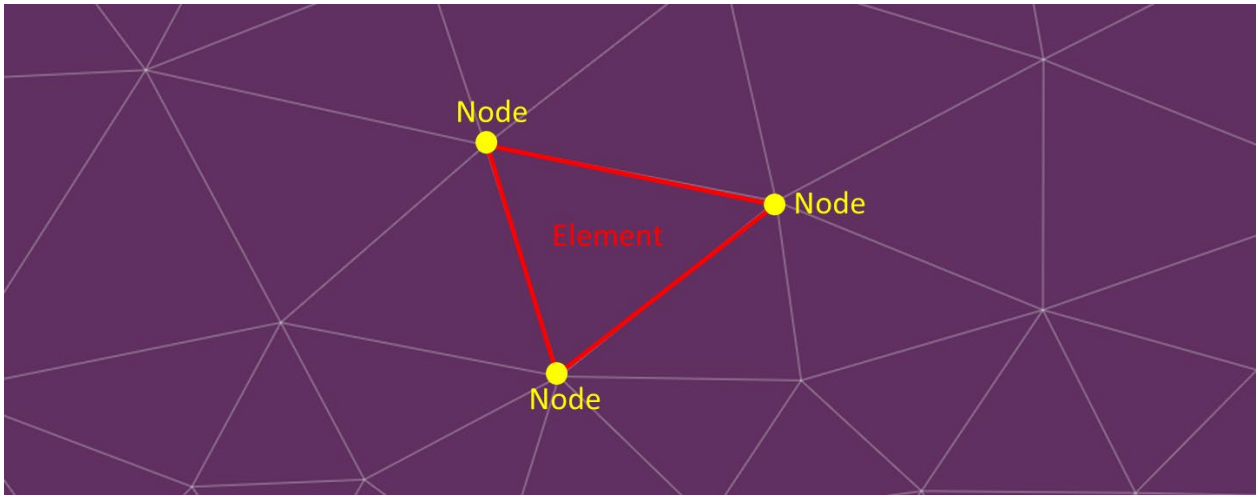

Figure 3-1: Finite element mesh with one element (red) and surrounding nodes (yellow) highlighted.

The vertical and horizontal discretisation, in other words the density of the finite element mesh, defines both the spatial resolution of parameter assignment (for example, different hydrogeological units in their lateral and vertical extent) as well as the numerical accuracy of the simulation. The higher the mesh density (i.e. the smaller the distance between the computational nodes) the more accurately the model can simulate the flow/heat transport. Higher mesh density is required where, for example, steep hydraulic gradients or other rapid spatial changes in parameters are expected.

The finite element mesh is created by first constructing a 2D planar framework, called a “Supermesh”. The Supermesh allows areas and locations that require higher or lower density of the finite element mesh to be defined. The Supermesh is then filled with finite elements and extended to 3D by defining additional layers. Note that the computation nodes are located on the surfaces separating the different layers, and these surfaces are called “slices” in FEFLOW ®. The layers consist of prismatic elements that lie in between the slices (i.e. slice 1 defines the top of layer 1, slice 2 defines the top of layer 2, etc..).

In this case, the model domain (i.e. the space represented by the model) is a rectangular prism 9000m (length) × 4000m (width) × 300m (depth). There are 13 horizontal layers (14 slices) from 50m AOD (slice 1) to -250m AOD (slice 14). Each layer contains 35,740 elements. Element size varies between 0.3m and 250m in the x and y directions, with higher a higher density mesh in the centre of the model where thermal plume transport is focused.

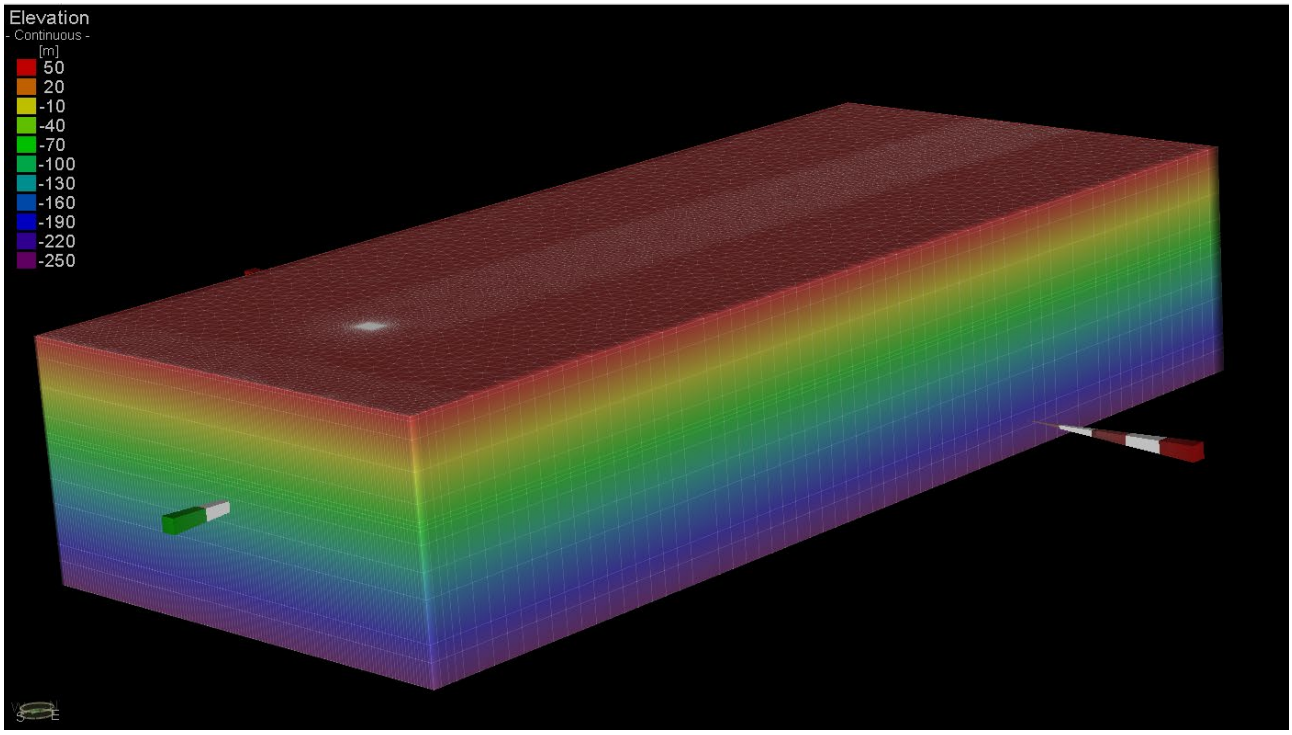

Figure 3-2: 3D model layers with elevation (m AOD) and model axis directions (x=red arrow, y=green arrow).

In FEFLOW®, BHEs are modelled as 1D representations of the real geometry of the piping material and borehole (BH) filling (DHI-WASY, 2010; Diersch and others, 2011b) through nodes on the top of each of the model layers (and bottom of the model). The nodes are linked and BCs applied to these nodes. The horizontal 2D mesh was locally refined between the BHE nodes, downstream in the direction of groundwater and thermal front migration. An overview of model discretisation is shown in Figure 3-3.

Observation points were placed towards the centre of the BHE array, along the plume axis and aligned with the modelled flow direction, so indicative of the maximum plume extent from the BHE locations.

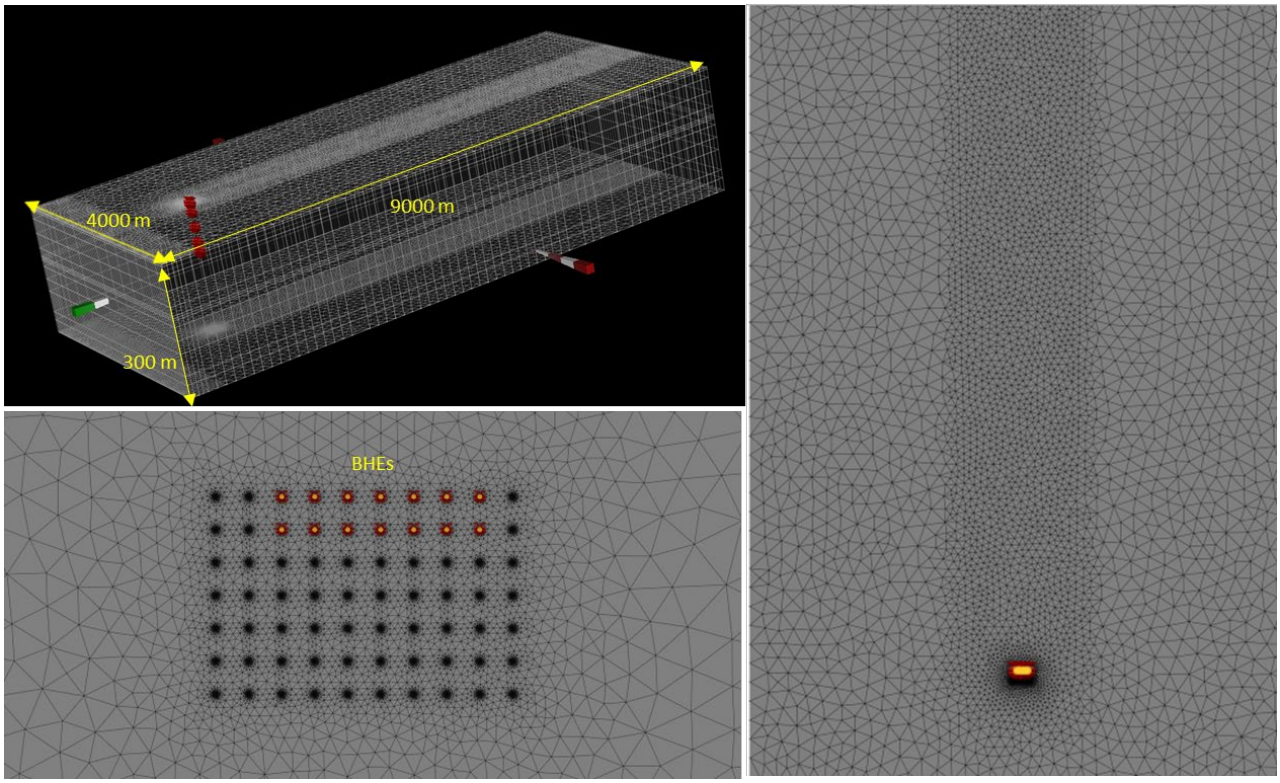

Figure 3-3: Overview of model domain discretisation in 3D (top left), around the BHE array (bottom left) and top layer showing discretisation downstream of the BHE array (right).

3.3.2 Closed-loop system configuration

The baseline scenario considers a closed-loop BHE system designed for cooling (heat rejection to ground), in a saturated sandstone aquifer.

A 45kW peak heat rejection rate to the ground was selected, because this corresponds to the upper limit for ground source heat pump eligibility in the Microgeneration Certification Scheme (MCS, Environment Agency, 2024b). The MCS scheme is targeted at domestic installations, though it is acknowledged that (i) 45 kW would be a very large domestic GSHC system, and (ii) a domestic system would typically extract, rather than reject heat to the ground.

Therefore, the baseline model represents a cooling system for a modestly-sized building. The system rejects heat to the ground continuously at the maximum rate of 45kW (1080kWh/d) for 3 months/year (i.e. 2160 full load equivalent hours or FLEQ). Net discharge of heat to the aquifer is equal to 97.2MWh/year.

For boreholes designed for cooling, there is no upper temperature design standard for heat injection recommended by MCS or the GSHPA. However, to remain efficient and relatively competitive with air source heat pumps, we have assumed that the fluid temperature leaving the BHE should not exceed 25°C for long periods.

The Earth Energy Designer (EED) a computer program for vertical BHE design[21] (Blomberg and others, 2019) was used to estimate an appropriate BHE array setup based on possible energy demand, cyclicity and thermal properties for the baseline scenario conditions.

Property	Value
BHE Geometry	Single U-shape
Name	
Borehole Diameter (D)	0.14 [m]
Pipe Distance (w)	0.07 [m]
Inlet Pipe Diameter (d-in)	0.04 [m]
Inlet Pipe Wall Thickness (b-in)	0.0037 [m]
Outlet Pipe Diameter (d-out)	0.04 [m]
Outlet Pipe Wall Thickness (b-out)	0.0037 [m]
Computational Method	Quasi-stationary (Eskilson & Claesson)
Heat-transfer coefficients	Computed
Inlet Pipe Thermal Conductivity (tc-in)	0.42 [J/m/s/K]
Outlet Pipe Thermal Conductivity (tc-out)	0.42 [J/m/s/K]
Grout volume thermal conductivity (tc-gr...	1.7 [J/m/s/K]
Pipes-in to grout	0.3027 [m s K/J]
Pipes-out to grout	0.3027 [m s K/J]
Grout to grout (1)	-0.2647 [m s K/J]
Grout to grout (2)	0 [m s K/J]
Grout to soil	0.02984 [m s K/J]
Refrigerant volumetric heat capacity (Ref. heat cap.)	3.95 [10+6 J/m³/K]
Refrigerant thermal conductivity (Ref. cond.)	0.47 [J/m/s/K]
Refrigerant dynamic viscosity (Therm. visc.)	3.5 [10-3 kg/m/s]
Refrigerant density (Ref. mass dens.)	1.035 [10+3 kg/m³]

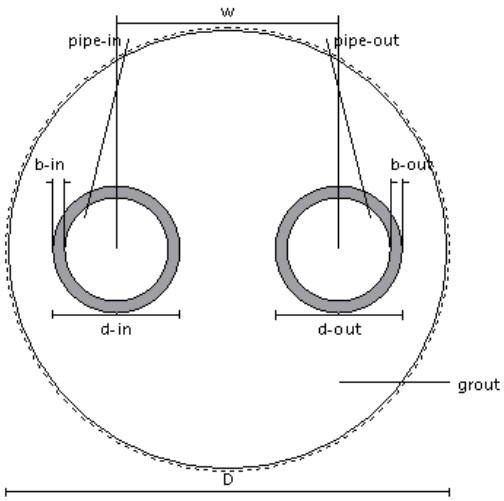

Figure 3-4: BHE properties and geometry from the EED

[21] EED provides a conservative design (i.e. more rather than fewer BHE for a given energy demand) as it does not account for advection by groundwater flow.

Based on indications from EED modelling, the BHE closed-loop GSHC system for the baseline scenario used an array of 14 BHE with total heat rejection rate divided equally between the BHEs. The BHE separated by 15m and up to 120m depth (from 0 to 120 metres below ground level (mbgl)). This spacing and length are in-line with industry practice, where BHE installation depths for similar systems and applications are commonly between 60 and 200m. Design details and material specification for BHE are provided in Figure 3-4.

3.3.3 Model border and hydraulic boundary conditions

Head boundary conditions define the groundwater inflow and outflow across the model borders. Boundary conditions are the starting point for the computation of the water levels, flow rates and thermal transport within the rest of the model domain.

To keep the saturated aquifer bulk thermal properties and transmissivity constant across the model domain (and prevent complication of results due to variable unsaturated thickness), the model was set up to represent confined conditions, with groundwater head at or above ground elevation. A regional groundwater flow was applied by assigning constant hydraulic head BC values of +80m AOD on the southern (upgradient) model edge and of 50m AOD on the northern (downgradient) edge (Figure 3-5). Initial hydraulic head conditions across the model were then assigned by running the model in steady state and groundwater flow only (no heat flow) mode as shown in Figure 3-5.

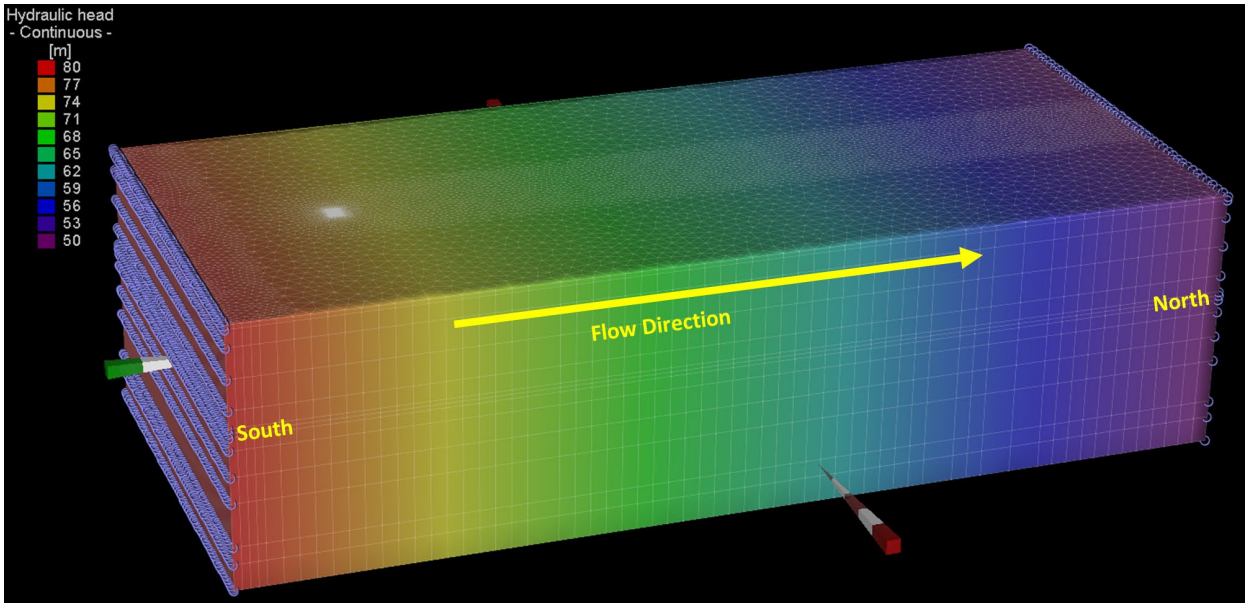

Figure 3-5: Hydraulic head and head boundary conditions applied in the model, with groundwater flow direction.

3.3.4 Heat transport boundary conditions

The undisturbed thermal condition of the aquifer was generated by imposing a constant temperature upper boundary condition of 10.5°C in slice 1, representing a typical English annual average soil temperature (Met Office, 2024).

A constant heat flux boundary condition of 0.06W/m^2 was imposed on the lowest slice to represent the upward geothermal heat flux, based on the British Geological Survey (BGS) geothermal heat flux map (Busby, 2010), which calculated values between 0.04 and 0.1W/m^2 across the UK.

A steady state heat transport simulation was used to find the initial temperature conditions across the model domain. This model used the baseline thermal and hydrogeological parameters specified in Section 3.3.5. Hydraulic heads calculated from the steady-state hydraulic head conditions described in section 3.3.3 were applied. FEFLOW® calculated a vertical thermal gradient accounting for heat advection effects. This acted as the initial condition for the transient simulations.

Temperature BC were set at the inflow (southern) and the outflow (northern) model edges for each slice by applying a constant temperature BC matching the starting temperature conditions calculated with the steady state run. The temperature starting conditions and the temperature boundary conditions applied to the model domain are shown in Figure 3-6.

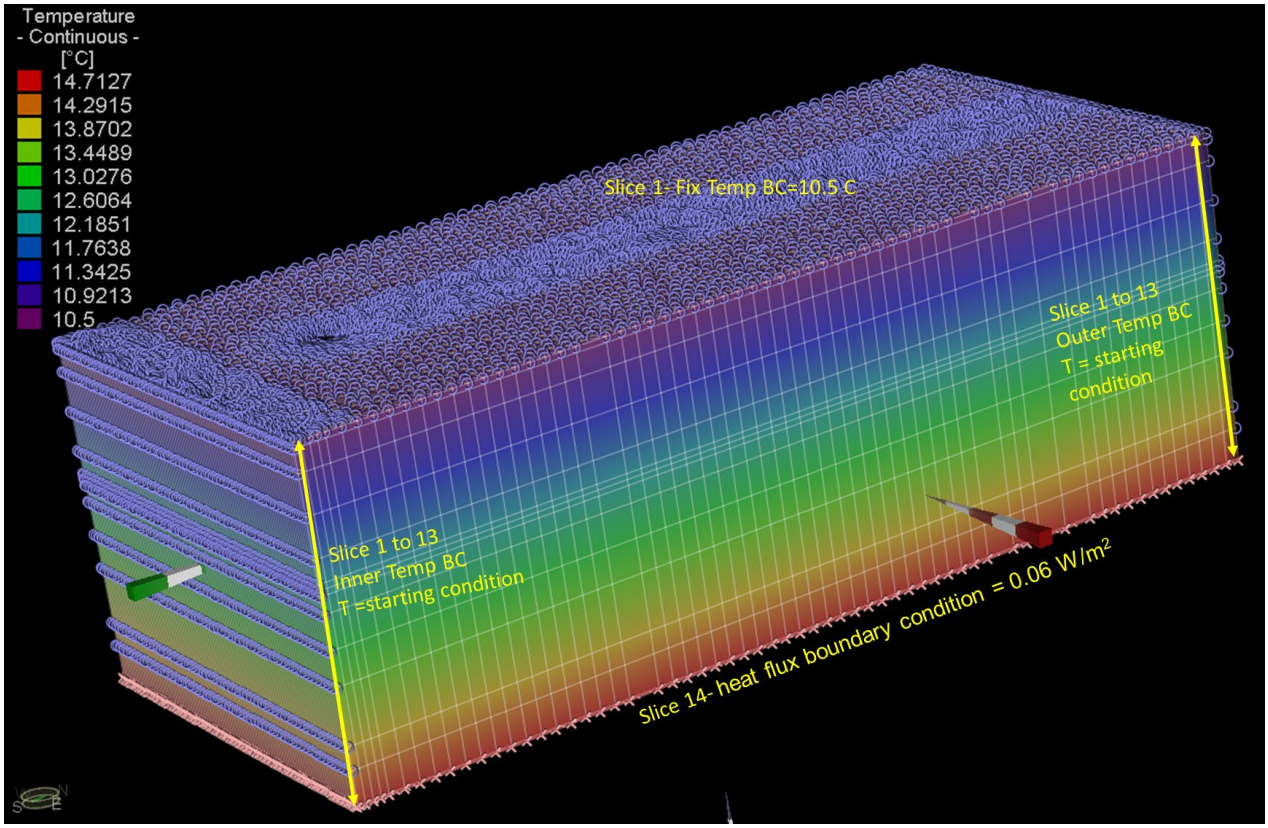

Figure 3-6: Model starting temperature and heat transport boundary conditions.

3.3.5 Thermo-hydrogeological model parameters

The baseline scenario essentially consists of a homogeneous, isotropic[22], saturated sandstone aquifer (typical of Permo-Triassic sandstones), where all layers share the same bulk thermal properties and hydrogeological parameters. However, a thin superficial layer (layer 1, 5m thickness) with lower hydraulic conductivity and lower porosity, was set to act as an aquitard to ensure uniformly confined conditions.

The geothermal and hydraulic properties implemented in the model were based on typical values representative of a saturated sandstone aquifer as identified from the literature review (for example, Banks 2012, Blomberg and others 2019, Energy Technologies Institute 2011, MCS 2011). A bulk volumetric heat capacity value of 2.2MJ/m^3/K and a bulk

[22] The physical properties are identical at each point within the model (homogeneous) and in all directions (isotropic).

thermal conductivity of 2.5W/m/K were considered representative for saturated sandstones and were therefore implemented in the baseline scenario.

Hydraulic conductivity and effective porosity for the sandstone aquifer were identified from BGS reports and manuals (Allen 1997). A value of 5m/d was used for hydraulic conductivity and 10% for porosity, which are within the plausible range and close to the median value determined for the Sherwood Sandstone aquifer.

There is limited information regarding thermal dispersivity in aquifers in the literature. De Marsily (1986) notes that the dispersivities of heat and (solute) tracers are generally comparable and values depend on the spatial scale of the observed phenomenon.

Domenico & Schwartz (1990) document the results of a number of field-scale tests of solute dispersivity and for a scale of 1000 to 3000 m; they suggest values in the range 10 to 500 m for longitudinal dispersivity, depending on the spatial scale of the observed phenomenon. In a number of heat tracer tests over distances of around 10m, the longitudinal thermal dispersivity was confirmed to be around 10% of path length (Carbon Zero Consulting, 2010). In the baseline scenario model, a value of 20m was assigned for longitudinal dispersivity and 2m for transversal dispersivity.

Properties for the idealised saturated sandstone aquifer are summarised in Table 3-2.

Table 3-2: Hydraulic and thermal properties for an isotropic saturated sandstone aquifer used in the baseline FEFLOW® model.

Parameter	Model value	Source of information
Saturated thermal conductivity	2.5W/m/K	Banks (2012), Energy Technologies institute (2011), MCS (2011), EED, Blomberg and others. (2019)
Saturated volumetric heat capacity	2.2MJ/m^3/K	Banks (2012), Energy Technologies institute (2011), MCS (2011), EED, Blomberg and others. (2019)
Matrix thermal conductivity which yields saturated thermal conductivity.	2.93W/m/K	Calculated on the basis of geometric mean, with a conductivity of 0.6 W/m/K for water and an effective porosity of 10%.
Matrix volumetric heat capacity which yields saturated volumetric heat capacity.	1.98MJ/m3/K	Calculated on the basis of arithmetic mean, with a vol. heat capacity of 4.19 MJ/m^3 /K for water and an effective porosity of 10%.
Hydraulic conductivity*	Kh=5m/d Kv=0.5m/d	Allen and others. (1997)
Effective Porosity*	10%	Allen and others. (1997)
Thermal dispersity	20m (longitudinal) 2m (transverse)	De Marsily (1986)

* The same parameters were applied to all model layers (layers 2 to 13) except that for the top layer (layer 1 - 5m thickness), where lower porosity (1%) and lower hydraulic conductivity (0.5m/d) were set to simulate aquitard conditions.

3.3.6 Model simulation time

Model simulations were run for 50 years, to represent long term impacts over the operational lifetime of a GSHC system, with a maximum time step length of 10 days.

3.4 Baseline model results

In this section the results and outputs obtained from the baseline scenario model introduced in Section 3.3 are presented. As discussed in Section 2.3.3, the thermal plume boundary considered for the assessment refers to the contour line corresponding to a 1°C (1K) change from the initial subsurface temperature, unless otherwise stated.

The lengths of the thermal plume were calculated after 50 years of operation of a closed-loop GSHC system, at the end of the last cycle of heat rejection (17,975 days). Model outputs were extracted from:

- slice 4, at 50% of total BHE installation depth i.e. 60mbgl for a 120 m BHE, and
- slice 2 at 5mbgl, to evaluate interaction with surface.

Thermal plume contour maps, extracted from slice view outputs for the baseline scenario are reported in Figure 3-7. In these contour maps, the “baseline” temperature is taken as the initial temperature at the depth of the slice in question. North-south cross-sections, longitudinal to flow direction through the closed-loop BHE Array and detailing thermal plume vertical distribution, are shown in Figure 3-8 and Figure 3-9.

Figure 3-7 shows a smaller plume at 5m bgl (slice 2) than at 60m depth (slice 4). These differences are related primarily to vertical conductive heat loss to the atmosphere due to the BC of 10.5°C implemented on top of layer 1, to represent air/soil temperature at ground level. Observing the shape of the plume in cross sections in Figures 3-8 and 3-9, it is evident that upwards heat attenuation is more significant than downward attenuation.

Considering a 1°C for the definition of a thermal plume boundary, with the current model settings the plume doesn’t exceed 11m length either at 5m bgl or 60m bgl.

Figures 3-10 and 3-11 show the increase in ground temperature (ΔT) over time at observation points located downstream of the BHE at 25m, 50m and 100m in slice2 and slice4.

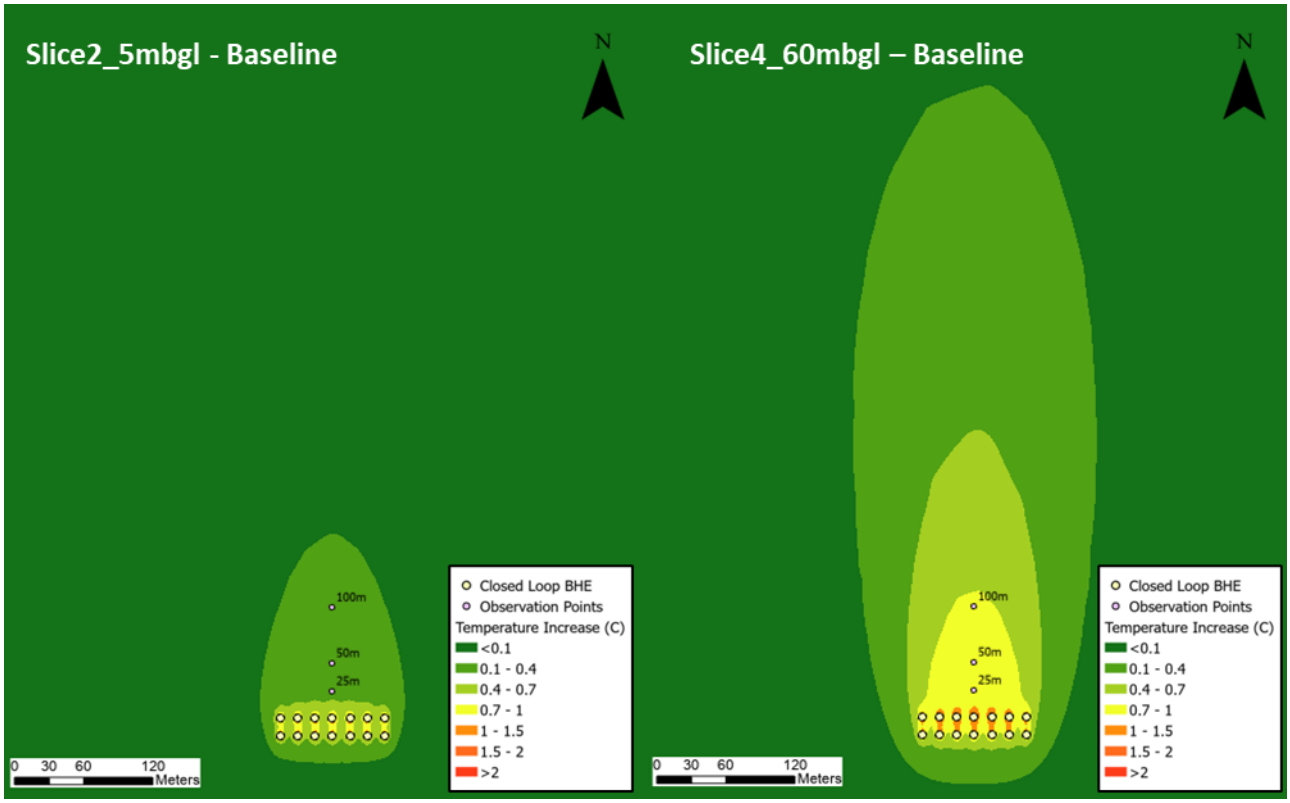

Figure 3-7: Extent and temperature change of the simulated thermal plume after 50 years for the baseline scenario, in a homogeneous sandstone aquifer at 5m and 60m bgl.

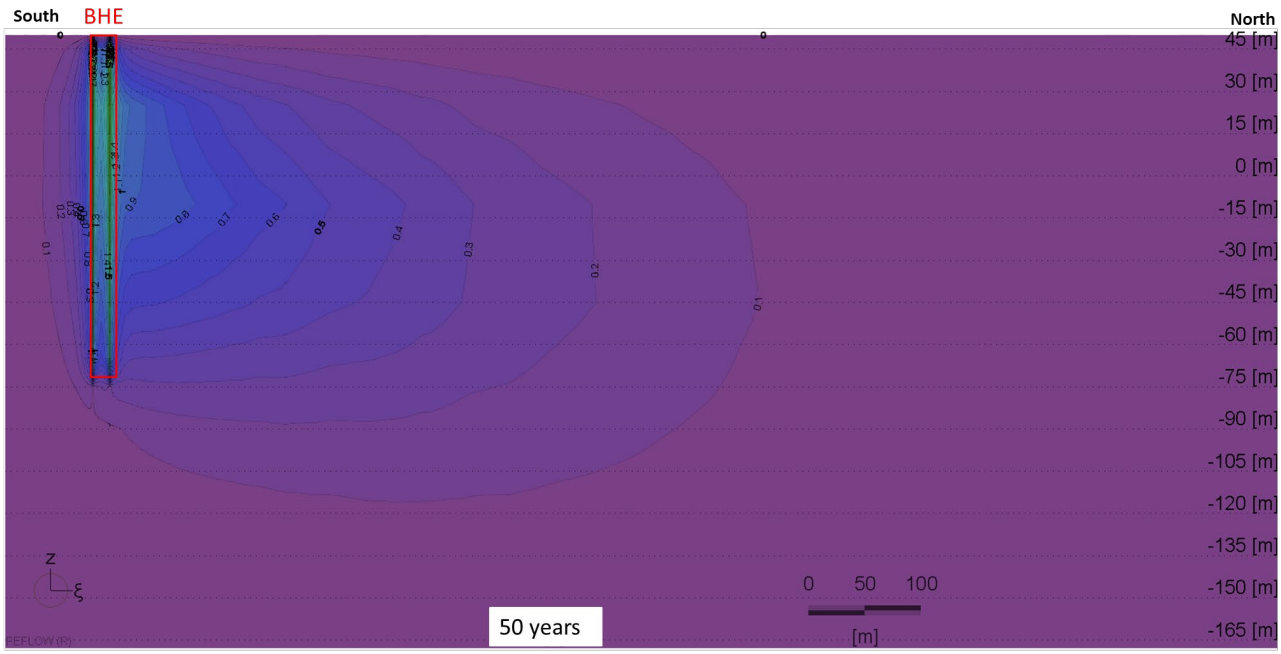

Figure 3-8: Cross section view through the baseline scenario model showing vertical (z) and longitudinal (ξ) distribution of the thermal plume after 50 years, temperature change from background (∆T °C)shown as iso-contour lines. Scale along right side is m AOD.

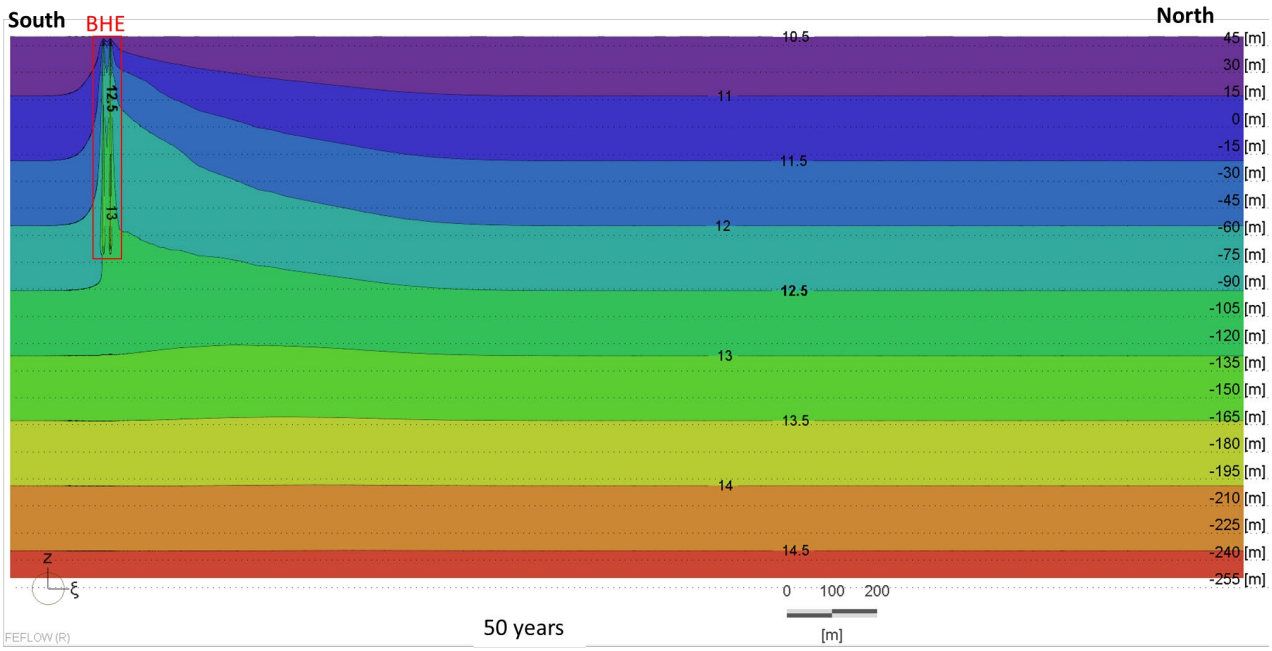

Figure 3-9: Cross section view through the baseline scenario model showing vertical (z) and longitudinal (ξ) distribution of the thermal plume after 50 years, absolute temperatures (°C) shown as iso-contour lines. Scale along right side is m AOD.

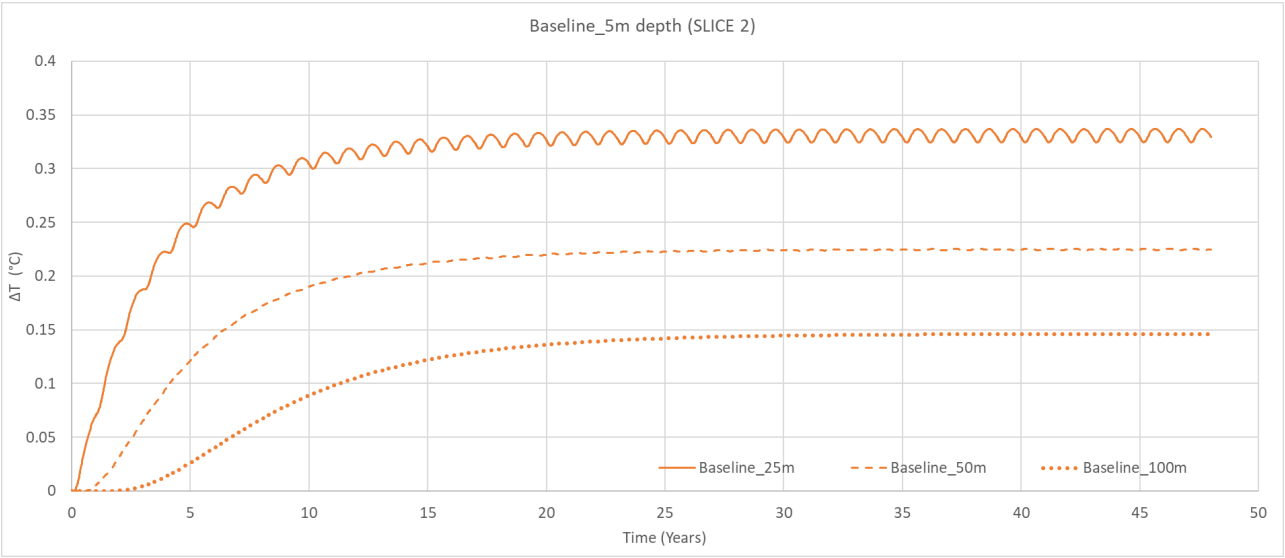

Figure 3-10: Change in temperature (ΔT) from initial conditions during the operational period (50 years) of the BHE array at slice 2 (5m bgl)

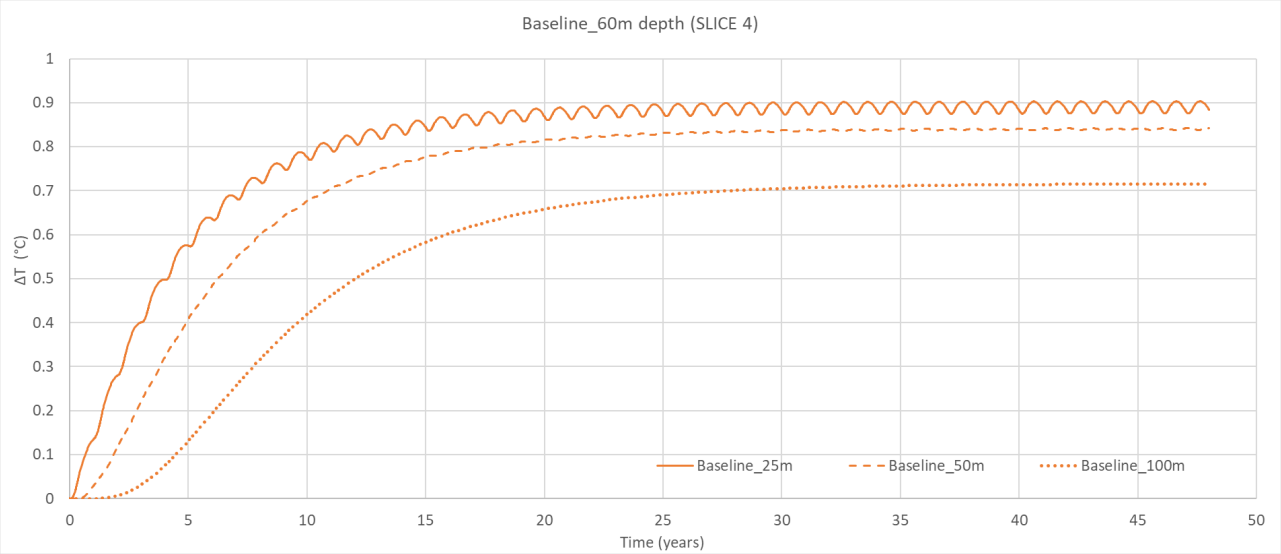

Figure 3-11: Change in temperature (ΔT) from initial conditions during the operational period (50 years) of the BHE array at slice 4 (60m bgl)

The baseline scenario results show that temperature changes close to the BHE are higher and approach steady-state conditions quicker than those further from the borehole. In both slices, the temperature time series extracted from observation points located further than 50m from the BHE do not reflect the cyclicity from BHE heat rejection activities (i.e. fluctuations are completely smoothed at a distance of 50 m). Fluctuations are, however, evident at 25m distance.

A summary of the results for thermal plume length and temperatures increase simulated after 50 years is given in Table 3-3.

Table 3-3: Thermal plume length and temperature changes at observation BH after 50 years of heat rejection for the baseline model.

Depth	Thermal plume length (1°C ΔT)	ΔT observed at 25m distance	ΔT observed at 50m distance	ΔT observed at 100m distance
5m depth (Slice 2)	~4m	~0.35°C	~0.25°C	~0.15°C
60m depth (Slice 4)	~11m	~0.9°C	~0.85°C	~0.7°C

3.5 Sensitivity analysis

A sensitivity analysis for a total of 24 simulation runs was undertaken to assess the importance of hydrogeological and thermal properties and GSHC system parameters on the development of the thermal plume during BHE operation. The analysis focussed on

the length, time evolution and temperatures of thermal plumes for different model parameters.

The sensitivity analysis was carried out changing one factor at a time; all hydrogeological and thermal parameters and GSHC system parameters were kept constant, except for the parameter that was being investigated. This approach allowed assessment of the importance of individual parameters and identification of the parameters that have the strongest influence on thermal plume development.

Thermal plume characteristics were processed and analysed using the same assumptions adopted for the baseline scenario, where the plume dimensions were determined considering 1°C contour of temperature change, relative to the starting temperature (T_0) simulated for each run (and for each layer). Thermal plumes were extracted at the end of the simulation after 50 years of heat rejection, at 5m depth and 60m depth.

Table 3-4 reports the complete parameter set, including baseline values and the ranges tested for this analysis. The main results are discussed in the following sections and further details, including temperature changes for observation BH, are provided in Appendix B.

Table 3-4: Parameter values assigned in the simulations for the sensitivity analysis.

Parameter	Baseline values	Values tested in sensitivity analysis
Target bulk saturated thermal conductivity (W/m/K)	2.5(W/m/K)	1,2,3,4 (W/m/K)
Target bulk saturated volumetric heat capacity	2.2(MJ/m^3/K)	1.9, 2.05, 2.3, 2.4 (MJ/m^3/K)
Darcy flux (m/d)*	0.017 (hydraulic gradient = 0.0033, K=5m/d)	0 (i= 0) 0.00017 (i= 0.0033 and K=0.05m/d) 0.0017 (i= 0.0033, K=0.5m/d) 0.17 (i= 0.0033, K=50m/d)
Effective porosity**	10%	1%, 20%, 30%
Thermal dispersity	20m	10m, 40m
Heat rejection rate at BHE array***	45kW heat rejection @ 2160 FLEQ, rejecting 97.2 MWh/year (3 months operational, 9 months non-operational)	10kW heat rejection @ 2160 FLEQ, rejecting 21.6 MWh/year 100kW heat rejection @ 2160 FLEQ, rejecting 216 MWh/year 200kW heat rejection @ 2160 FLEQ, rejecting 432 MWh/year (3 months operational, 9 months non-operational)
BHE operation cyclicity	45 kW heat rejection . 1080kWh/day – 3 months on and 9 months off. Rejecting 97.2 MWh/year	22.1 kW heat rejection. 531kWh/day – 6 months on and 6 months off Rejecting 97.2 MWh/year
BHE depth (m)	120m	50m, 90m, 150m

* Hydraulic conductivity for Layer1 (0.5m/d) maintained as per Baseline scenario.
** Porosity for Layer1 (1%) maintained as per Baseline scenario.
*** Number of BHE were revised according to the changes in system power capacity and energy demand

3.5.1 Bulk saturated thermal conductivity

In FEFLOW®, thermal conductivity (TC) is split into conductivity of the fluid (groundwater) and the matrix (solid). FEFLOW derives bulk saturated thermal conductivity from the thermal conductivities of the mineral (matrix) and fluid (groundwater) components, and the porosity. The effect of bulk saturated thermal conductivity on the evolution of the thermal plume was investigated for 4 different values varying from 1 to 4W/m/K, covering a plausible range associated with various rocks and sediments categories, as indicated by MCS standard for BHE design (MCS, 2011), where lower thermal conductivities are typically assigned to clay and silt materials while higher values are normally reported for sands and sandstones.

The thermal conductivity of groundwater (λ_w) was kept equal to 0.6 W/m/K, while 4 different values were considered for the solid phase conductivity (λ_s). Bulk thermal conductivity was calculated using Equation (4), and applied to the model domain.

Thermal plume contour maps for the sensitivity analysis runs are shown in Figure 3-12 and Figure 3-13 and results are summarised in the following table.

Table 3-5: Thermal plume lengths (1°C ∆T isocontour) after 50 years for different values of thermal conductivity (TC)

Plume length 1°C ∆T isocontour	Baseline thermal conductivity	TC#1	TC#2	TC#3	TC#4
Matrix thermal conductivity (λ_s	2.93W/m/K	1.06W/m/K	2.29W/m/K	3.59W/m/K	4.94W/m/K
***Target bulk saturated thermal conductivity**	2.5W/m/K	1W/m/K	2W/m/K	3W/m/K	4W/m/K
5 m depth – Slice 2	~4m	~8m	~5m	~3m	~2m
60 m depth – Slice 4	~11m	~25m	~12m	~8m	~7m

* Assuming bulk thermal conductivity is calculated using a weighted geometric mean of matrix and fluid conductivities, with a porosity of 10%.

The model outputs show plume length is inversely related to thermal conductivity, so the higher the thermal conductivity the smaller the 1°C isocontour – in aquifers with higher thermal conductivity, more of the aquifer may have been impacted by temperature change but by a smaller amount as heat is effectively dissipated. The thermal conductivity of the rock controls the amount of heat that can disperse from the plume to the surface (and also laterally and to underlying strata). As the thermal conductivity increases, the amount of heat lost increases and the dimension of the thermal plume in the aquifer decreases.

Temperature change is also impacted by thermal conductivity, with a greater build up of heat with a lower thermal conductivity. Simulated temperature gradients in proximity of BHE are higher for runs where lower values of thermal conductivity were used. These effects can be attributed to

(i) Higher temperature gradients being required to conduct heat away from the BHEs in a low conductivity medium, and
(ii) a lower vertical conductive heat loss through the ground surface, when the aquifer has a lower thermal conductivity.

Based on the distribution of the thermal plume contours plotted in Figure 3-12 and Figure 3-13, thermal conductivity exhibits an important influence on the plume length, however, considering a 1°C isocontour for the definition of a thermal plume boundary, the plume never exceeds 25m length either in Slice 2 or Slice 4.

This conclusion applies to relatively shallow, near surface aquifers. In deeper aquifers, the rate of attenuation of the plume is likely to be more dependent on the thermal conductivity

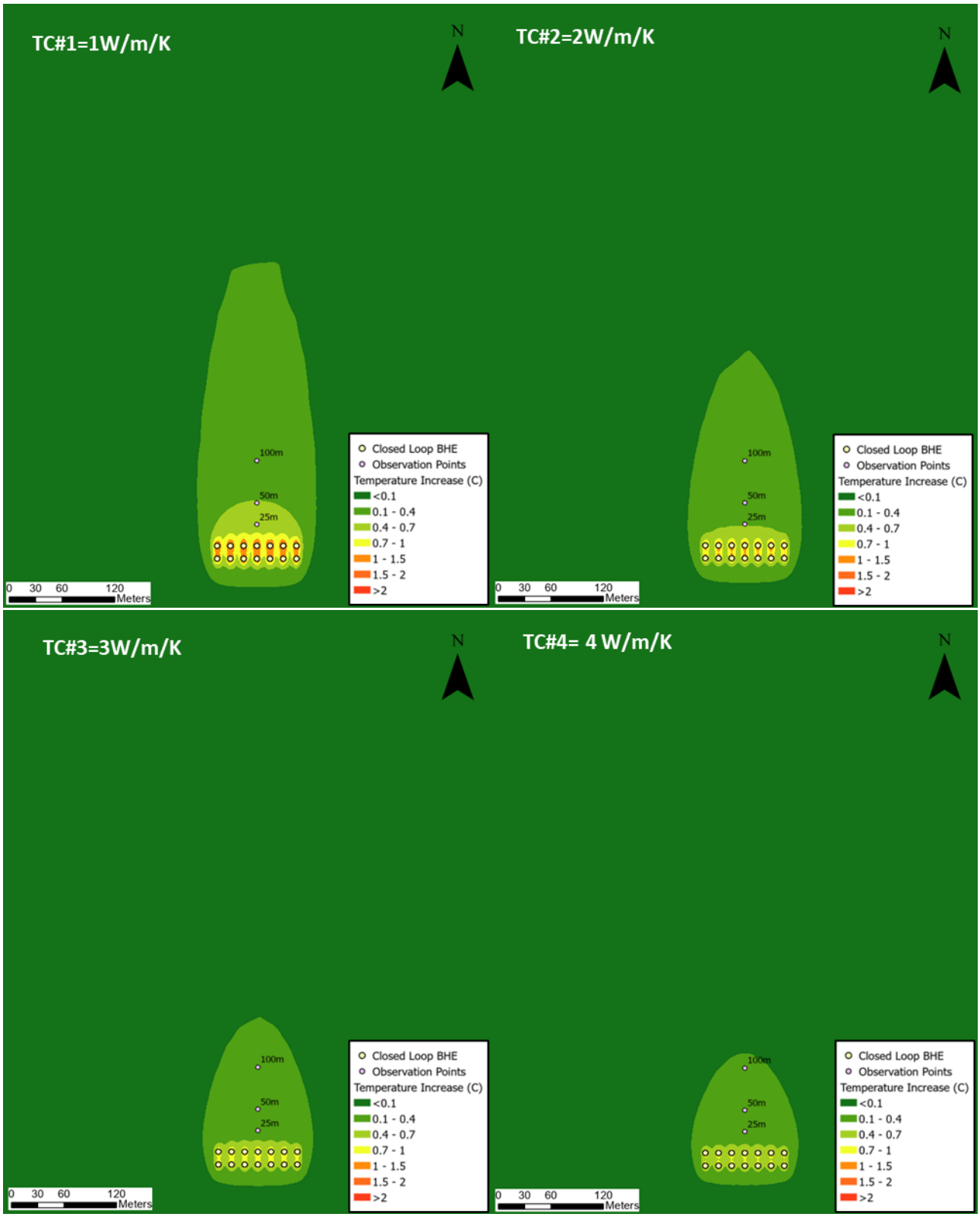

of the overlying (for example confining) strata – see Section 4.4.

Figure 3-12: Extent and temperature change of the simulated thermal plume after 50 years for different thermal conductivities at 5m bgl (slice 2).

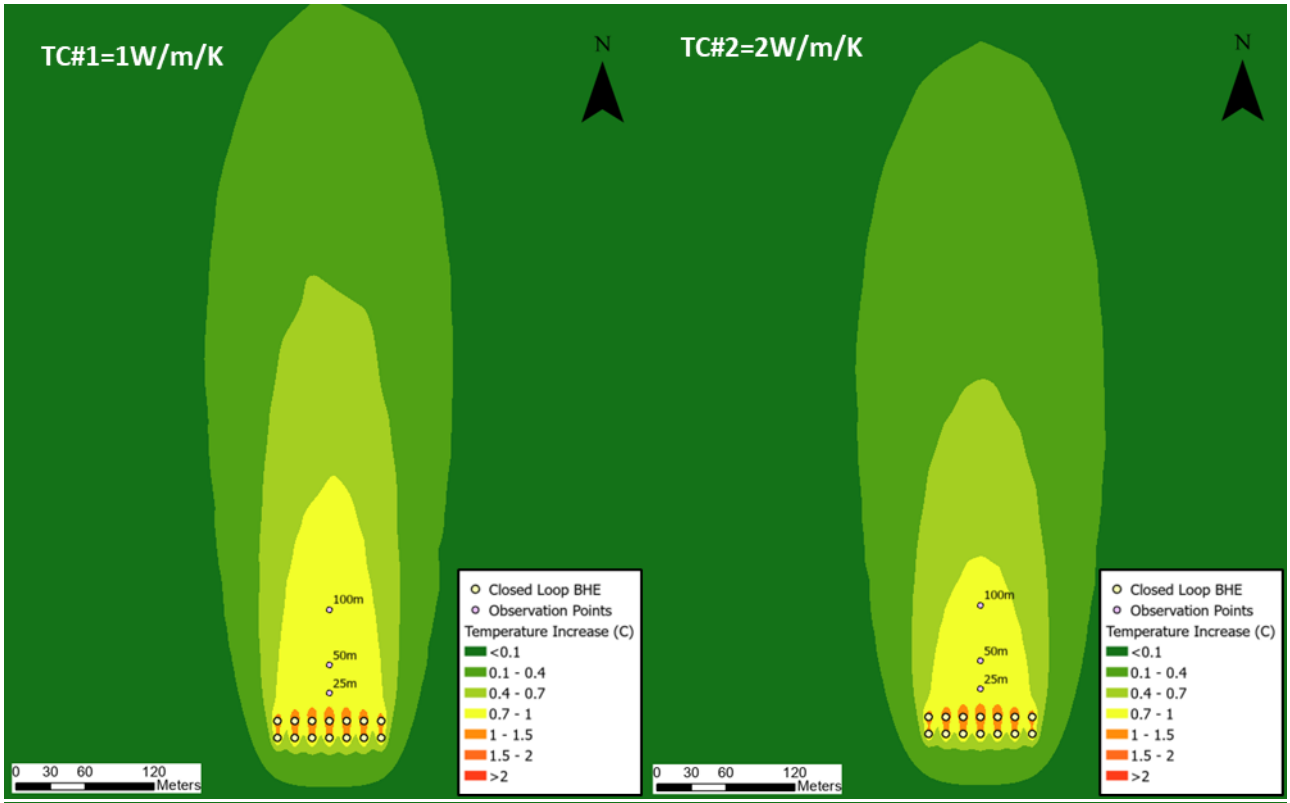

Figure 3-13: Extent and temperature change of the simulated thermal plume after 50 years for different thermal conductivities at 60m bgl (slice 4).

3.5.2 Bulk saturated volumetric heat capacity

Volumetric heat capacity (VHC) is the energy needed to increase the temperature of a certain volume of a medium by a certain temperature interval. In FEFLOW®, the bulk saturated heat capacity of the porous medium can be calculated as a weighted average of the heat capacities of the fluid and the matrix (solid), based on the porosity.

A similar approach was adopted for the saturated bulk volumetric heat capacity (ρc) of the aquifer, which was assigned using Equation (2) and literature reference values varying between 1.9 and 2.4MJ/m^3/K, for a range of rock materials, plausible for formations present in England. As for the thermal conductivity, a fixed value was set for the fluid phase ($\rho_w c_w$ = 4.19MJ/m^3/K), while 4 different values were adopted for the matrix phase.

Outputs showing the thermal plume temperature change isocontours for slices 2 and 4 for the VHC are reported in Figures 3-14 and 3-15, and results are summarised in the following table.

Table 3-6: Thermal plume lengths (1°C ΔT isocontour) after 50 years for different values of VHC.

Plume length of 1°C ΔT isocontour	Baseline VHC	VHC#1	VHC#3	VHC#4	VHC#2
Matrix VHC	1.98MJ/m^3/K	1.65MJ/m^3/K	1.81MJ/m^3/K	2.09MJ/m^3/K	2.2MJ/m^3/K
***Target bulk saturated VHC**	2.2MJ/m^3/K	1.9MJ/m^3/K	2.05MJ/m^3/K	2.3MJ/m^3/K	2.4MJ/m^3/K
5 m depth – Slice 2	~4m	~4m	~4m	~4m	~4m
60 m depth – Slice 4	~11m	~11m	~11m	~10m	~10m

* Bulk VHC calculated using a weighted arithmetic mean of matrix and fluid VHC, with a porosity of 10%

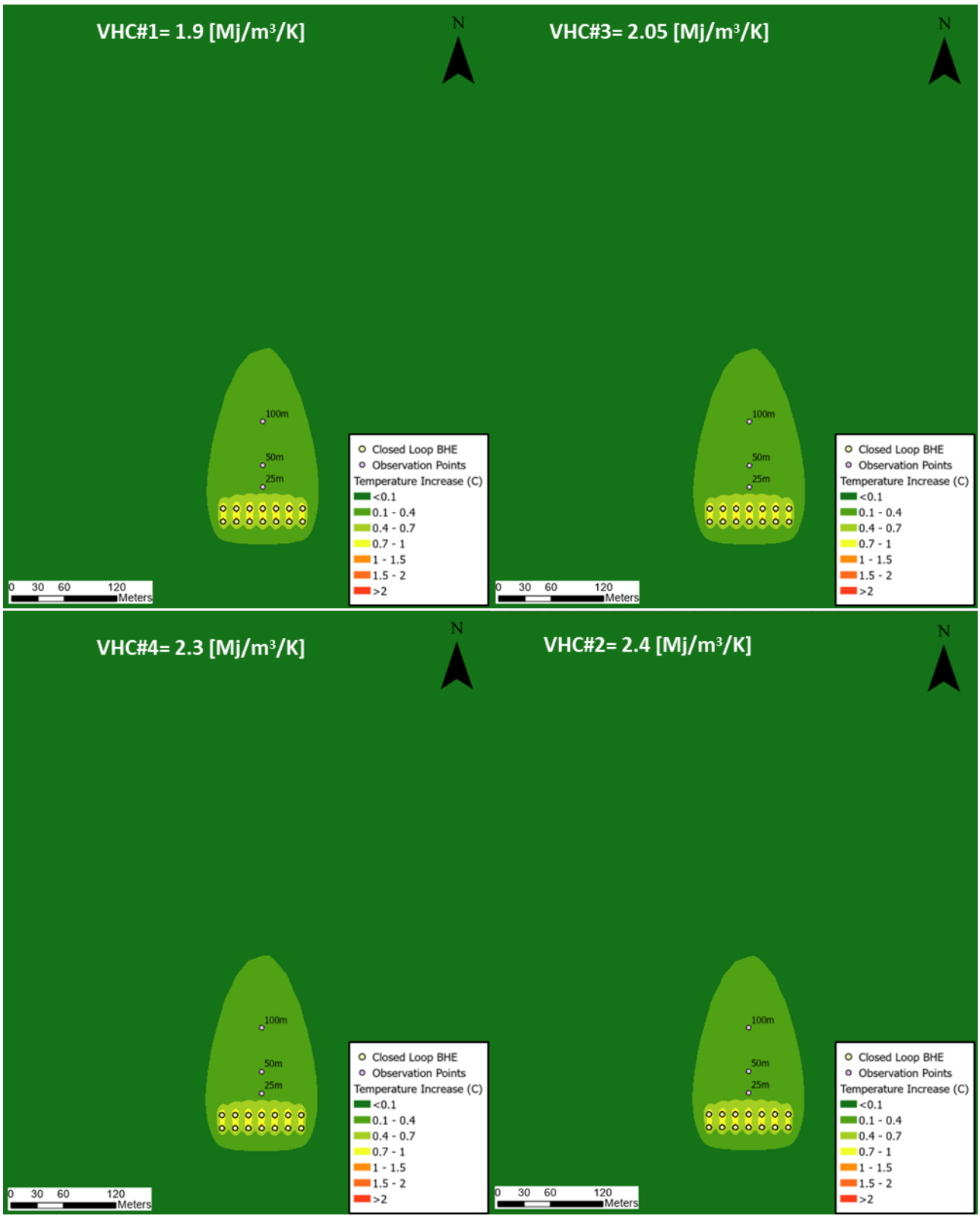

Figure 3-14: Extent and temperature change of the simulated thermal plume after 50 years for different VHC at 5m bgl (slice 2)

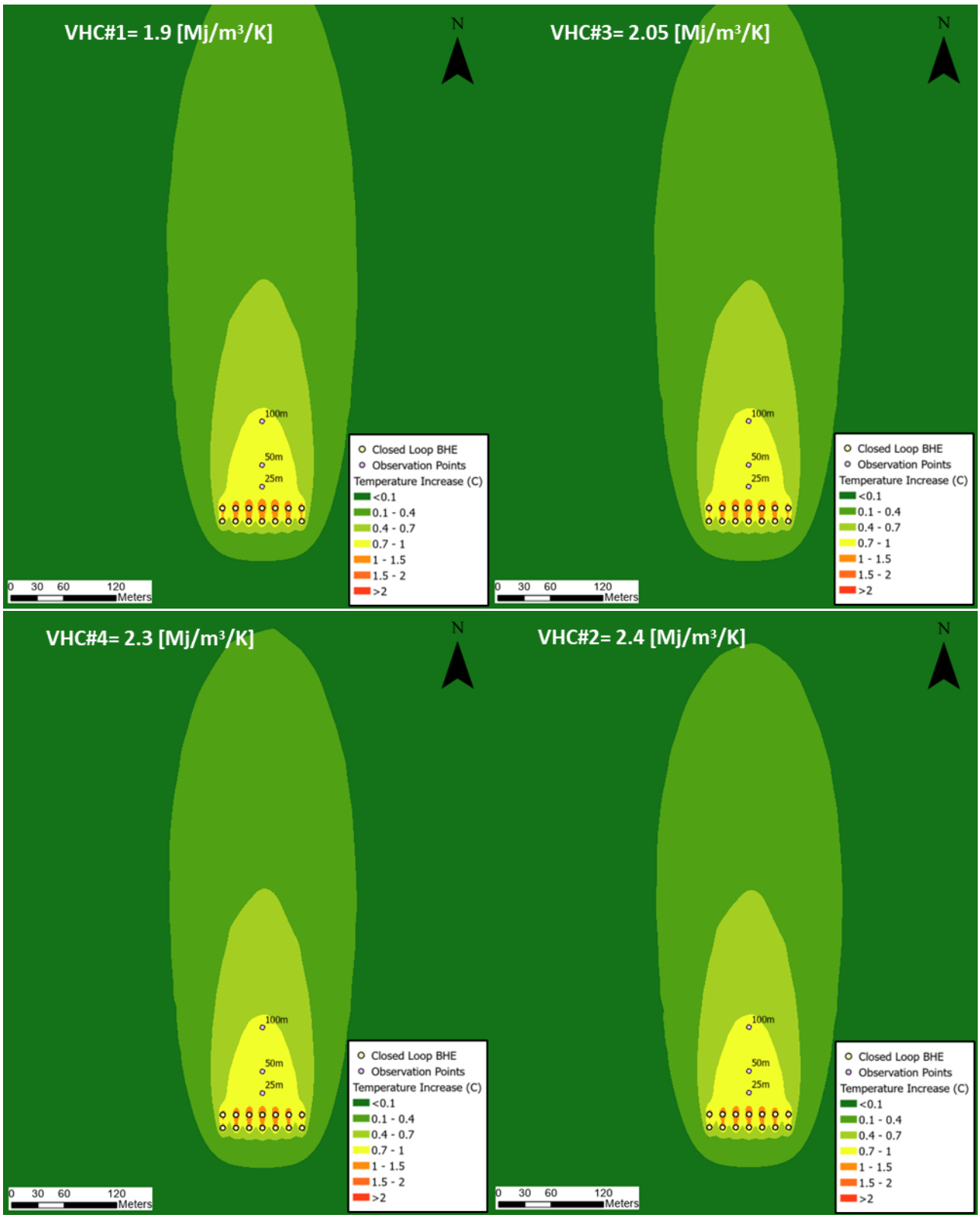

Figure 3-15: Extent and temperature change of the simulated thermal plume after 50 years for different VHC at 60m bgl (slice 4).

Considering a 1°C threshold for the definition of a thermal plume boundary, no significant differences between these runs are visible in Slice 2 outputs (5mbgl), while minor changes in the plume shape are visible for outputs extracted from Slice 4 (60mbgl). Based on the distribution of the thermal plume contours VHC does not have a large influence on the thermal plume length. What little effect it does have is inversely related to the plume length simulated under each run (i.e. slightly longer plume for lower heat capacity). This is because for low VHC heat is less efficiently absorbed into the rock matrix, involving less retardation and faster thermal transport.

3.5.3 Effective porosity

For the heat transport simulation, effective porosity[23] is used to calculate bulk parameters for heat conductivity and heat capacity. Three different simulations were completed for the porosity sensitivity analysis, using a range of representative values reported in literature (Kruseman and de Ridder, 2000), varying from 1% to 30% and plausible for rock types found in England. These changes were applied to layers 2 to 13, while no change in effective porosity was applied to layer 1, which was kept at 1% for all the simulations.

Altering porosity changes the proportion of fluid-filled pore space and matrix in the bulk rock, which also has the potential to alter the bulk thermal conductivity and heat capacity of the rock. In order to keep the same “target” bulk saturated thermal conductivity (2.5 W/m/K) and volumetric heat capacity (2.2 $MJ/m^3/K$), the matrix properties were adjusted at the same time as porosity to retain the same bulk properties as in the baseline scenario.

Simulation outputs for slice 2 and slice 4, showing thermal plume contour maps for the porosity sensitivity analysis runs, are reported in Figure 3-16 and Figure 3-17, while results are summarised in Table 3-7.

[23] Note that porosity and effective porosity are essentially the same in FEFLOW® (i.e. all available porosity is treated as effective).

Table 3-7: Thermal plume lengths (1°C ΔT isocontour) after 50 years for different values of effective porosity.

Plume length of 1°C ΔT isocontour	Baseline porosity 10%	Porosity#1 1%	Porosity#2 20%	Porosity#3 30%
5m depth – Slice 2	~4m	~4m	~4m	~3m
60m depth – Slice 4	~11m	~11m	~10m	~9m

Altering effective porosity has very little impact on plume evolution or length. Only at 30% effective porosity is a measurable difference between these runs present in Slice 2 outputs (5mbgl), while minor changes in the plume shape are visible for outputs extracted from slice 4 (60mbgl). Based on the distribution of the thermal plume contours, an increase of porosity results in a slight decrease in the plume length.

According to Equations 6 and 7, the thermal transport velocity is given by:

$$v_{th} = \frac{v_e}{R_{th}} = \frac{v_D n_e \rho_w c_w}{n_e \rho c} = \frac{v_D \rho_w c_w}{\rho c}$$

and is not explicitly dependent on the effective porosity n_e. If the assumption of instantaneous thermal equilibration between water and matrix is correct, and if bulk thermal conductivity and heat capacity remain the same, one would not expect to see a dependence of thermal transport velocity on effective porosity.

The reason for the slight sensitivity of the plume length to effective porosity may be that "target" bulk saturated thermal conductivity has been calculated using a simple weighted geometric mean of water and matrix thermal conductivities. There is no "100% correct" method for calculating thermal conductivity a priori and it is possible that FEFLOW® uses a slightly alternative algorithm – leading to a slight apparent dependence on porosity.

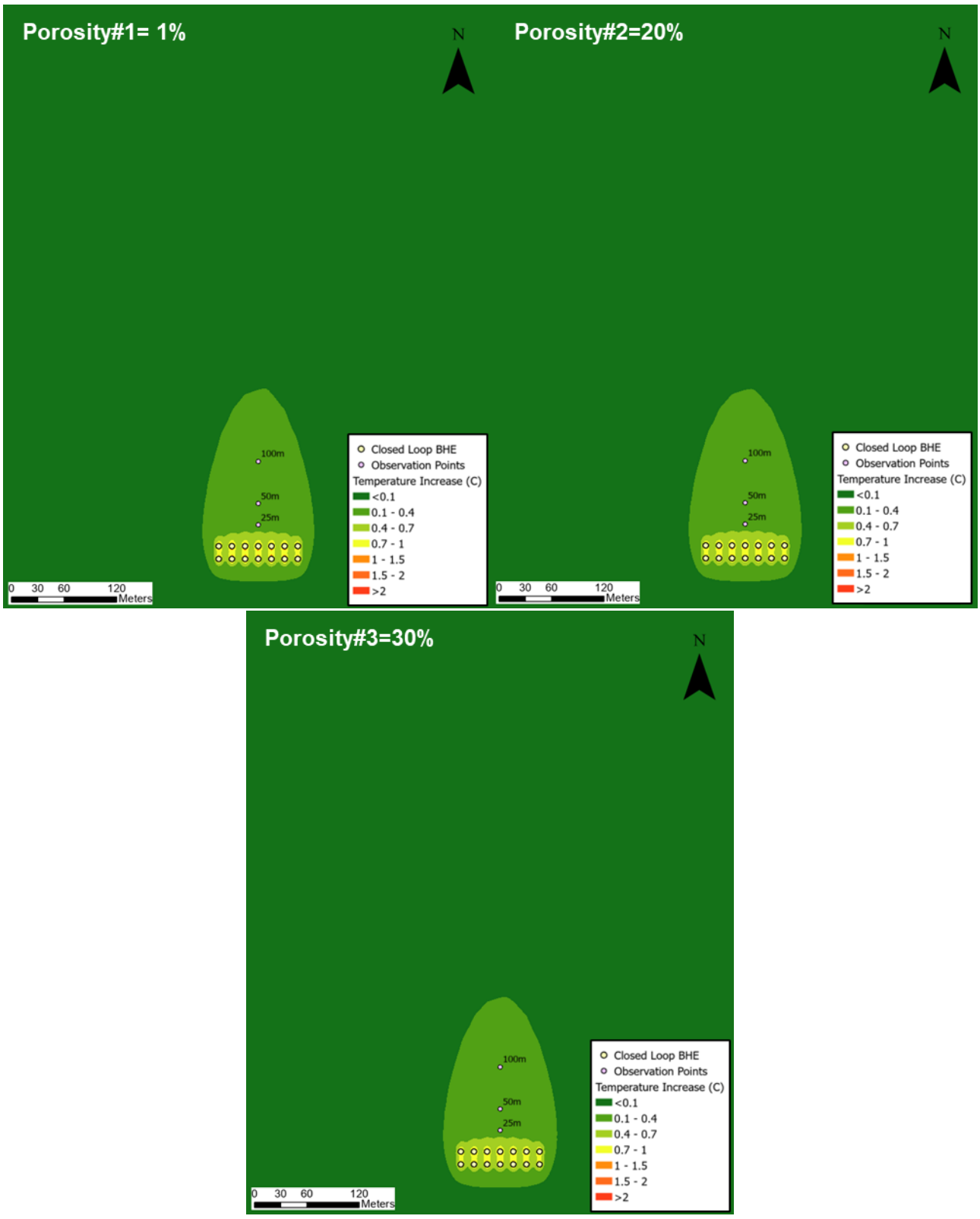

Figure 3-16: Extent and temperature change of the simulated thermal plume after 50 years for different effective porosities, at 5m bgl (slice 2)

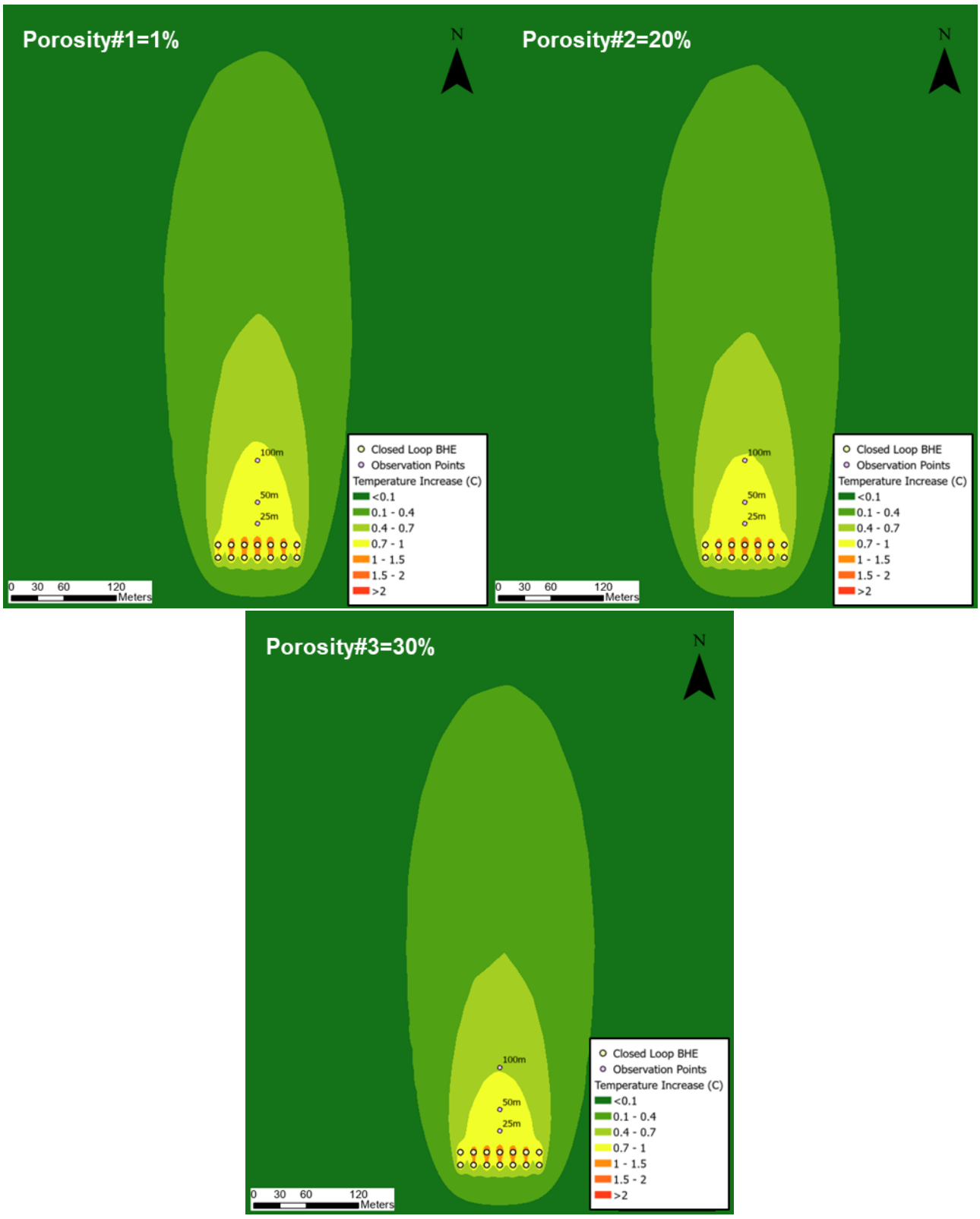

Figure 3-17: Extent and temperature change of the simulated thermal plume after 50 years for different effective porosities at 60m bgl (slice 4)

3.5.4 Darcy Flux

A range of Darcy fluxes between 0 and 0.17 m/d were simulated as part of the sensitivity analysis to evaluate relative importance of advective transport for the thermal plume

distribution. As the model's head gradient was held constant (see below), the various Darcy fluxes applied in this analysis were derived by varying hydraulic conductivity in the range 0.05 m/d to 50m/d. These changes were applied to layers 2 to 13, while no change in hydraulic conductivity was applied to layer 1, which was kept at 0.5 m/d for all the sensitivity runs.

Hydraulic gradient was maintained the same for all the simulations (i=0.0033), with the exception of run n.1, where no groundwater flow was applied to the model (i=0) to analyse the evolution of thermal plume under static groundwater conditions.

Thermal plume contour maps, extracted from slice view outputs for the sensitivity analysis runs are reported in Figure 3-18 and Figure 3-19, while results are summarised in Table 3-8.

Table 3-8: Thermal plume lengths (1°C ΔT isocontour) after 50 years for different values of Darcy flux.

Plume length of 1°C ΔT iso-contour	Baseline: Darcy Flux=0.017 m/d (K_{xy}=5m/d, i=0.0033)	Darcy Flux#1=0 m/d (K_{xy}=5m/d, i=0)	Darcy Flux#2=0.00017 m/d (K_{xy}=0.05m/d, i=0.0033)	Darcy Flux#3=0.0017 m/d (K_{xy}=0.5m/d, i=0.0033)	Darcy Flux#4=0.17 m/d (K_{xy}=50m/d, i=0.0033)
5m depth – Slice 2	~4m	~8m	~8m	~8m	<1m
60m depth – Slice 4	~11m	~47m	~50m	~72m	<1m

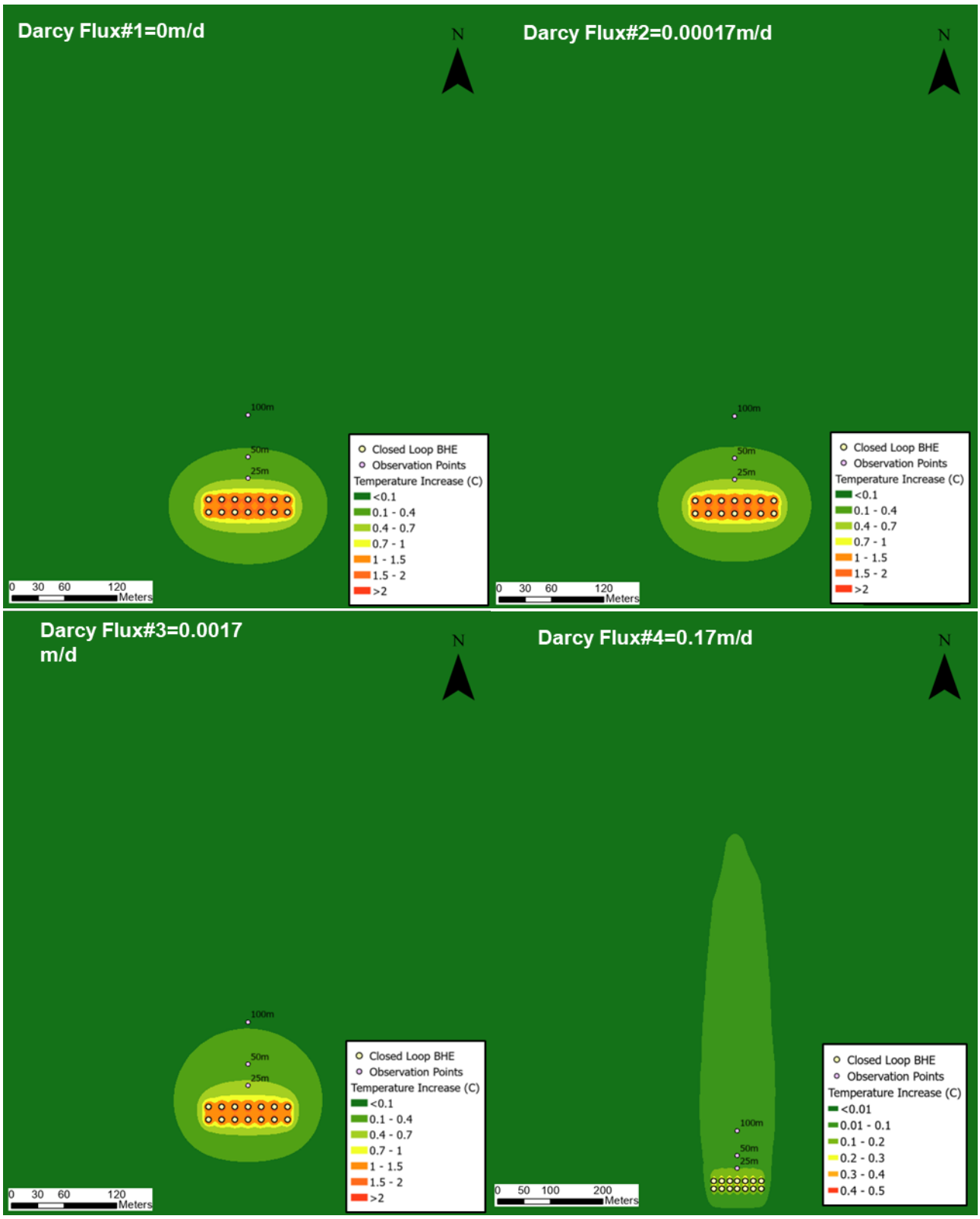

Figure 3-18: Extent and temperature change of the simulated thermal plume after 50 years for different Darcy fluxes, at 5m bgl (slice 2)

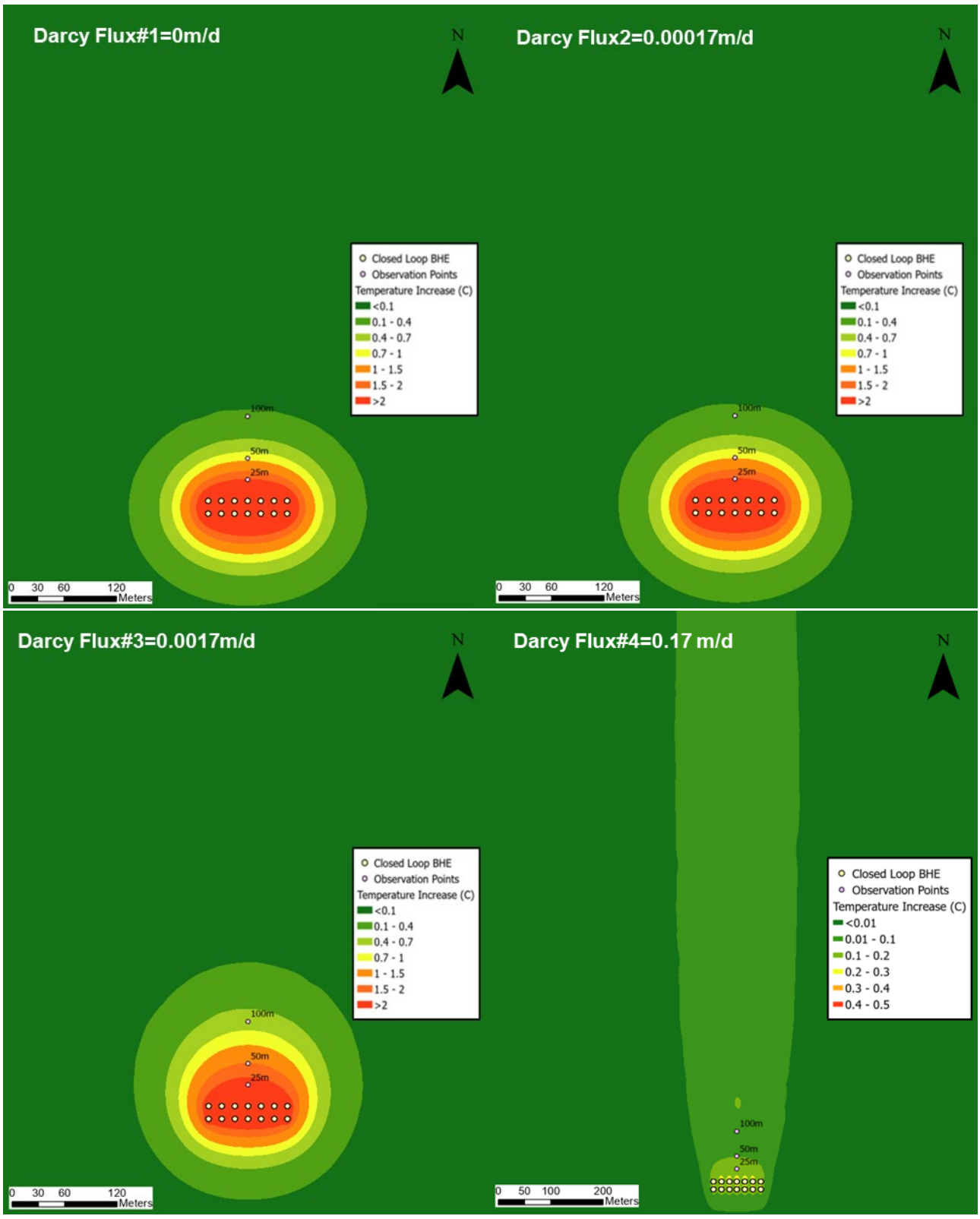

Figure 3-19: Extent and temperature change of the simulated thermal plume after 50 years for different Darcy fluxes, at 60m bgl (slice 4)

The results show that higher values of Darcy flux lead to a considerable increase in the plume length, however these differences are not as evident in slice 2, closer to ground level, where heat loss to the surface dominates heat transport.

Groundwater model outputs extracted from slice 4 (60mbgl) show that for low Darcy fluxes (< 0.017 m/d) the heat accumulates in a pseudo-circular area around the BHE system and does not migrate substantially down gradient within the timeframe of the model (50 years). This results in overall shorter but wider thermal plumes, generating much higher temperature in the vicinity of the BHEs. Up to 0.017 m/d (the baseline scenario), an increasing flux does result in a modest extension of the plume (identified as the 1°C temperature change isocontour)

At higher Darcy flux rates (0.017 m/d and above), the groundwater flow is effective at dispersing the heat, such that it does not accumulate around the BHE array, and the length of the plume (as judged by the 1°C contour) becomes shorter. The contour maps indicate that, if one were to judge the plume shape by a much lower temperature change criterion, the plume actually becomes longer, narrower and generally cooler, as dilution and dispersion effectively attenuate the higher temperature core of the plume.

At the highest groundwater flux (0.17 m/d) there are almost no measurable impacts downstream of the BHE array, considering threshold temperature change of 1°C.

3.5.5 Dispersivity

Dispersivity accounts for the effects of several inhomogeneities not otherwise considered in the model properties. Including microscale inhomogeneities such as pore directions not parallel to flow direction, macroscale properties such as rock formation layers and lenses not considered due to treatment of the matrix as a homogenous porous medium, and model discretization.

As discussed in Section 3.3.5, dispersivity values depend on the spatial scale of the observed phenomenon. In a number of heat tracer tests over distances of around 10 m, the longitudinal thermal dispersivity was confirmed to be around 10% of path length (Carbon Zero Consulting, 2010).

With these assumptions in mind, three pairs of longitudinal and transverse thermal dispersivity values were selected, with transverse dispersivity set at one tenth of longitudinal dispersivity (Carbon Zero Consulting, 2010), which ranged between 10m and 40m. The baseline scenario used dispersivities of 20 m (longitudinal) and 2 m (transverse)

Thermal plume contour maps, extracted from slice view outputs for the sensitivity analysis runs for dispersivity, are reported in Figures 3-20 and 3-21, while results are summarised in Table 3-9.

Table 3-9: Thermal plume lengths (1°C ΔT isocontour) after 50 years for different values of dispersivity.

Plume length of 1°C ΔT iso-contour	Baseline: Dispersivity=20m, 2m	Dispersivity#1=10m, 1m	Dispersivity#2=40m, 4m
5m depth – Slice 2	~4m	~5m	~2m
60m depth – Slice 4	~11m	~12m	~5m

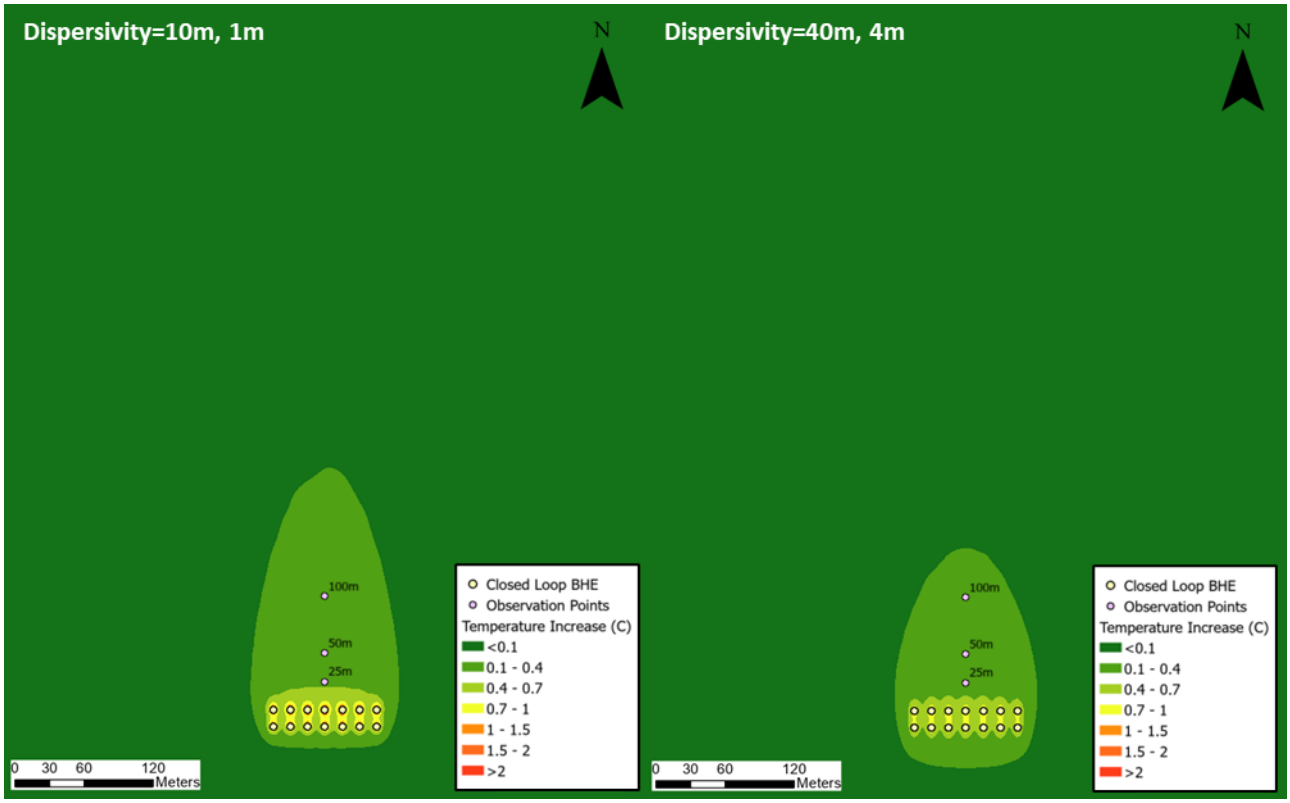

Figure 3-20: Extent and temperature change of the simulated thermal plume after 50 years for different dispersivities, at 5m bgl (slice 2)

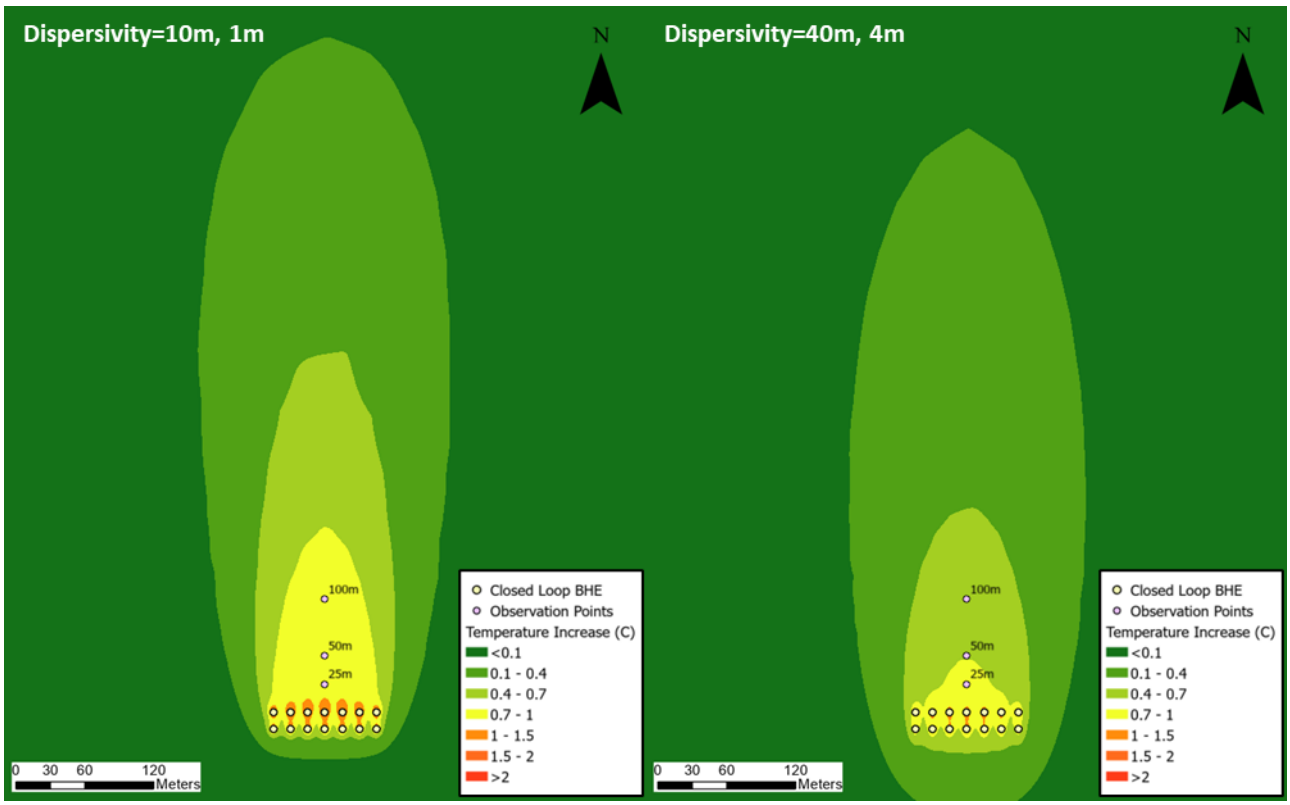

Figure 3-21: Extent and temperature change of the simulated thermal plume after 50 years for different dispersivities, at 60m bgl (slice 4)

The simulated outputs identify a correlation between dispersivity values and the evolution of the thermal plume in the aquifer, with dispersivity inversely related to the plume length. This is because, for higher values of dispersivity, heat dissipation in the aquifer increases, attenuating the concentration of heat in the direction of groundwater flow, and therefore generating shorter geothermal plumes. Numerical modelling shows that higher values of dispersivity result in a greater attenuation of the thermal plume.

However, considering a 1°C for the definition of a thermal plume boundary, with the current model settings, the plume doesn't exceed 12m length either in slice 2 or slice 4.

3.5.6 GSHC system operational cyclicity

Besides thermal and hydrogeological parameters, variables related to the operation of the GSHC system were also assessed.

The baseline scenario modelled a continuous discharge of heat to the aquifer of 45 kW (1080 kWh/day) for 90 days each year, equal to 97.2MWh/year. The alternative scenario, considered here, also modelled the discharge of 97.2MWh/year, but at a rate of 531 kWh/day (22.1 kW) continuously for 183 days per year (6 months).

In both scenarios, 14 BHE (2 x 7 array) were active.

Thermal plume contour maps, extracted from slice view outputs for the sensitivity analysis runs, are shown in Figure 3-22, while results are summarised in Table 3-10.

Table 3-10: Thermal plume lengths (1°C ∆T isocontour) after 50 years for different GSHC system cyclicity.

Plume length of 1°C ∆T isocontour	Baseline: 1080kWh/d for 90 days=97.2MWh/year	Cyclicity#1 531kWh/d for 183 days=97.2MWh/year
5m depth – Slice 2	~4m	~2m
60m depth – Slice 4	~11m	~4m

In the baseline scenario, a peak heat rejection rate of 45 kW was applied (27 W/m borehole). In the alternative scenario, a peak heat rejection rate of 22.1 kW was applied (13 W/m borehole). This results in lower BHE heat transfer fluid temperatures and lower core temperatures in the BHE array. Thus, as judged by the 1°C temperature change scenario, the alternative (longer heat rejection season) scenario results in apparently shorter plumes and lower thermal gradients, in the immediate vicinity of the BHE. Considering the 1°C temperature change criterion, the plume never exceeds 11m length either in slice 2 or slice 4 with either setting.

However, because the same bulk amount of heat is being rejected each year (97.2MWh/year), the distal effects and plume evolution, as judged by, say, the 0.1°C temperature contour, are very similar (Figure 3-22). There are some minor differences, however: spreading the same amount of energy over a longer period, results in a slightly shorter overall distal thermal plume length.

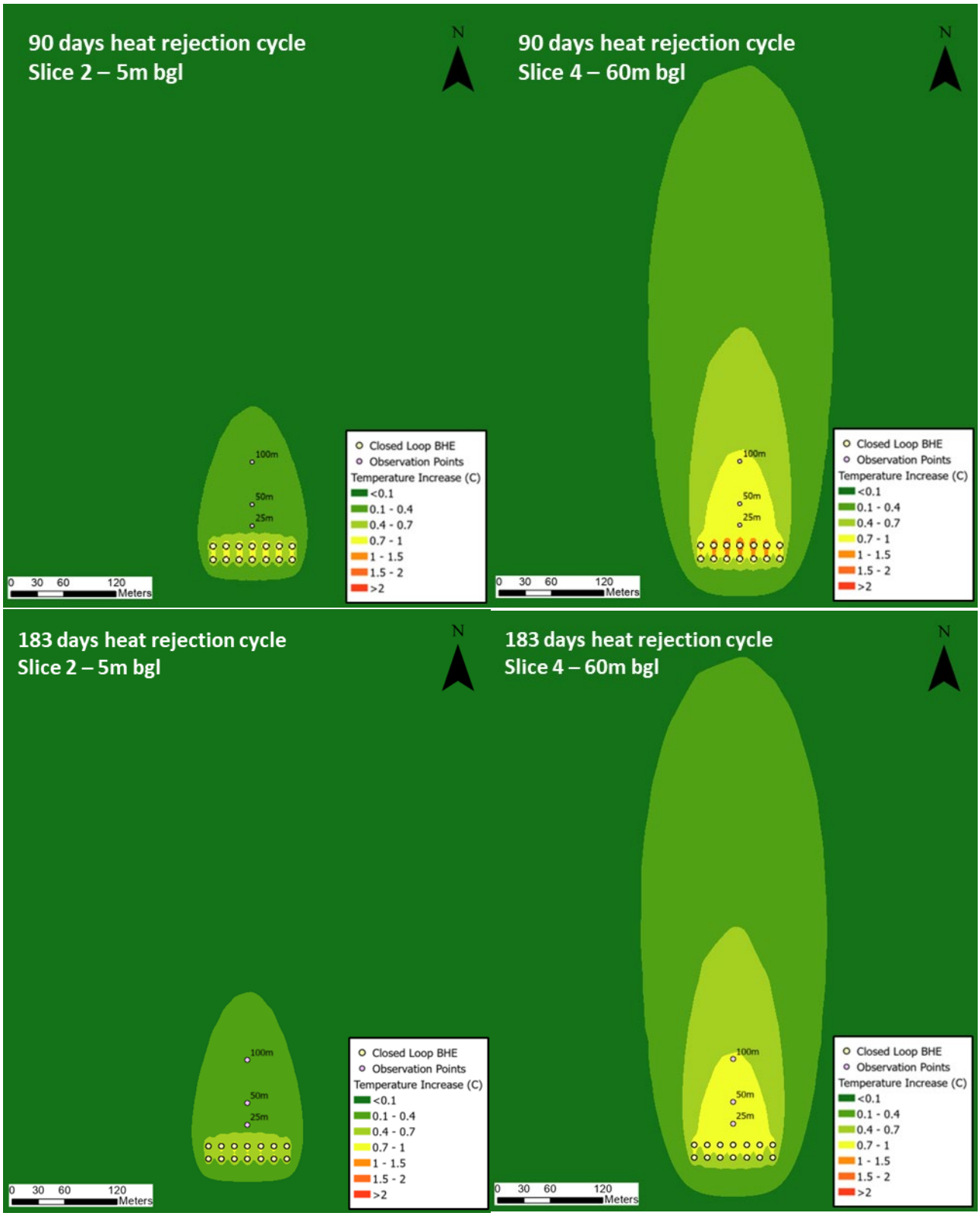

Figure 3-22: Extent and temperature change of the simulated thermal plume after 50 years for different GSHC system cyclity, at 5m bgl (slice 2, baseline, 1080 kWh/day for 90 days) (top) and 60 m bgl (slice 4, 531 kWh/d for 183 days/year) (bottom).

3.5.7 GSHC system power capacity

The effects of different heat capacities of GSHC systems were assessed as part of the sensitivity analysis. Peak heat rejection rates investigated were 10kW, 100kW and 200kW. The annual heat rejection rate simulated for these runs is equivalent to each system operating continuously at full capacity for 2160 FLEQ (90 days/year), as per the baseline scenario setting. The number of BHE and the array geometry varied according to the peak heat rejection rate, based on preliminary assessments carried out with EED modelling in order to meet energy demands for each simulation. Details of geometry and number of boreholes for each system are provided below:

Table 3-11: BHE/array system details for system power capacity sensitivity analysis

	Baseline system power capacity	BHE system power capacity#1	BHE system power capacity#3	BHE system power capacity#2
Power capacity	45kW	10kW	100kW	200kW
Yearly full load equivalent hours (FLEQ)	2160	2160	2160	2160
Peak load heat rejection rate	1080 kWh/d	240kWh/d	2400kWh/d	4800kWh/d
Yearly heat rejection rate	97.2MWh/year	21.6MWh/year	216MWh/year	432MWh/year
BHE number (and array shape)	n.14 (7 x 2)	n.2 (1 x 2)	n.30 (10 x 3)	n.70 (10 x 7)
BHE spacing	15m	15m	15m	15m
BHE length	120m	120m	120m	120m
Power extracted per unit length of BHE (W/m)	~27 W/m	~42 W/m	~28 W/m	~24 W/m
Yearly system cyclicity	3 months on full operative, 9 months off			

Thermal plume contour maps, extracted from slice view outputs for the sensitivity analysis runs are reported in Figures 3-23 and 3-24, while results are summarised in the table below.

Table 3-12: Thermal plume lengths (1°C ∆T isocontour) after 50 years for different values of BHE/array power capacity.

Plume length of 1°C ∆T isocontour	Baseline system power capacity 45kW - 1080 kWh/d	BHE system power capacity#1 10kW - 240kWh/d	BHE system power capacity#3 100kW - 2400kWh/d	BHE system power capacity#2 200kW - 4800kWh/d
5 m depth – Slice 2	~4m	~5	~6	~10
60 m depth – Slice 4	~11m	~6	~165	~310

Overall higher heat rejection rate leads to a considerable increase in plume size and temperature gradient.

A system with 10kW peak heat rejection rate (21.6 MWh/year), show a limited thermal plume extent, up to 6m length in slice 4 (60m depth). However, a system with yearly heat rejection rate >200 Mwh/year (a 100 kW system here), generate much greater temperature gradients in the vicinity of the BHEs, and also generate larger thermal plumes. The simulation results for run 2 (100kW heat rejection rate, or 216 MWh/year) and run 3 (200kW heat rejection rate, or 432 MWh/year) show, respectively, thermal plumes longer than 150m and 300m in slice 4, as defined by the thermal plume isocontour of 1°C. These differences are smaller in slice 2, closer to ground level, where heat loss to the surface is effective in reducing the higher temperature core of the plume and hence limiting longitudinal and transverse heat propagation.

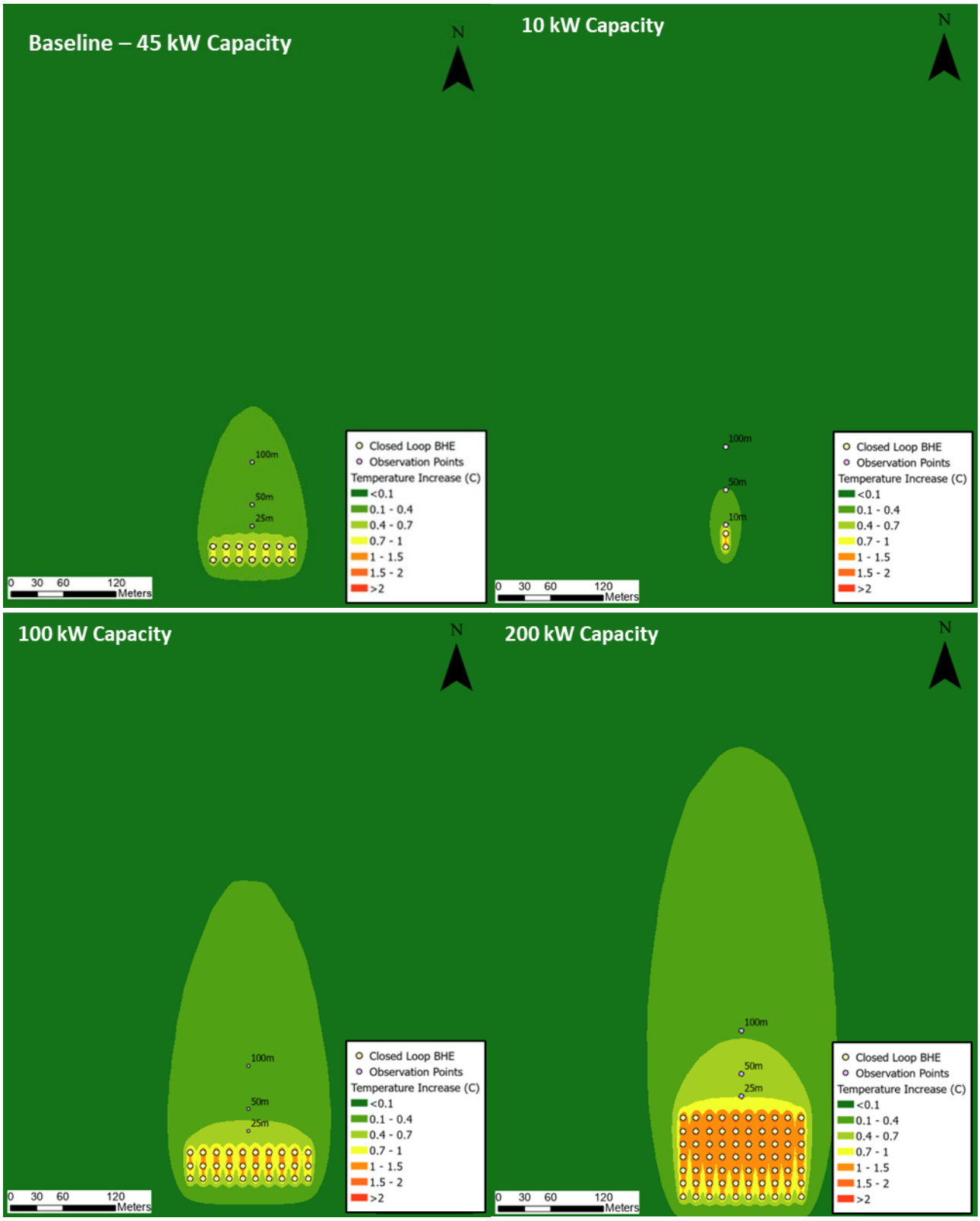

Figure 3-23: Extent and temperature change of the simulated thermal plume after 50 years for different BHE power capacity, at 5m bgl (slice 2)

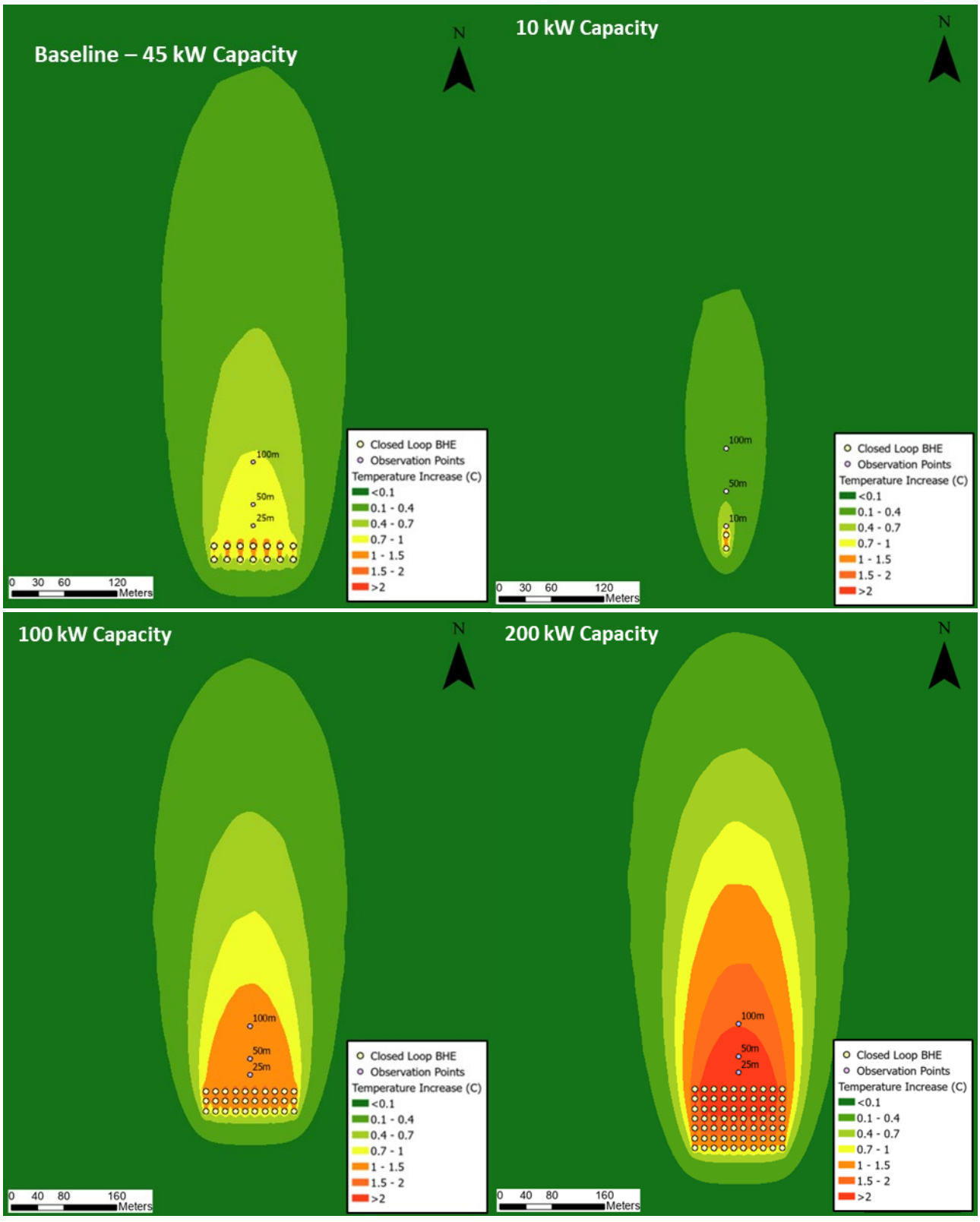

Figure 3-24: Extent and temperature change of the simulated thermal plume after 50 years for different BHE power capacity, at 60m bgl (slice 4)

3.5.8 BHE length

The sensitivity analysis investigated variable BHE installation depths. The objective was to estimate the different impacts of the same heat injection peak rate applied in the baseline model (1080 KWh/d), dispersed across a variable depth interval.

Three additional runs were completed to address these impacts, assuming BHE depths of 50m, 90m, 150m as shown in Table 3-13. The number of boreholes, geometry of the array and the heat rejection rate were maintained as per the baseline scenario settings, however the vertical discretisation of these models was slightly modified to fit these changes in BHE boundary conditions (i.e. slices elevations are not always matching between models). Varying the borehole depth did, of course, alter the heat rejection intensity (W per m of borehole) and it is this that controls the circulating heat transfer fluid temperature in the BHE. The heat rejection rate of 64.3 W/m in the shortest BHE (50 m BHE) is arguably higher than would be acceptable for a real operational GSHC system, as it would result in high heat transfer fluid temperatures and an operational efficiency that would compare poorly with conventional cooling systems.

Table 3-13: BHE and heat injection rate details for BH of varying lengths

BHE details	Baseline BHE length= 120m	BHE length#1= 50m	BHE length#2= 90m	BHE length#3= 150m
BHE length	120m	50m	90m	150m
Peak heat injection rate	1080Kwh	1080Kwh	1080Kwh	1080Kwh
Power capacity	45kW	45kW	45kW	45kW
Number of BHEs used	14	14	14	14
Power extracted per unit length of BHE (W/m)	26.8	64.3	35.7	21.4

Thermal plume contour maps, extracted from slice view outputs for the sensitivity analysis runs, are reported in Figures 3-25 and 3-26, while results are summarised in Table 3-14.

Table 3-14: Thermal plume lengths (1°C ∆T isocontour) after 50 years for different BH lengths.

Plume length of 1°C ∆T isocontour	Baseline BHE length= 120m (~27W/m)	BHE length#1= 50m (~64W/m)	BHE length#2= 90m (~36W/m)	BHE length#3= 150m (~21W/m)
5m depth, slice 2	~4m	~9m	~5m	~3m
Variable depth, ~50% of BHE length	~11m (at 60m bgl)	~65 (at 25m bgl)	~58 (at 45m bgl)	~7m (at 60m bgl)

Model outputs were extracted from slice 2 (5m bgl) to evaluate interaction with surface and from slices at elevation matching approximately 50% of BHE depths applied in each run.

Based on the outputs generated for these runs, little difference is evident in slice 2 (5m bgl) while considerable differences are noticeable at deeper elevations (~50% BHE depths). Broadly speaking, the plume lengths are related to the intensity of heat rejection in W/m borehole.

Results for sensitivity runs for BHEs installed to 50m and 90m depth, having power per unit length of 64W/m and 36 W/m respectively, show overall higher temperatures in the BHE vicinity after 50 years of heat injection. This resulted in thermal plumes longer than 60m, based on the 1°C temperature change isocountour, simply because the same heat injection rate (1080 KWh/d) is concentrated across a thinner depth interval, thereby generating higher temperature gradients.

On the other hand, results from sensitivity run with BHE installed to 150m depth and having power per unit length of 21W/m, show overall lower temperatures and a plume shorter than 10m at 60m depth.

Based on these outputs, it is observed that, increasing power applied per BHE unit length, produce considerable higher temperature in the BHE vicinity and longer thermal plumes. The thermal power per metre of borehole has thus been confirmed as an important variable when considering the impact of closed-loop BHE system design. In fact, this set of sensitivity runs really examined the impact of varying thermal power per metre, rather than borehole depth per se.

Of course, the vertical thickness of the plumes will vary also: the plume from the 50 m boreholes will be less than half as thick as that from the 150 m boreholes.

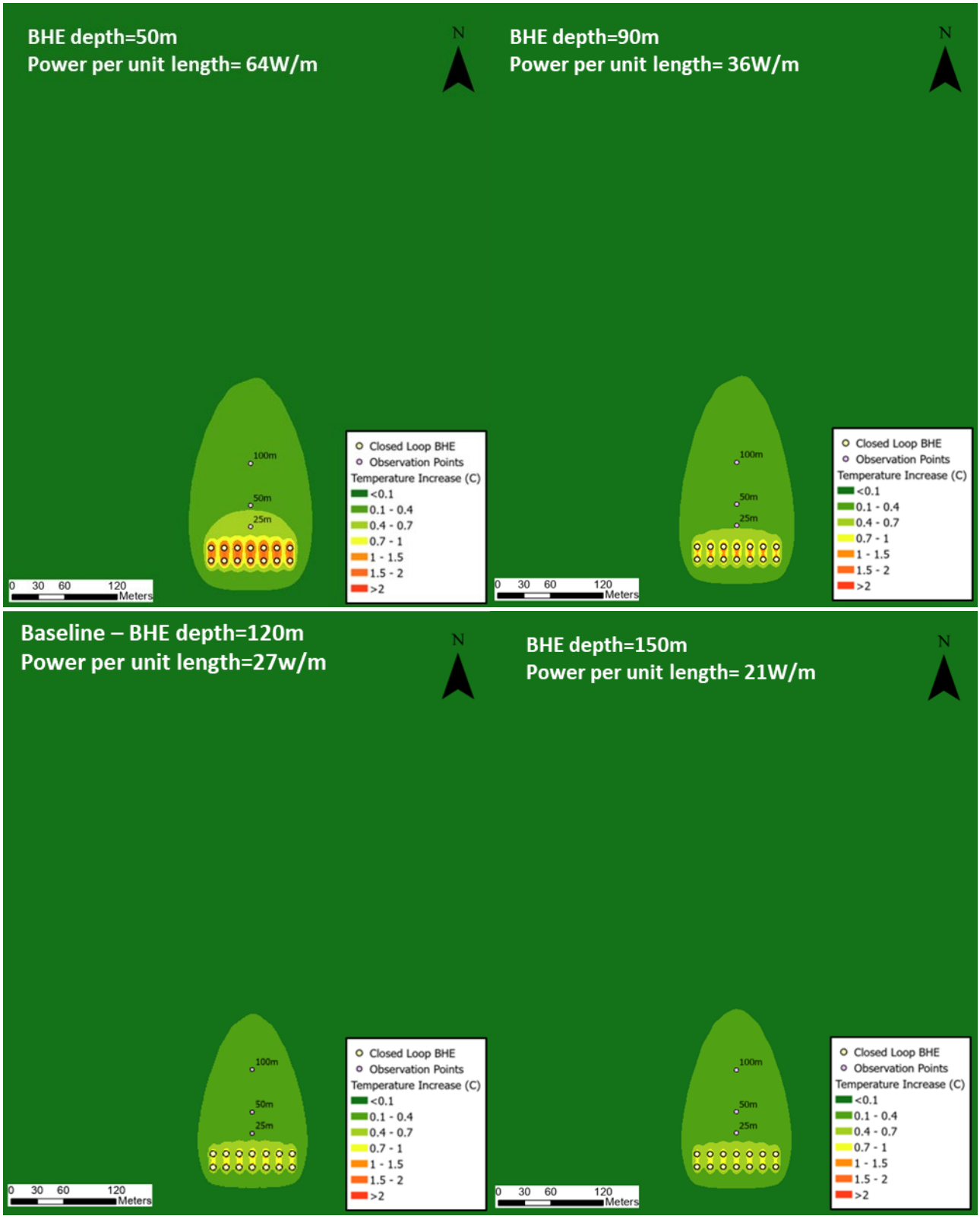

Figure 3-25: Extent and temperature change of the simulated thermal plume after 50 years for different BH depths at 5m bgl (slice 2)

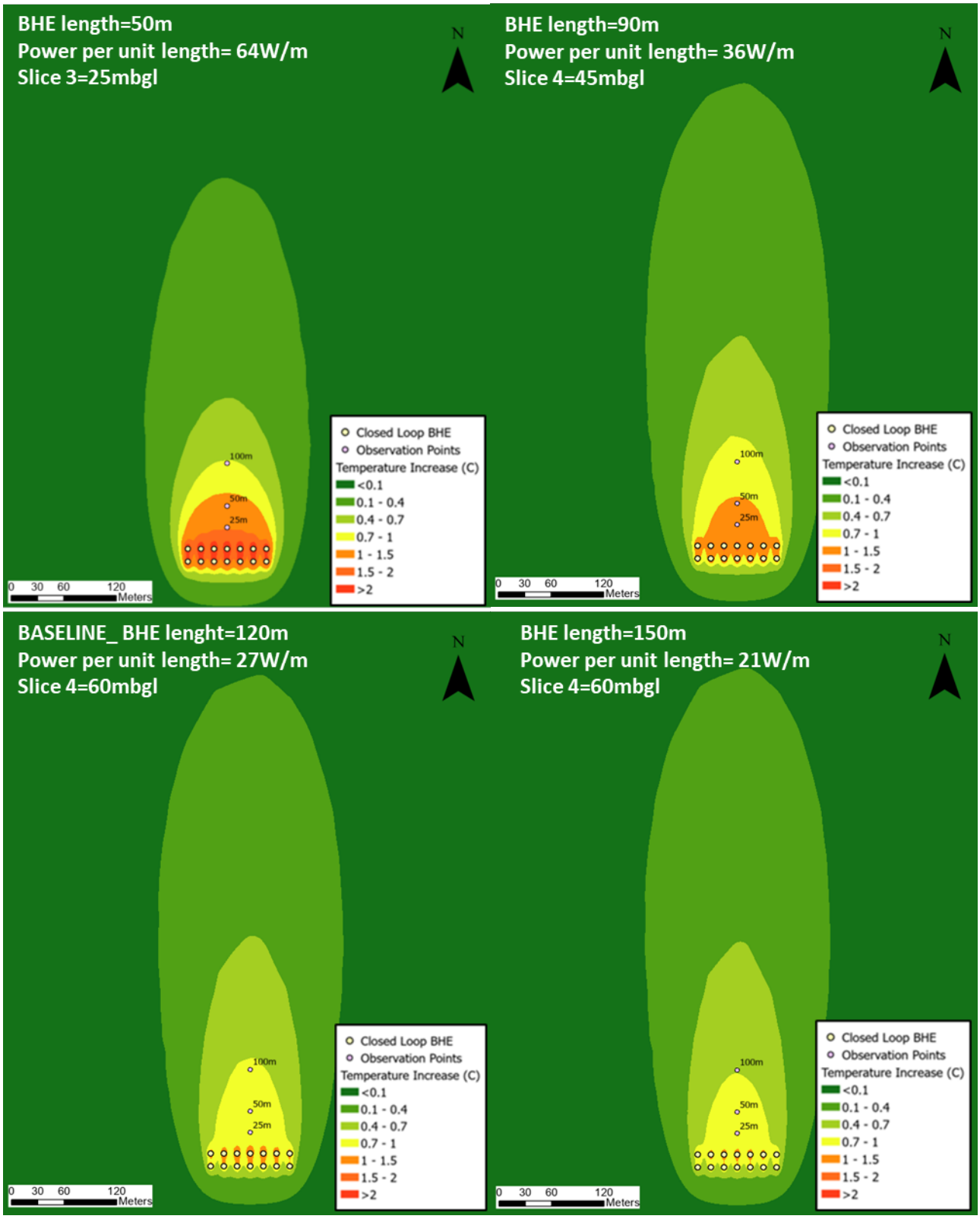

Figure 3-26: Extent and temperature change of the simulated thermal plume after 50 years for different BH lengths for variable depths matching ~50% of BHE lengths.

3.6 Baseline model and sensitivity analysis summary

The objective of the first part of the modelling work described in this report was to evaluate and compare the influence of thermal and hydrogeological subsurface properties, as well as GSHC system characteristics, on the evolution and spatial distribution of the thermal plume from a BHE array.

A closed-loop BHE system, in cooling mode (rejecting heat into the ground), with maximum capacity of 45kW and peak load of 1080kWh/d, delivering a net discharge of heat to the aquifer equal to 97.2MWh/year over a 3-month period per year (i.e. summer cooling) within a saturate sandstone aquifer was simulated in a baseline scenario. Model simulations were extended for a time period of 50 years, to represent long term impacts over the operational lifetime of a GSHC system.

The simulated thermal plume, resulting from 50 years of heat rejection operations, shows upwards heat loss to overlying strata and ultimately the atmosphere, which was set at a constant temperature boundary of 10.5 °C, cooler than the aquifer. Using 1°C as the definition of a thermal plume boundary, the plume simulated for the baseline scenario was less than 11m long between 5 and 60 mbgl.

A sensitivity analysis was undertaken with a total of n.24 simulation runs, to assess the importance of different hydrogeological and thermal properties, and BHE operational setup on the development of temperature alteration during system operation. The focus of the analysis was on the length and time evolution of thermal plumes as subject to varying model parameters. The following parameters were investigated:

- Thermal conductivity;
- Volumetric heat capacity;
- Effective porosity;
- Darcy flux;
- Dispersivity;
- GSHC system operational cyclicity;
- GSHC system power capacity/energy demand;
- BHE depth (power per unit length).

Plume length and temperatures are summarised in Table 3-15.

Table 3-15: Summary of thermal plume lengths (1°C isocontour) for sensitivity analyses and temperature changes for at observation BH for the baseline model. Orange cells indicate plume lengths that exceed 50 m from BHE.

Baseline Model – 50 years simulation time	Plume length – 1°C ΔT	ΔT observed at 25m distance	ΔT observed at 50m distance	ΔT observed at 100m distance
5m depth (Slice 2)	~4m	~0.35°C	~0.25°C	~0.15°C
60m depth (Slice 4)	~11m	~0.9°C	~0.85°C	~0.7°C

Plume length 1°C ΔT					
Thermal conductivity	1W/m/K)	2W/m/K	2.2W/m/K (Baseline model)	3W/m/K	4W/m/K
5 m depth – Slice 2	~8m	~5m	~4m	~3m	~2m
60 m depth – Slice 4	~25m	~12m	~11m	~8m	~7m
Volumetric heat capacity	1.9MJ/m^3/K	2.05MJ/m^3/K	2.2MJ/m^3/K) (Baseline model)	2.3MJ/m^3/K	2.4MJ/m^3/K
5 m depth – Slice 2	~4m	~4m	~4m	~4m	~4m
60 m depth – Slice 4	~11m	~11m	~11m	~10m	~10m
Effective porosity	1%	10% (Baseline model)	20%	30%	
5m depth – Slice 2	~4m	~4m	~4m	~3m	
60m depth – Slice 4	~11m	~11m	~10m	~9m	
Darcy flux	Darcy Flux#1=0m/d (Kxy=5m/d, i=0)	Darcy Flux#2=0.00017m/d (Kxy=0.05m/d, i=0.0033)	Darcy Flux#3=0.0017m/d (Kxy=0.5m/d, i=0.0033)	Darcy Flux=0.017m/d (Kxy=5m/d, i=0.0033) (Baseline model)	Darcy Flux#4=0.17m/d (Kxy=50m/d, i=0.0033)
5m depth – Slice 2	~8m	~8m	~8m	~4m	<1m
60m depth – Slice 4	~47m	~50m	~72m	~11m	<1m
Dispersivity (X,Y)	Dispersivity#1=10m, 1m	Dispesivity=20m, 2m (Baseline case)	Dispersivity#2=40m, 4m		
5m depth – Slice 2	~5m	~4m	~2m		
60m depth – Slice 4	~12m	~11m	~5m		
System cyclicity	1080kWh/d for 90 days=97.2MWh/year (Baseline model)	Cyclicity#1 531kWh/d for 183 days=97.2MWh/year			
5m depth – Slice 2	~4m	~2m			
60m depth – Slice 4	~11m	~4m			
System power capacity	10kW - 240kWh/d	45kW - 1080 kWh/d (Baseline model)	100kW-2400kWh/d	200kW-4800kWh/d	
5 m depth – Slice 2	~5m	~4m	~6m	~10m	
60 m depth – Slice 4	~6m	~11m	~165m	~310m	
BHE Length	BHE Length#1= 50m (~64W/m)	BHE Length#2= 90m (~36W/m)	BHE Length= 120m (~27W/m) (Baseline model)	BHE Length#2= 150m (~21W/m)	
5m depth – Slice 2	~9m	~5m	~4m	~3m	
Variable depth ~50% of BHE length	~65m (at 25mbgl)	~58m (at 45mbgl)	~11m (at 60mbgl)	~7m (at 60mbgl)	

Based on the results observed with the sensitivity analysis results, the main outcomes are:

- An increase in thermal conductivity results in a decrease in plume length due to greater conductive heat loss through the surface and surrounding rocks and resulting reduction in the size of the thermal plume in the aquifer.

- VHC does not have a large influence on the thermal plume length, although it is demonstrated to be weakly inversely correlated to the plume length. This is because, for low VHC, heat is less efficiently absorbed into the rock matrix, involving less retardation and greater thermal transport.

- Effective porosity has minimal impact on the dimensions of the resultant plume (provided that the assumption of instantaneous thermal equilibrium between matrix and groundwater, made in the model, is true).

- Darcy flux has a significant impact on plume development. For low Darcy fluxes the heat accumulates in a pseudo-circular area around the BHE system and does not migrate substantially down gradient within the time-frame of the model. This results in overall shorter but wider thermal plumes, generating much higher temperature in the vicinity of the BHEs. For high groundwater flux rate, the plume becomes longer and narrower and dilution and dispersion effectively attenuate the higher temperature core of the plume.

- When the value of dispersivity increases, heat dissipation in the aquifer increases, resulting in shorter thermal plumes in the direction of groundwater flow. Numerical modelling suggests that higher values of dispersivity result in a greater degree of attenuation of the plume.

- The simulated outputs varying operational cyclicity show that, spreading the same amount of energy over a longer rejection period each year results in lower temperatures in the vicinity of the BHE, and a shorter thermal plume (as defined by the contour of 1°C temperature change) in the vicinity of the BHE. Overall, however, the same amount of heat is being discharged to the rock and the distal plume length (as defined by, say, the 0.1°C temperature contour) is only affected by operational cyclicity to a minor extent.

- A series of plausible high BHE system power demands were also associated with significantly increased plume size and temperature gradient. Scenarios simulating systems with yearly heat rejection rates >200 MWh/year generate high temperature gradients in the vicinity of the BHEs, and also longer thermal plumes. The simulation results for run 2 (100kW rejection rate, and 216 MWh/year) and run 3 (200kW rejection rate, and 432 MWh/year) yield heat plumes in excess of (respectively) 150m and 300m at 60mbgl (based on the 1°C temperature change contour)

- The peak heat exchange rate per m of borehole is one of the more important variables in closed-loop system design (as well as the total heat exchange with the ground over the course of a year).

- It is observed that the plumes are overall significantly smaller at shallow depths (i.e. 5mbgl) than the ones calculated at deeper elevations (i.e. 60m depth). These differences are related primarily to vertical conductive heat loss to the atmosphere through the temperature BC implemented on top of layer 1, to simulate effects of air/soil temperature at ground level.

Of the parameters tested as part of the sensitivity analysis, those showing the strongest influence on the thermal plume migration, as a result of BHE heat rejection operations, are the Darcy flux, the total heat rejection per annum (MWh/yr) and peak rate per BHE metre (W/m). However sensitivity analysis results show that also the thermal conductivity and the dispersivity are also important for heat propagation. This is in-line with findings from the literature.

4 Model scenarios

The evolution of the thermal plumes from closed-loop GSHC schemes, were simulated for a series of scenarios representing a range of different aquifer conditions that might be characteristic of English hydrogeology, and operational scenarios for the closed-loop system. The scenarios simulated and analysed as part of this study are listed below. Settings and results are discussed in the following sections:

- Closed-loop system for heat extraction;
- Baseline scenario with a partially unsaturated aquifer;
- Closed-loop system with alternating heat abstraction and injection phases.
- London Basin aquifer;
- Mudrock aquitard (i.e. Mercia Mudstone Group);
- Fluvial sand and gravels aquifer;
- Conservative / worst case scenario

Model simulations for these scenarios were run for a period of 50 years to represent long term impacts over the operational lifetime of a GSHC scheme.

4.1 Closed-loop system for heat extraction

For this scenario, the effects of a closed-loop system designed for heating purposes (i.e. heat extraction from the ground resulting in a cool thermal plume) were investigated. The simulation implemented a system of 45kW (1080 kWh/day) instantaneous heat extraction rate, continuously operative for 3 months/year (2160 hours/year), equal to 97.2MWh/year extracted from the aquifer. This is essentially the baseline scenario with inverted “polarity”.

Based on preliminary indications from EED modelling, to verify design feasibility, the BHE closed-loop system for this scenario implemented n.14 BHE, with 15 m spacing, installed to 120m depth (i.e. from 0 to 120mbgl). BHE properties and geometry specifications are the same as the baseline scenario, as shown Figure 3-4.

The groundwater model geometry and all the settings applied in this scenario are the same as used for the baseline scenario, summarised in Section 3.3.1 and 3.3.3.

The lengths of the thermal plume were calculated after 50 years of an active BHE system, at the end last cycle of heat extraction (17,975 days). Model outputs were extracted from Slice4, at 50% of total BHE installation depth (60mbgl), and from slice2 (5mbgl) to evaluate interaction with surface.

Thermal plume isocontour maps, extracted from slice view outputs for this scenario, are reported in Figure 4-1.

Figure 4-1: Extent and temperature change of the simulated thermal plume after 50 years for a heat extraction scenario at 5m and 60m bgl.

Similarly to the baseline scenario for the case of heat injection, the plume simulated in the down-gradient direction (north) is significantly shorter at 5 mbgl than the one calculated at 60m depth. These effects are related to attenuation of the plume by vertical conductive heat migration from the surface (constant temperature boundary condition at 10.5°C, implemented on top of layer 1, to simulate effects of ground level temperature).

Considering -1°C change for the definition of a thermal plume boundary, with these model settings the plume does not extend further than 11m in length either in slice 2 or slice 4. This threshold is exceeded only in the close vicinity of the BHE array.

Figures 4-2 and 4-3 show temperature change from starting conditions from observation points located downstream the BHE at various distance (25m, 50m, 100m) in slice 2 and slice 4.

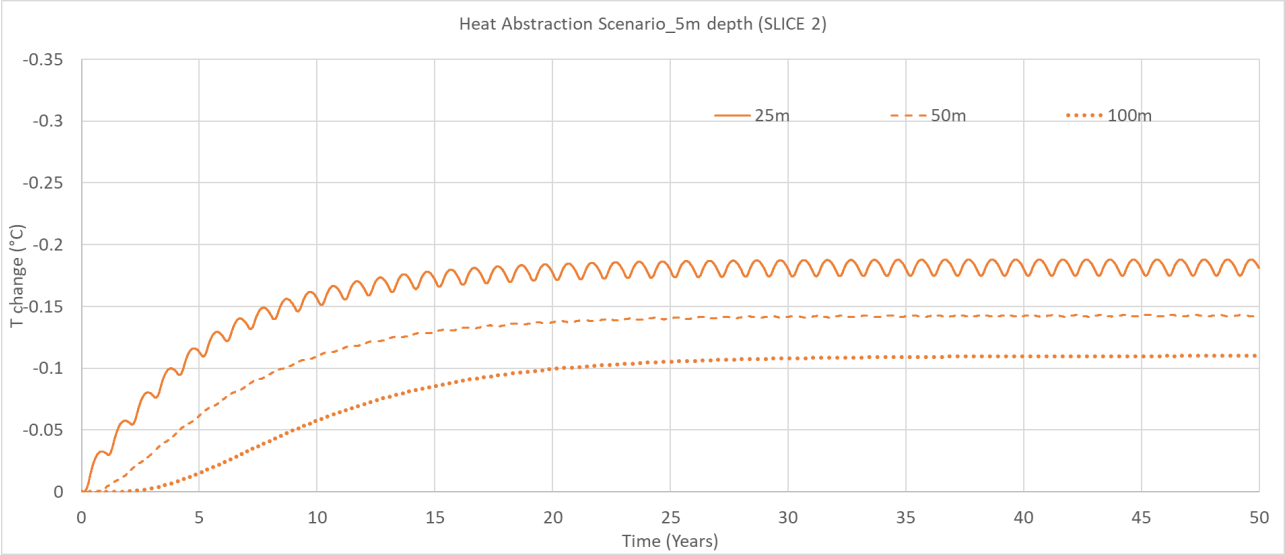

Figure 4-2: Change in temperature (ΔT) from initial conditions during the operational period (50 years) of the BHE array for the heat extraction scenario at slice 2 (5m bgl)

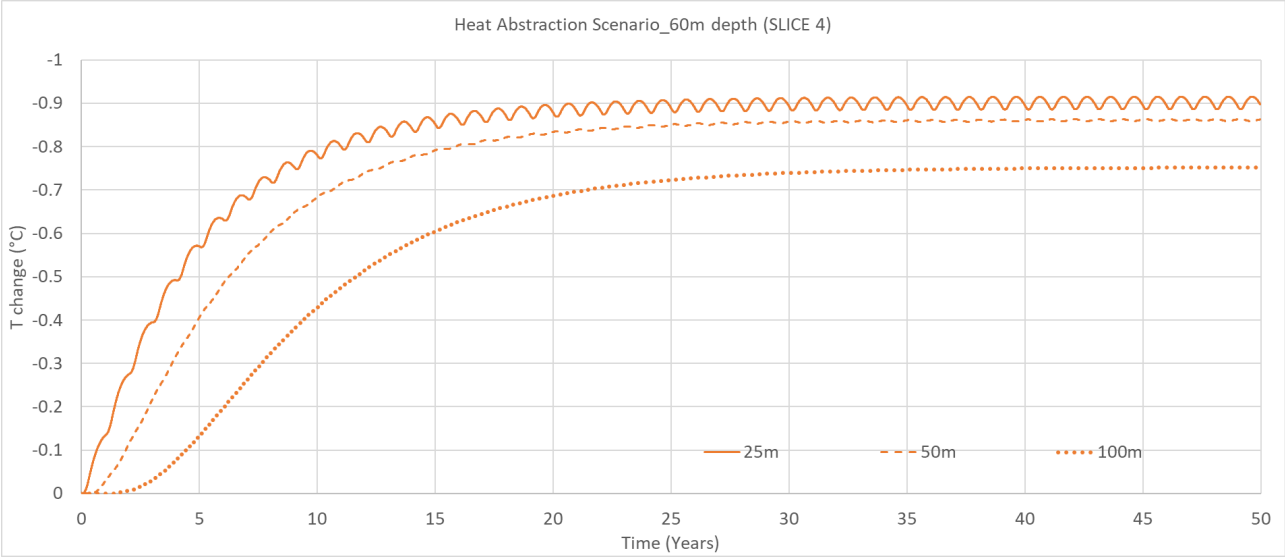

Figure 4-3: Change in temperature (ΔT) from initial conditions during the operational period (50 years) of the BHE array for the heat extraction scenario at slice 4 (60m bgl)

It is notable that temperature changes at 5 m depth and 25 m distance are lower in magnitude (-0.2°C) than the change in the baseline heat rejection scenario (+0.35°C – Figure 3-12). Thus, the heat extraction scenario is not an exact mirror image of the heat rejection scenario. This is due to the unidirectional (upward) nature of the geothermal gradient, which is not reversed in the two scenarios and which thus “breaks” the exact symmetry. The explanation for this is revealed by considering a scenario where the BHE has no external load imposed, but merely passively circulates a heat transfer fluid around its length. The heat transfer fluid circuit acts as a thermal “short circuit”, transporting a

small amount heat from depth to the surface (“up” the geothermal gradient), slightly heating the shallow subsurface and slightly cooling the rocks at the base of the BHE. This is the reason why there is a small “deficit” of “coolth” (-0.2°C at 25 m) in the near-surface slice during heat extraction compared to the small “excess” of heat (+0.35°C at 25 m) in the near-surface slice under heat rejection (Figure 3-12). At the borehole’s mid-point (60 m bgl), the plots for heat extraction (Figure 4-3) and heat rejection (Figure 3-13) are almost identical.

The time series (Figures 2-3 and 2-4) show that temperatures increase and also approach steady-state conditions more quickly in proximity to the BHE than those further from the BHE array. In both slices, the temperature time series extracted from observation points located further than 50m from the BHE show no cyclicity (i.e. it is smoothed at this distance) from BHE heat rejection activities, while these fluctuations are evident for closer observation point located at 25m distance.

In this scenario, the temperature decreases by approximately -0.1°C at 100m distance from the BHEs in slice 2 and by -0.7 °C at 100m in slice 4.

A summary of the results for the thermal plume length and temperatures at the observation BHs after 50 years, are summarised in the following table.

Table 4-1: Thermal plume length and temperature changes at observation BH after 50 years for the heat extraction scenario.

50 years simulation time	Plume length 1°C ΔT	ΔT observed at 25 m distance	ΔT observed at 50 m distance	ΔT observed at 100 m distance
5m depth (Slice 2)	~ 9m	~ - 0.2 (°C)	~ -0.15 (°C)	~ - 0.1 (°C)
60m depth (Slice 4)	~ 4m	~ -0.9 (°C)	~ - 0.9(°C)	~ - 0.75 (°C)

4.2 Partially saturated aquifer conditions

This scenario modelled the effects of a heat rejection GSHC system under partially saturated aquifer conditions. This is in contrast with the baseline scenario where the simulation was completed under fully saturated conditions.

To account for partially saturated conditions, the simulated water table was set between 10mbgl and 40mbgl across the model domain, resulting in approximately 15m of unsaturated aquifer thickness at the location of the BHE array. This was implemented by applying constant hydraulic head values of 40m AOD on the southern model edge

(upgradient) and 10m AOD on northern model edge (downgradient). The head difference along the length of the model domain remains 30 m (as in the baseline case).

Other than the flow boundary conditions discussed above, the groundwater model geometry, parameters and closed-loop system settings applied in this scenario are the same as for the baseline scenario, as previously summarised in Table 3-1 and 3-2. In the unsaturated zone, the model recalculates the bulk thermal conductivity and volumetric heat capacity, based on the proportion of residual air and water in the pore spaces; this results in a decrease in both conductivity and heat capacity in the unsaturated zone.

The length of the resulting thermal plumes was calculated after 50 years of an active BHE system, at the end of the last heat rejection cycle (17,975 days). Model outputs were extracted from slice 4, at 50% of total BHE installation depth (60mbgl), and from slice 2 (5mbgl) to evaluate interaction with surface.

Thermal plume contour maps, extracted from slice view outputs for this scenario, are reported in Figure 4-4.

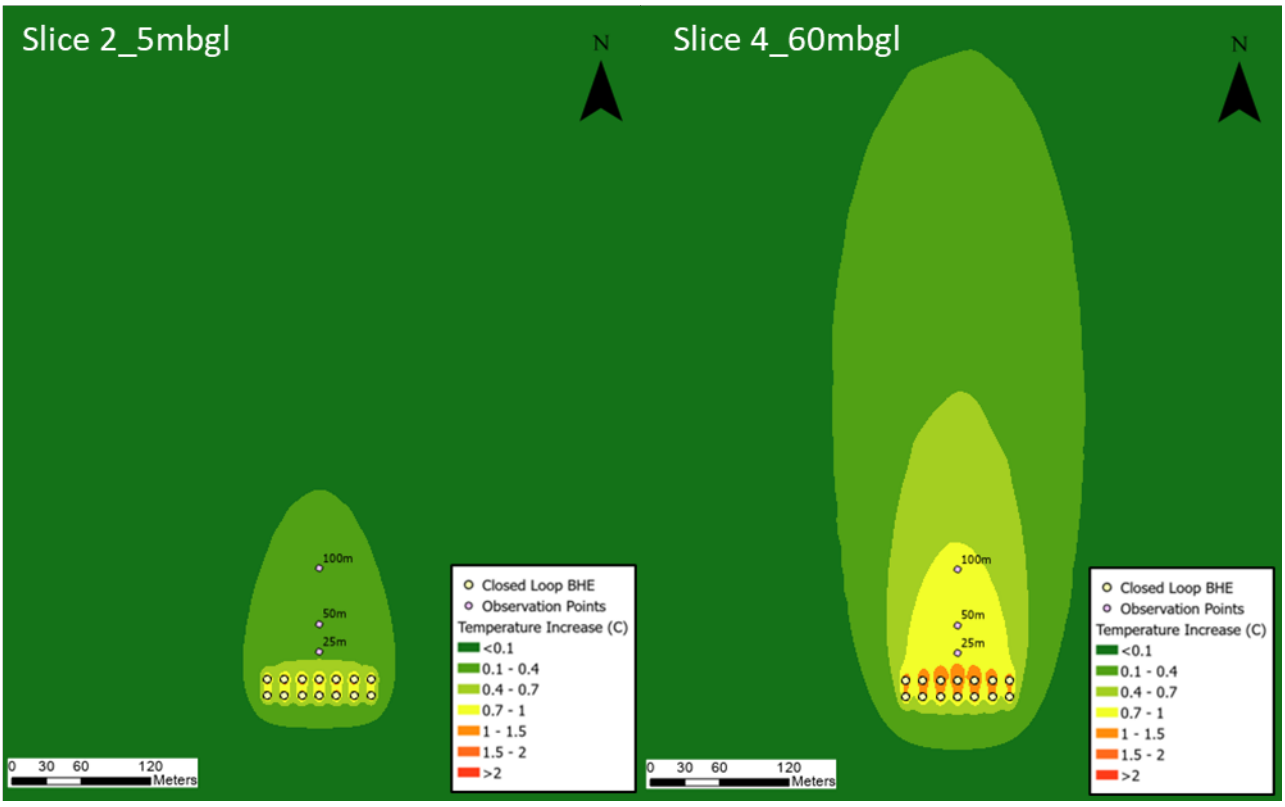

Figure 4-4: Extent and temperature change of the simulated thermal plume after 50 years for a scenario with partially saturated aquifer conditions at 5m and 60m bgl.

The outputs generated with the partially saturated aquifer conditions are very similar to the results observed for the baseline scenario (Section 3.4), both in terms of plume length and overall temperature distribution, as shown in Tables 3-3 and 4-2.

Table 4-2: Thermal plume length and temperature changes at observation BH after 50 years of heat rejection for a partially saturated scenario.

Depth	Plume length (1°C ΔT)	ΔT observed at 25m distance	ΔT observed at 50m distance	ΔT observed at 100m distance
5m depth (Slice 2)	~4m	~0.35°C	~0.25°C	~0.15°C
60m depth (Slice 4)	~14m	~1.0°C	~0.9°C	~0.75°C

In theory, a thicker unsaturated zone would be anticipated to have an insulating effect at the top of the aquifer, leading to enhanced plume length, but for the geological conditions specified (10% effective porosity in the sandstone; 1% effective porosity in the 5m thick surface aquitard) this effect is small.

4.3 Alternate phasing between heat extraction and injection (balanced system).

This scenario provides indications about the potential thermal impacts from “reversible” GSHC schemes, operated by alternating heat extraction and heat injection phases, on a yearly cycle.

As opposed to the baseline case, this scenario modelled a closed-loop BHE system designed for both heating and cooling, with a maximum heat exchange rate of 45kW. The yearly operational cyclicity applied to the BHE array is shown in Figure 4-5 and considers a system operating continuously at peak load of 1080kWh/d (45 kW) for 3 months/year under heat injection mode (injecting 97.2MWh/year to the aquifer) and a subsequent standby period of 1.5 months (45 days) with no ongoing heat exchange activities. This period is then followed by a heat extraction phase, with BHEs running continuously for 6 months/year at 540kWh/d (extracting 97.2MWh/year from the aquifer) and a final standby period of 50 days without ongoing operations.

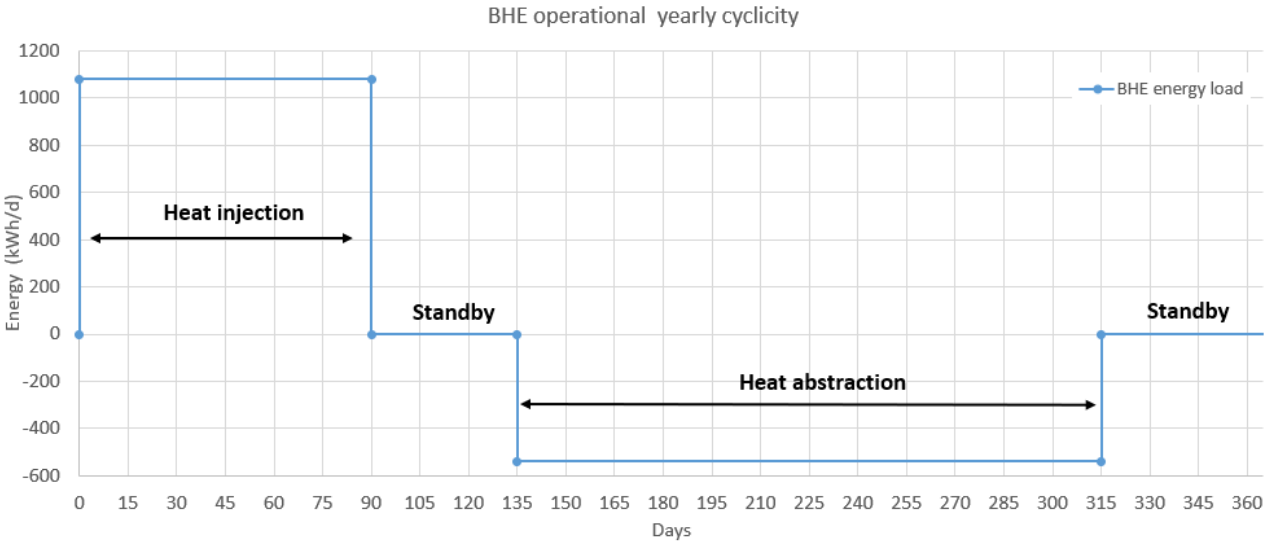

Figure 4-5: Yearly cyclicity of BHE system energy demand

Other than the BHE operational cyclicity mentioned above, the groundwater model geometry and all the settings applied in this scenario are the same as for the baseline scenario, as previously summarised in Tables 3-2 and 3-3.

Temperature change (from initial conditions) time series at observation points located downstream from the BHE at 25m, 50m, 100m in slice 2 and slice 4 are shown in Figures 4-6 and 4-7.

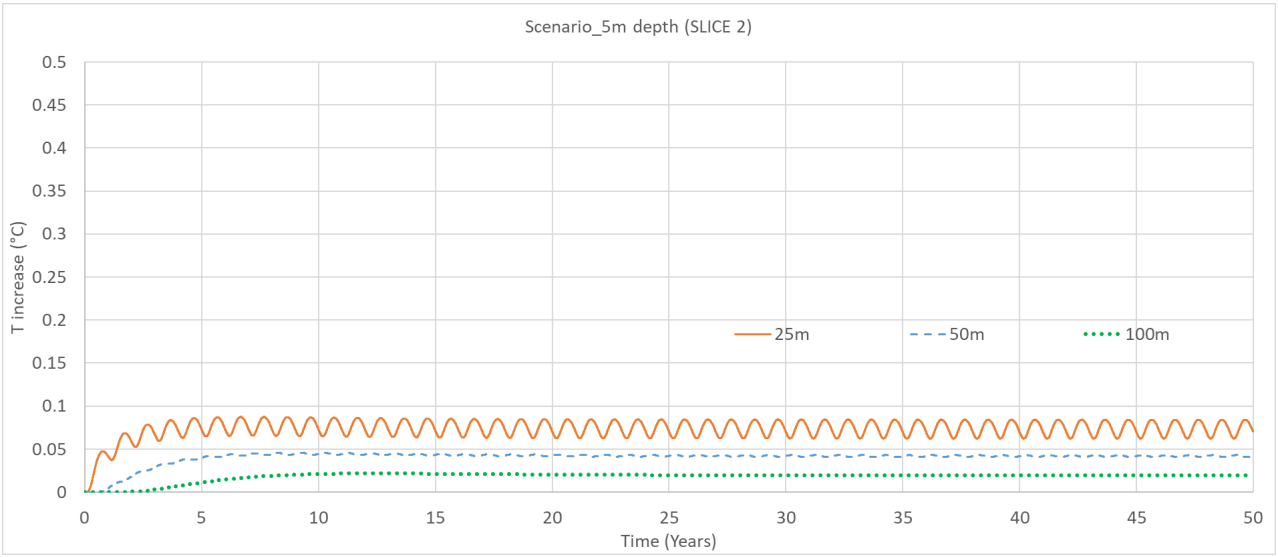

Figure 4-6: Change in temperature (∆T) from initial conditions during the operational period (50 years) of the BHE array for the alternating heat extraction and injection scenario at slice 2 (5m bgl).

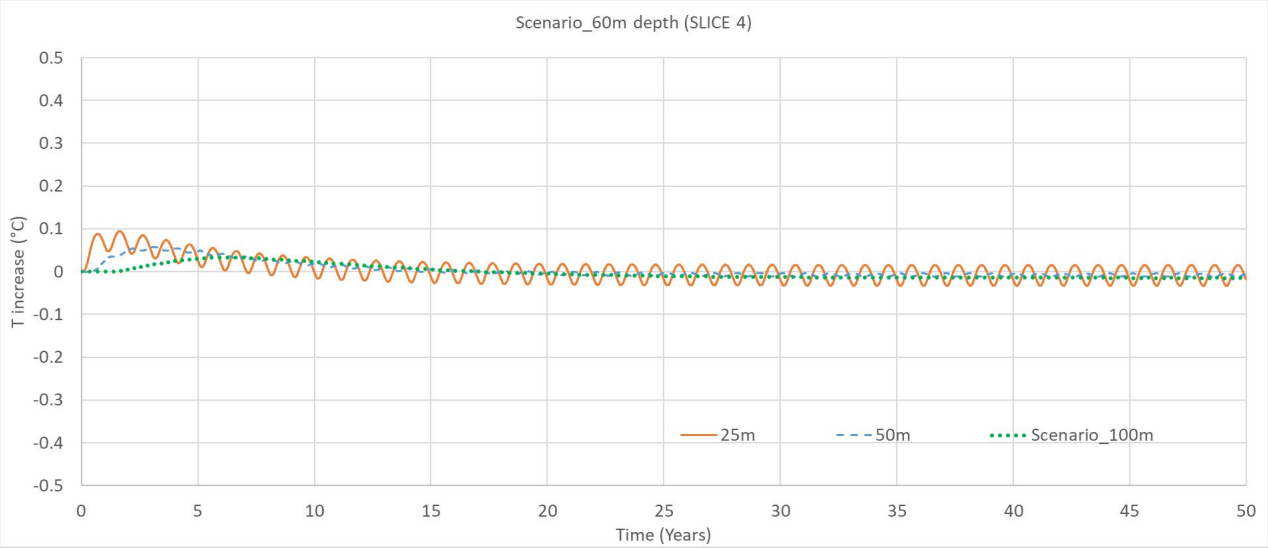

Figure 4-7: Change in temperature (∆T) from initial conditions during the operational period (50 years) of the BHE array for the alternating heat extraction and injection scenario at slice 4 (60m bgl).

The results show minimal temperature changes across the model domain, with ∆T always <0.1°C for both slice 2 (5mbgl) and slice 4 (60mbgl). Due to the alternate operational BHE cyclicity implemented in this scenario the effects on underground temperature produced by heat injection phases are compensated by the subsequent heat abstraction periods and there is little net change and no extensive thermal plume.

The reason for a slight net increase in temperature in slice 2 (shallow subsurface) is the same as the explanation given in Section 4.1. Consider a scenario where the BHE has no net external load imposed, but merely passively circulates a heat transfer fluid around its length. The heat transfer fluid circuit acts as a thermal “short circuit”, resulting in a small net transport of heat from depth to the surface (“up” the geothermal gradient), slightly heating the shallow subsurface and slightly cooling the rocks at the base of the BHE. One would expect, in this balanced scenario between heat extraction and rejection, a small net temperature decrease near the base of the BHE in the long term. At 60 m depth (the BHE mid-point) there is no long-term temperature change (Figure 4-7).

Table 4-3: Thermal plume length and temperature changes at observation BH after 50 years for the alternating heat extraction and injection scenario.

50 years simulation time	Plume length, 1°C ∆T	∆T (°C) observed at 25 m distance	∆T (°C) observed at 50 m distance	∆T (°C) observed at 100 m distance
5m depth (Slice 2)	NA	<0.1°C	<0.1°C	<0.1°C
70m depth (Slice 4)	NA	<0.1°C	<0.1°C	<0.1°C

4.4 London Basin aquifer

An additional scenario was set to represent GSHC systems installed in a geology typical of the London Basin (LB) area. To fit this case, the groundwater model was modified considering hydrogeological and geothermal conditions characteristic of this area, as detailed below.

The BHE system capacity, the array geometry and the yearly operational cyclicity applied in this simulation are the same as for the baseline scenario, as outlined in Section 3.3.2. (maximum heat rejection rate of 45kW (with peak load 1080kWh/d), for 3 months/year (2160 FLEQ), delivering a net discharge of heat to the aquifer equals to 97.2MWh/year.)

4.4.1 Model dimensions and boundary conditions

The X and Y model dimensions and discretisation for this scenario were the same as applied in the baseline scenario (Section 3.3.1.), however the vertical discretisation of the model was adjusted to reflect hydrogeological settings for the LB area (discussed in Section 4.4.3).

The hydraulic gradient applied in the groundwater model was based on groundwater levels for the LB area, from the Environment Agency report "Management of the London Basin Chalk Aquifer – status Report 2022[24]" (Environment Agency, 2023). The regional groundwater flow was reproduced by assigning constant hydraulic head values on the southern edge (upgradient) of 40m AOD and of 10m AOD to the northern (downgradient) edge. The head difference along the length of the model domain remains 30 m (as in the baseline case).

4.4.2 Heat transport boundary conditions

The thermal balance of the aquifer was reproduced by imposing a constant temperature upper boundary condition of 14°C in slice 1 (model top), since it is recognised that in London the baseline temperatures in the Chalk aquifer are higher than in rural areas.

A constant heat flux boundary condition of 0.06W/m^2 was imposed at the model bottom to represent the geothermal heat flux (the same as for the baseline scenario).

4.4.3 Thermo-hydrogeological model parameters

The geological succession characterising the LB area is summarised in Table 4-4, showing bedrock and their typical thickness. The Cretaceous Chalk Group is overlain by

[24] In particular, Figure 11.

the Palaeogene deposits of Thanet Formation (a fine sand; the Lambeth Group (sands, silts and clays); and Harwich Formation (sands and gravels).

These “Lower London Tertiary” sediments are overlain by the London Clay which forms a low permeability “cap”, confining the Chalk and Lower London Tertiary sandy strata (when these are fully saturated).

Hydraulically significant fractures and fissures are found in the upper part of the Chalk sequence across the London Basin. According to ESI (2010), the thickness of confined Chalk over which significant water bearing fractures are found is typically a few tens of metres and generally no more than 50 m. Thus, a thickness of “upper transmissive Chalk[25]” of 40 m has been selected for this model, beneath which the Chalk is modelled as a low permeability formation.

[25] The terms “upper transmissive Chalk” and “lower permeability Chalk” should not be confused with the (now superseded) stratigraphic convention of dividing the Chalk into Upper, Middle and Lower Chalk.

Table 4-4: Geology of the London Basin (from Ellison, 2004)

Era	Group	Formation	Thickness (m)
Palaeogene	Bracklesham	Barton Sand Bagshot	10–25
	Thames	London Clay (including Claygate Member)	30-90
		Harwich	0-10
	Lambeth	Woolwich and Reading Beds	10-20
		Upnor	5-7
	Montrose	Thanet	0-30
Cretaceous	Chalk		180-245

The hydrogeological settings for this scenario were conceptualised considering the geological succession mentioned above. In some cases the geological layers were simplified and grouped into the same model layers, maintaining the relevant aquifer structures/properties. A summary of the hydrogeological conceptual model and the groundwater model vertical discretisation is provided in Table 4-5 and shown in Figure 4-8.

Table 4-5: Model layers and vertical discretisation for the London Basin scenario.

Formation	Hydrogeological characteristics	Modelled Formation	Thickness (m)
London Clay	Aquitard	Single aquiclude - layer 1 to layer 6	90
Lambeth Group	Aquitard with aquifer horizons		
Thanet Sands	Thin aquifer, in hydraulic continuity with Chalk	Fractured Chalk aquifer - layer 7 to layer 11	40
Upper transmissive chalk	Fractured, fissured aquifer, higher hydraulic conductivity.		
Lower permeability chalk	Lower hydraulic conductivity	Low permeability Chalk aquifer - layer 12 to layer 17	170

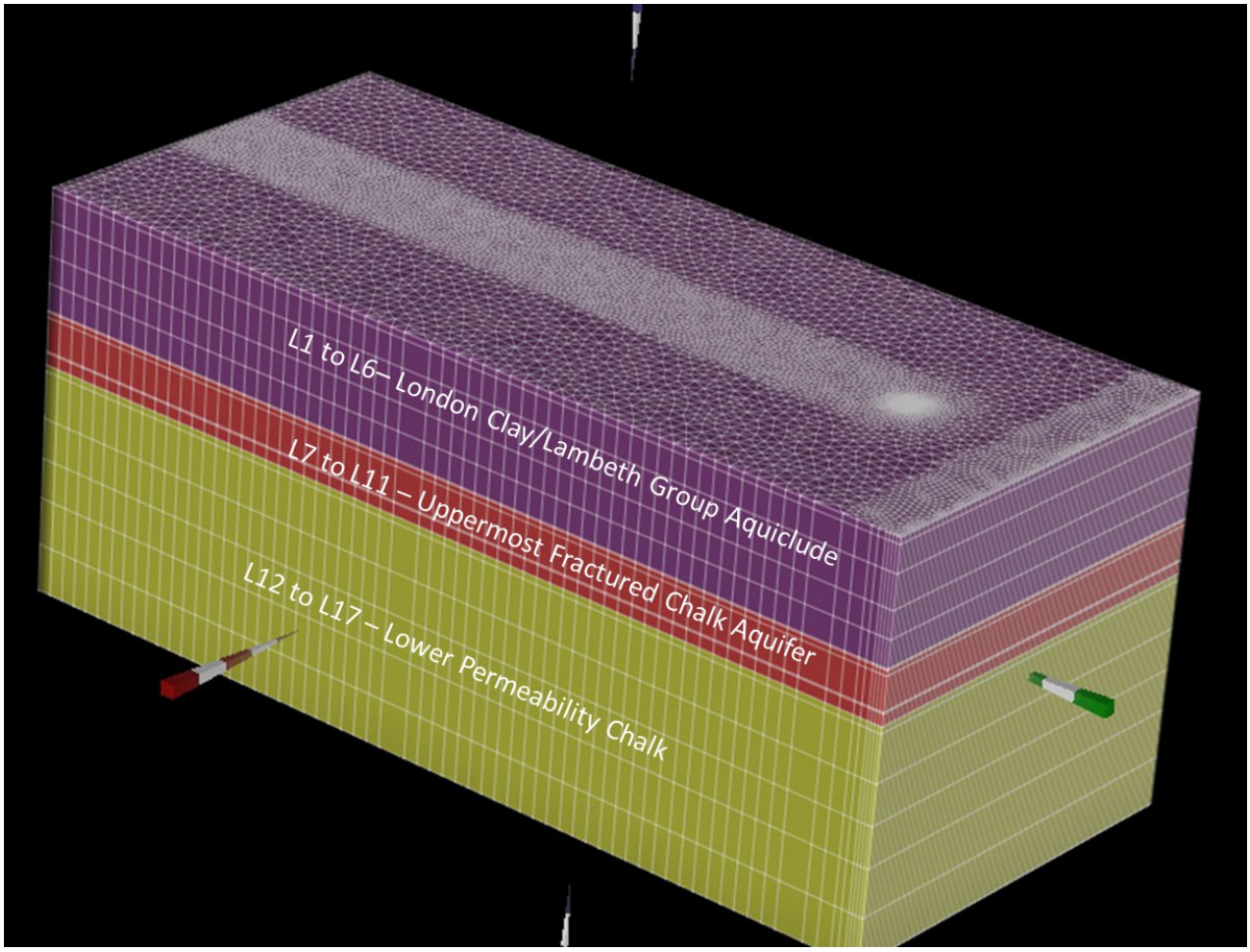

Figure 4-8: Model vertical discretisation and hydrogeological units reproduced in FEFLOW®.

Hydrogeological properties considered for this scenario were assigned based on ranges of values reported in Allen and others (1997) and from previous groundwater models available for the LB area (ESI 2010, 2011). Chalk hydraulic conductivity values were derived considering a total transmissivity for the Chalk group of 405 m^2/d, in-line with average Chalk transmissivities used for the London Basin groundwater model and assuming 80% of Chalk transmissivity occurring in the top 40 m of this formation (ESI, 2010).

The thermo-geological properties applied to the different model layers were also selected following a review of several literature sources (Table 4-6) to identify parameters representative of these formations.

A summary of hydrogeological and geothermal parameters applied to the LB scenario, together with the relevant literature sources consulted, are listed in the table below.

Table 4-6: Hydraulic and thermal properties applied in the LB scenario. L refers to model layers.

Parameter	Model value	Source of information
Bulk saturated thermal conductivity	London Clay/Lambeth Group (L1 to L6) 1.7W/m/K	EED recommended parameters for clay and silt material (EED; Blomberg and others, 2019)
	Chalk (L7 to L16) 1.9W/m/K	Thermal response testing through the Chalk aquifer in London (Loveridge and others, 2013)
Bulk saturated VHC	London Clay/Lambeth Group (L1 to L6) 2.3MJ/m^3/K	EED recommended parameters for clay and silt material (EED; Blomberg and others, 2019)
	Chalk (L7 to L16) 2.6MJ/m^3/K	Waples and Waples (2004)
Hydraulic conductivity	London Clay/Lambeth Group (L1 to L6) Kh=1E-5m/d, Kv=1E-6m/d	ESI (2010, 2011).
	Fractured Chalk (L7to L11) Kh=8m/d Kv=0.8m/d This implies a transmissivity of 40 m x 8 m/d = 320 m^2/d	ESI (2010, 2011).
	Low hydraulic conductivity Chalk (L12 to L17) Kh=0.5m/d Kv=0.05m/d This implies a transmissivity of 170 m x 0.5 m/d = 85 m^2/d	ESI (2010, 2011).

Effective Porosity	London Clay/Lambeth Group (L1 to L6) 2%	Johnson (1967)
	Chalk (L7 to L17) 1%	Allen (1997)
Thermal Dispersity	(L1 to L17) 20m	Domenico & Schwartz (1990)

4.4.4 Scenario results

The lengths of the thermal plume were calculated after 50 years of active BHE operation, at the end last cycle of heat rejection (17,975 days). Model outputs were extracted from slice 8 (95m bgl), to monitor the effects on the upper transmissive chalk layer, and from slice 2 (5m bgl) and slice 4 (50m bgl), to evaluate effects on the aquiclude layer and interaction with the surface.

Thermal plume contour maps, extracted from slice view outputs for this scenario, are reported at 20 years in Figure 4-9 and 50 years in Figure 4-10, and cross sections views are shown in Figures 4-11 and 4-12.

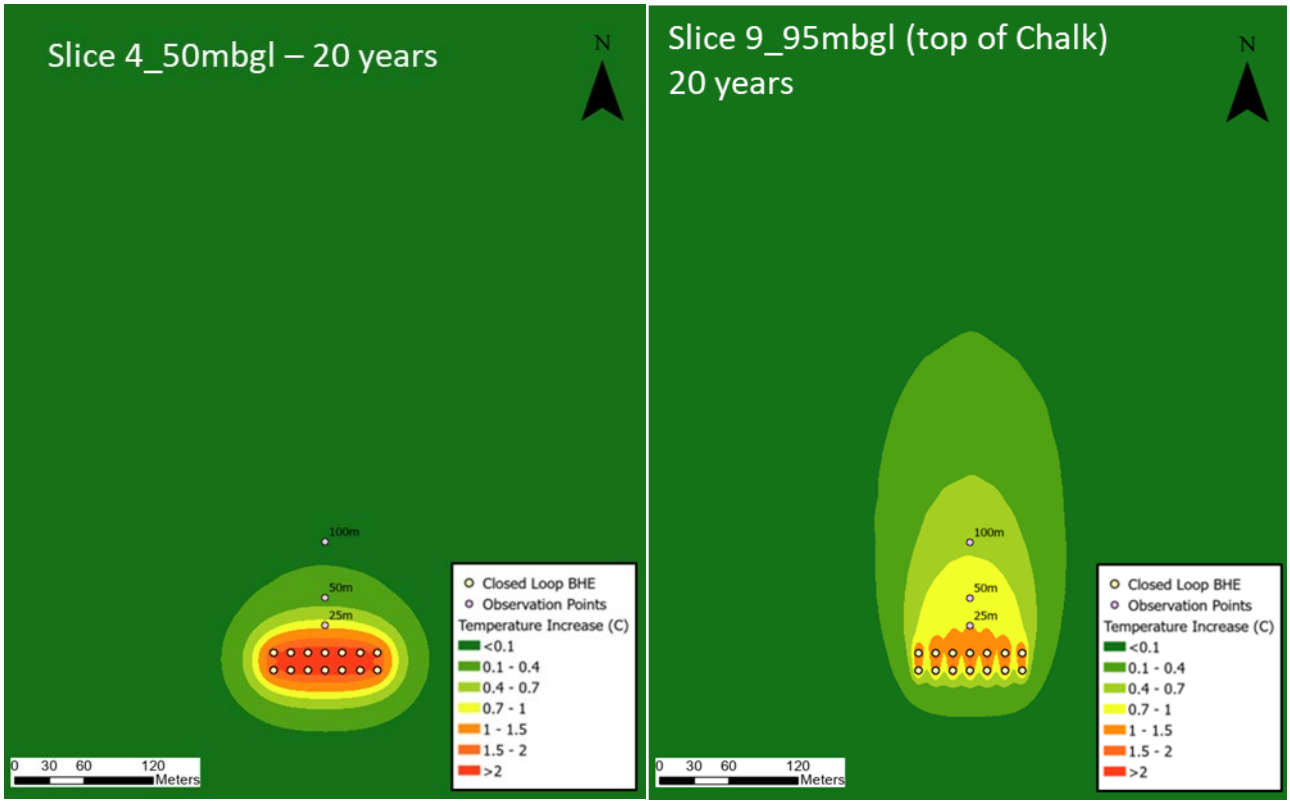

Figure 4-9: Extent and temperature change of the simulated thermal plume after 20 years for the London Basin Scenario at 50mbgl and 95mbgl – the top of the Chalk.

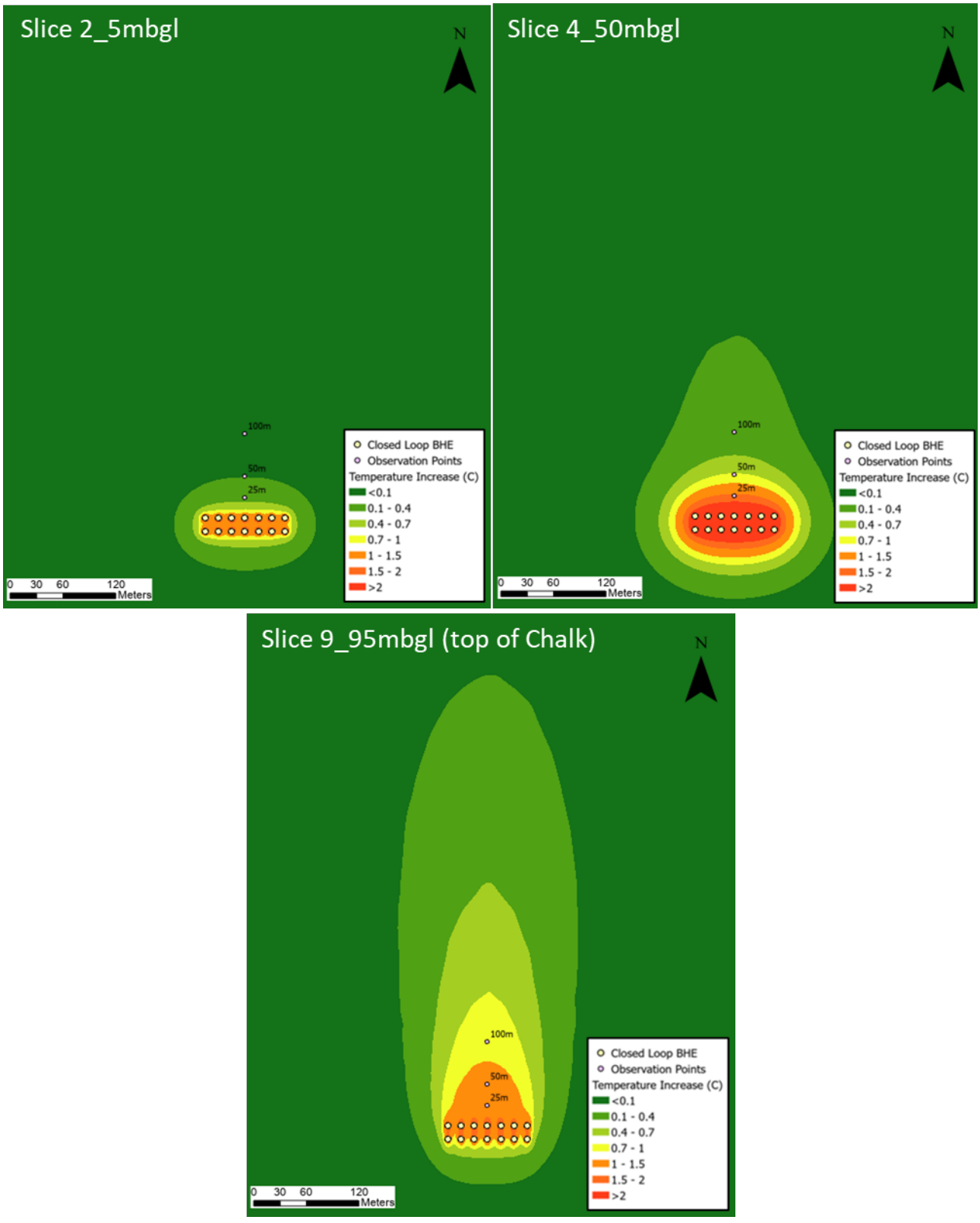

Figure 4-10: Extent and temperature change of the simulated thermal plume after 50 years for the London Basin Scenario at 5m bgl, 50m bgl, 95m bgl (the top of the Chalk)

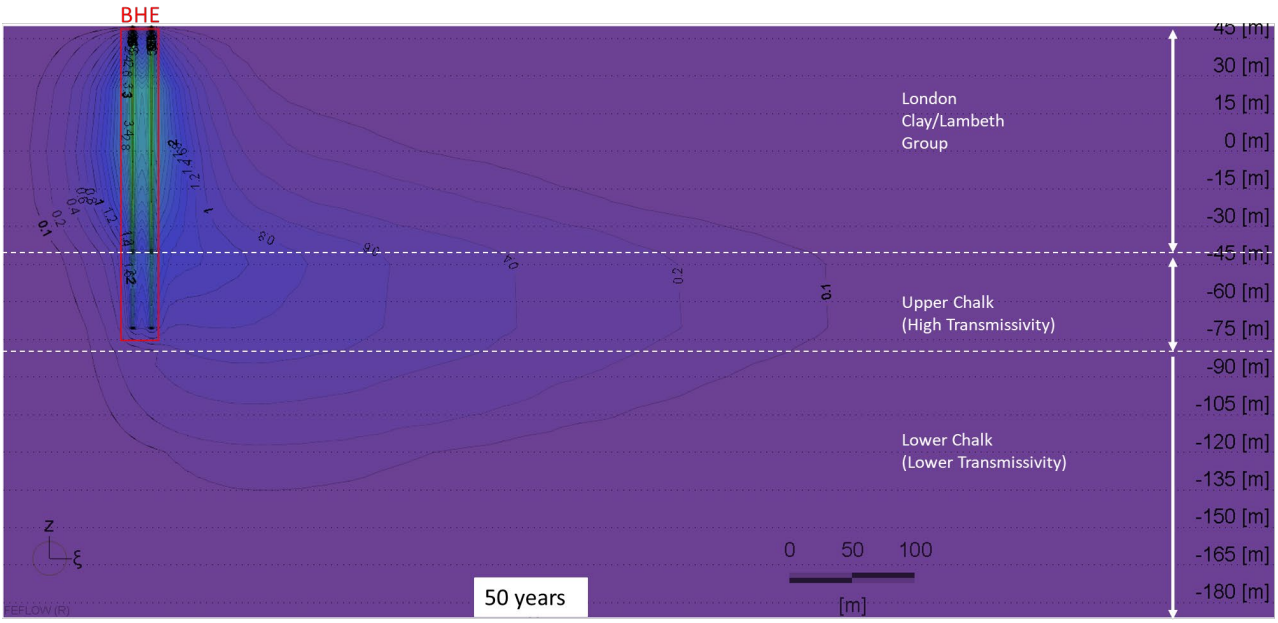

Figure 4-11: Cross section view through the London Basin scenario model showing vertical (z) and longitudinal (ξ) distribution of the thermal plume after 50 years, temperature change from background (∆T °C)shown as iso-contour lines. Scale along right side is m AOD.

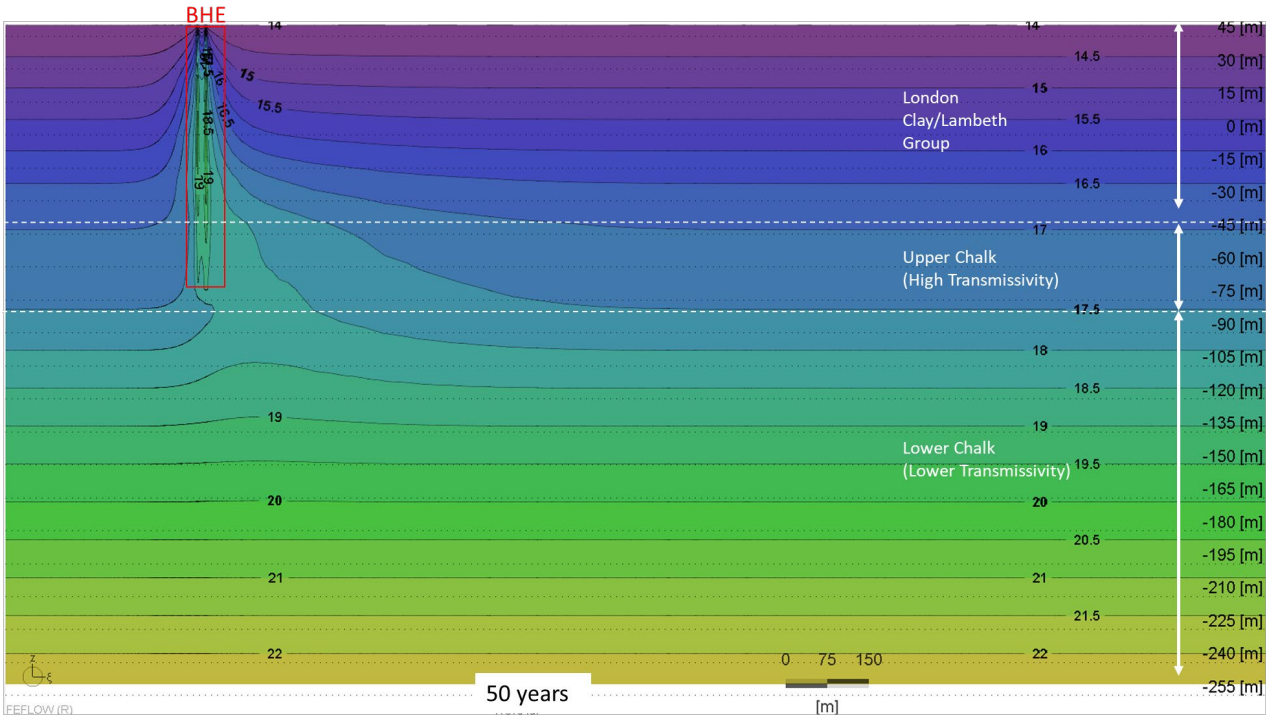

Figure 4-12: Cross section view through the London Basin scenario model showing vertical (z) and longitudinal (ξ) distribution of the thermal plume after 50 years, absolute temperatures (°C) shown as iso-contour lines. Scale along right side is m AOD.

Figure 4-10 shows thermal plume propagation in slice 2 (5m bgl), slice 4 (50m bgl) within the aquiclude layers and for the top of the chalk extracted from slice 9 (95m bgl) after 50 years of BHE operations.

Over 20 years, the thermal plume does not migrate significantly down-gradient within the aquitard layers because of the low Darcy flux (~$3x10^{-8}$m/d). Instead, the heat accumulates around the BHE, forming a slightly elongated, pseudo-elliptical heat core shape (Figure 4-9). However, after 50 years, the thermal plume at 50m bgl shows a more elongated shape, most likely due to the vertical conduction of heat from the thermal plume in the underlying Chalk. The combination of low thermal conductivity and low flow velocity result in a high temperature gradient, with temperature changes of more than 2°C observed in the vicinity of the BHEs in slice 4 (50m bgl), after 50 years. These effects are less prominent in slice 2 (5m bgl) due to vertical conductive heat loss to the surface (i.e. through the constant temperature BC implemented at the top of the model).

On the other hand, a long, relatively narrow thermal plume evolves in the upper transmissive Chalk layer (slice 9 at 95m bgl), due to the higher groundwater flux rate (~0.03 m/d) as shown in Figure 4-11. Temperature gradients produced by the BHE smooth with depth and isocontour lines stretch along the groundwater flow direction, within the Chalk layers characterised by higher transmissivity (-40m AOD to -80m AOD).

Figures 4-13, 4-14 and 4-15 show temperature change from initial conditions at 5m, 50m and 95 mbgl over 50 years at observation points 25m, 50m, 100m downstream of the BHE.

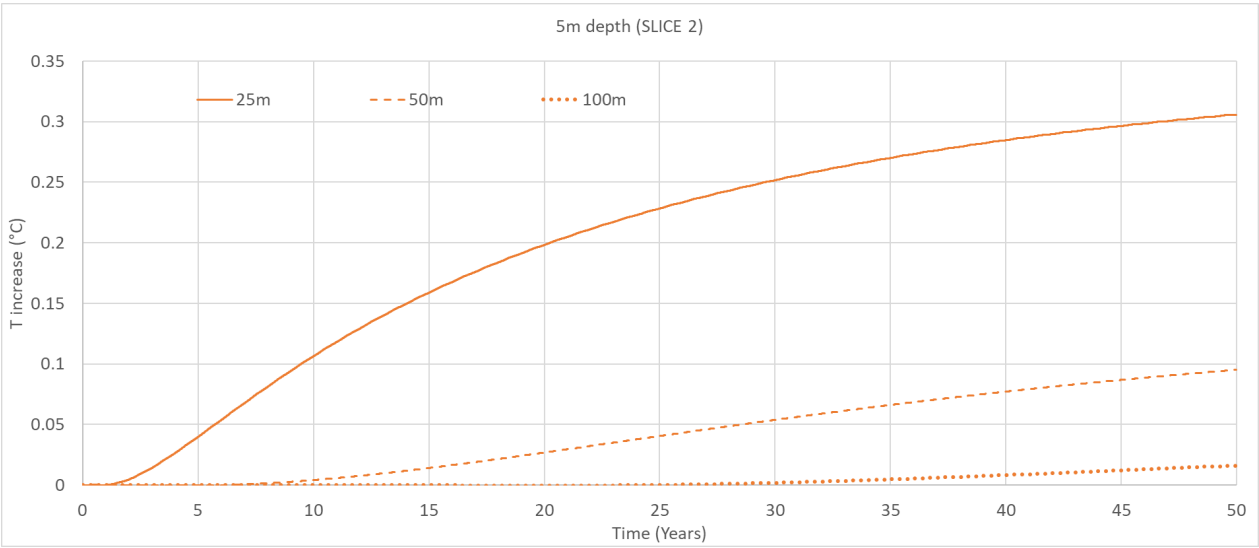

Figure 4-13: Change in temperature (∆T) from initial conditions during the operational period (50 years) of the BHE array for London Basin scenario at slice 2 (5m bgl).

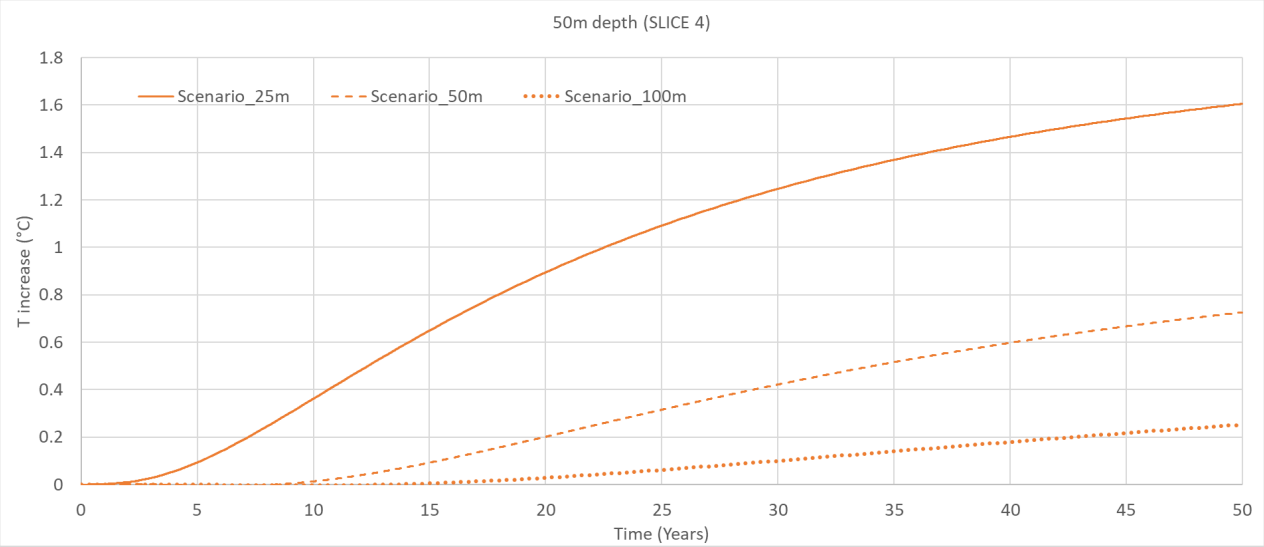

Figure 4-14: Change in temperature (ΔT) from initial conditions during the operational period (50 years) of the BHE array for London Basin scenario at slice 4 (50mbgl)

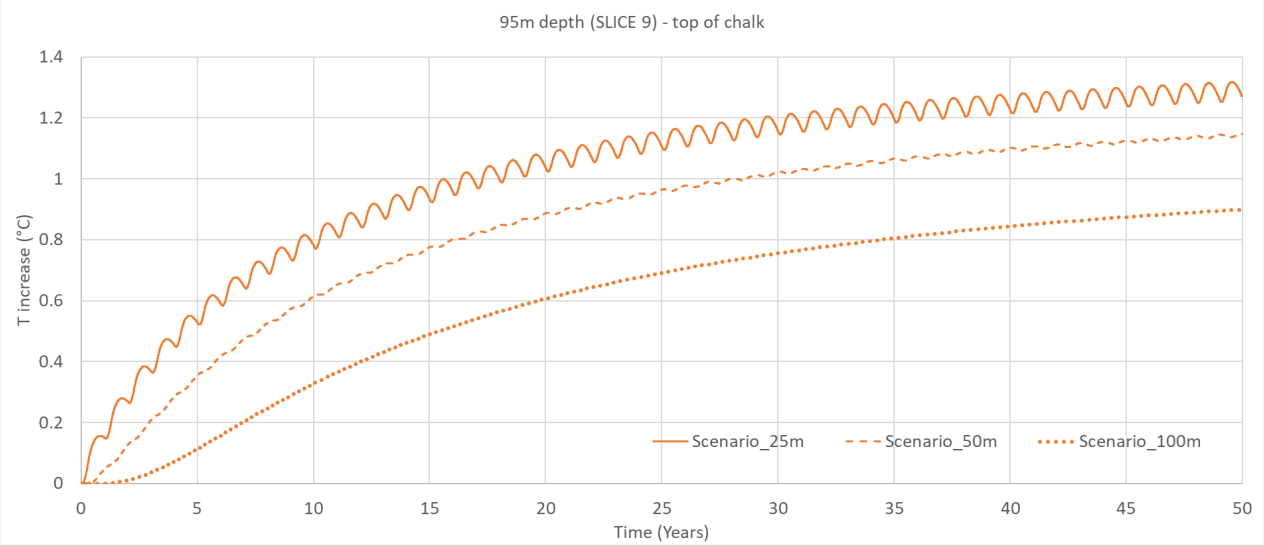

Figure 4-15: Change in temperature (ΔT) from initial conditions during the operational period (50 years) of the BHE array for London Basin scenario at slice 9 (95mbgl, top of the Chalk)

Thermal plume length and temperatures simulated after 50 years, are summarised in the following table.

Table 4-7: Thermal plume length and temperature changes at observation BH after 50 years for the London Basin scenario.

50 years simulation time	Plume length, 1°C ΔT	ΔT observed at 25 m distance	ΔT observed at 50 m distance	ΔT observed at 100 m distance
5m depth (Slice 2)	~6m	~0.3°C	~0.1°C	<1°C
50m depth (Slice 4)	~42m	~1.6°C	~0.8°C	~0.4°C
95m depth (Slice 9)	~80m	~1.2°C	~1.1°C	~0.9°C

4.5 Mudrock aquitard (Mercia Mudstone Group)

A scenario was set to investigate impacts from closed-loop BHE systems installed in mudstone/siltstone aquitards and similar lithologies. Reference values used for the thermal and hydraulic parametrisation in this scenario were based on values given for the Mercia Mudstone Group (MMG), widespread across England. Groundwater model settings and results for these scenarios are described in the following sections.

The BHE system capacity, array geometry and the yearly operational cyclicity were the same as the baseline scenario outlined in Section 3.3.2, assuming maximum heat rejection rate of 45kW (with peak load 1080kWh/d), for 3 months/year (2160 FLEQ), delivering a net discharge of heat to the aquifer equals to 97.2MWh/year.

4.5.1 Model dimensions and hydraulic boundary conditions

Model dimensions and vertical discretisation applied for this scenario are the same as those used for the baseline scenario (Section 3.3.1.), without any adjustments to the model layering.

The water table varied from 0 to 30m bgl, with partially saturated top layers and variable unsaturated thicknesses across the model domain (approximately 5m at the BHE array location) to simulate common MMG conditions. The regional groundwater flow was reproduced by assigning constant hydraulic head values on the southern edge (upgradient) of 50m AOD and of 20m AOD to the northern (downgradient) edge. The head difference along the length of the model domain was 30 m (as in the baseline case).

4.5.2 Heat transport boundary conditions

The same heat transport boundary conditions as in the baseline model were used in the mudrock scenario, imposing

- a constant temperature upper boundary condition of 10.5°C in Slice 1 to simulate annual average soil temperature, and
- a constant heat flux boundary condition of 0.06W/m^2 on the model bottom to simulate the geothermal heat flux.

4.5.3 Thermo-hydrogeological model parameters

The thermal and hydraulic properties used in the model were selected following a literature review to confirm the range of values representative of similar lithologies. This scenario represented a single lithology, with the same set of properties assigned to all the model layers, without any vertical discretisation of either thermal or hydrogeological parameters.

The EED recommended bulk volumetric heat capacity value for siltstone materials is 2.3MJ/m^3/K (EED; Blomberg and others, 2019), in line with the range of values provided by BGS (Parkes and others, 2021), resulting from geothermal testing performed on MMG. The same literature sources (EED; Blomberg and others, 2019, Parkes and others, 2021) suggest bulk thermal conductivity equal to 2.1W/m/K for the MMG. These values were implemented in the heat transport model.

Hydrogeological parameters assigned to the groundwater model, were selected based on BGS reports and other literature sources (Armitage and others, 2016) that provide a range of values determined for the Mercia Mudstone Group. Hydraulic conductivity of 0.01m/d and effective porosity of 9% fits with the range of data available in literature for this formation.

A summary of hydrogeological and thermal parameters applied in this scenario, together with the relevant literature sources, are listed in the table below.

Table 4-8: Hydraulic and thermal properties used for the mudrock aquitard scenario.

Parameter	Model value	Source of information
Bulk saturated thermal conductivity	2.1W/m/K	(EED; Blomberg and others, *2019;* Parkes and others, 2021*)*
Bulk saturated VHC	2.3MJ/m^3/K	(EED; Blomberg and others, 2019; Parkes and others, 2021)
Hydraulic conductivity	Kh=0.01m/d, Kv=0.001m/d	(Armitage and others, 2016)
Effective porosity	9%	(Armitage and others, 2016)
Thermal dispersivity	20m	(De Marsily, 1986)

4.5.4 Scenario results

The length of the thermal plume was calculated after 50 years of BHE operation, at the end of the last cycle of heat rejection (17,975 days). Model outputs were extracted from slice 4, at 50% of total BHE installation depth (60m bgl), and from slice 2 (5m bgl) to evaluate interaction with surface.

Thermal plume contour maps, for slice 2 (5mbgl) and slice 4 (60mbgl) outputs for this scenario, are shown in Figure 4-16 after 50 years.

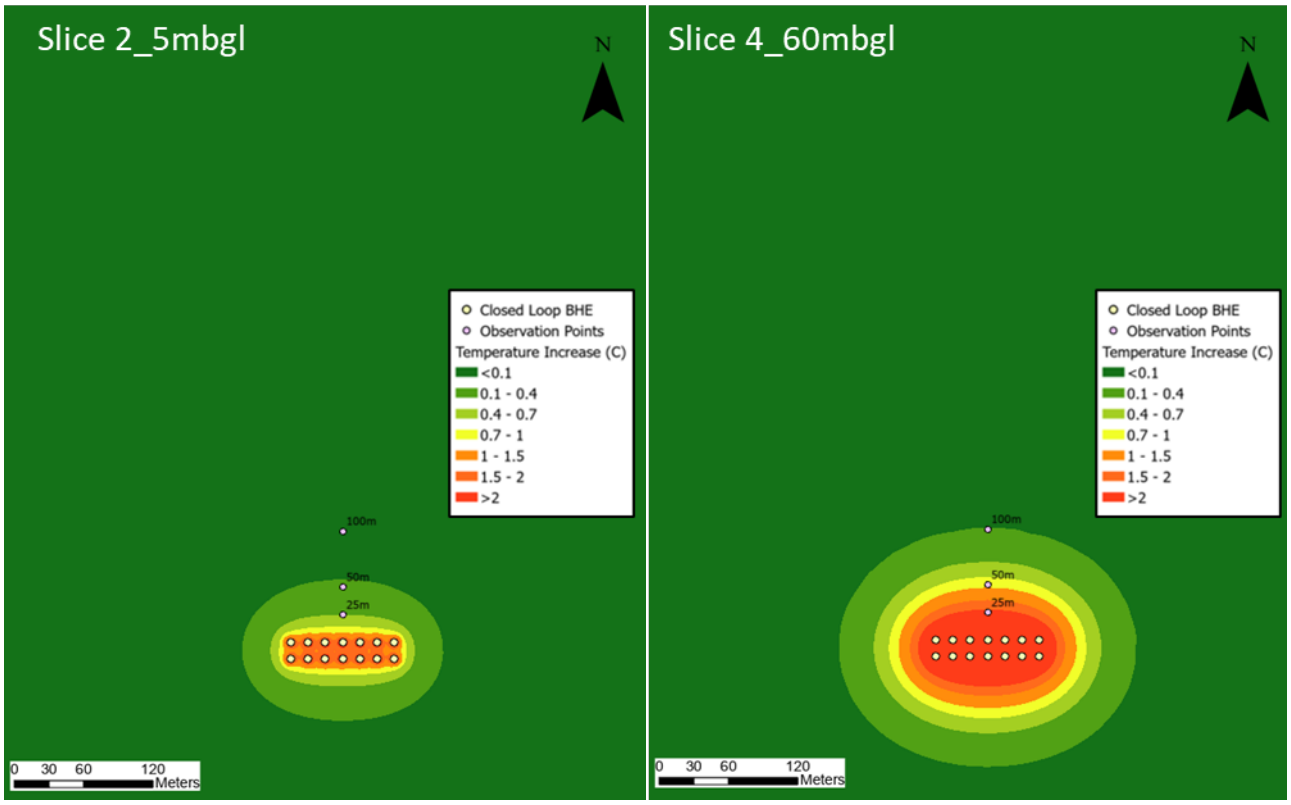

Figure 4-16: Extent and temperature change of the simulated thermal plume after 50 years for the Mudrock scenario at 5m bgl and 60mbgl.

As highlighted in Figure 4-16, due to the negligible Darcy flux in this simulation (~0.00003m/d), the heat generated by the closed-loop system accumulates in a pseudo-elliptical area around the BHE array and does not migrate substantially down-gradient within the timeframe of the model (50 years). This results a thermal “halo” around the BHE array and negligible thermal plume propagation with groundwater flow. Heat accumulates in the vicinity of the BHEs, resulting in a noticeable temperature alteration (considering 1°C temperature change threshold) up to 45 m distance from the BHE area in slice 4 (60mbgl). These effects are smaller in slice 2 (5mbgl) due to vertical conductive heat loss through the surface (constant temperature boundary condition implemented at the top of the model).

Temperature change (ΔT) from starting conditions at observation BH 25m, 50m, 100m downstream of the BHE over the 50 years of operations is shown in time series on Figures 4-17 and 4-18 for slices 2 and 4.

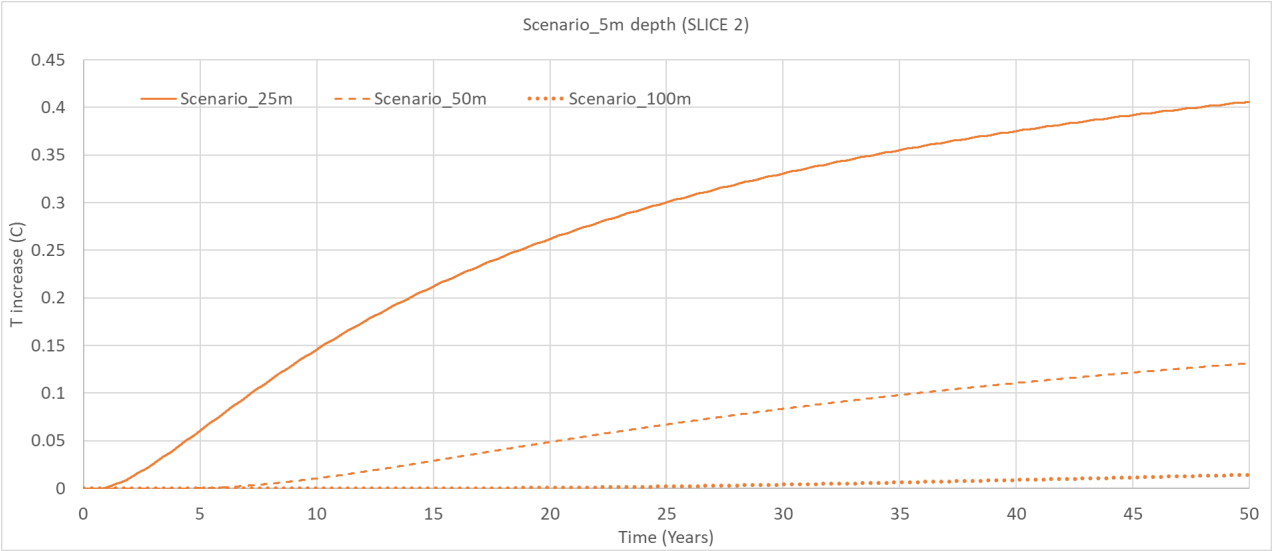

Figure 4-17: Change in temperature (∆T) from initial conditions during the operational period (50 years) of the BHE array for the Mudrock scenario at slice 2 (5m bgl).

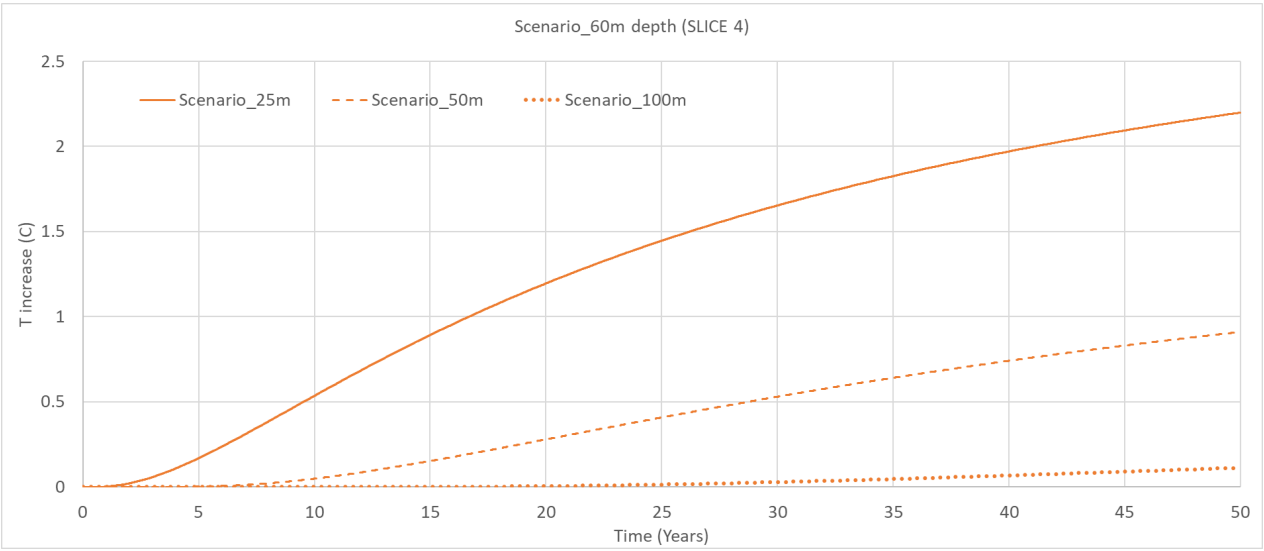

Figure 4-18: Change in temperature (∆T) from initial conditions during the operational period (50 years) of the BHE array for the Mudrock scenario at slice 4 (60m bgl).

The times series shows that the temperatures do not reach steady-state conditions at any of the observation BH after 50 years of heat injection activities. Annual fluctuations resulting from annual BHE operational cyclicity are already effectively “damped” by 25 m distance. These results show that for the mudrock scenario, the temperature increases approximately by 0.4 °C at 25m distance from the BHEs in slice 2 and by 2.2 °C at 25m in slice 4 after 50 years. A summary of the results for the thermal plume (or, in this case, “halo”) length and temperature build up simulated after 50 years, are summarised in the table below.

Table 4-9: Thermal plume length and temperature changes at observation BH after 50 years for the Mudrock scenario.

50 years simulation time	Plume length (slice 4), 1°C ΔT	ΔT (°C) observed at 25 m distance	ΔT (°C) observed at 50 m distance	ΔT (°C) observed at 100 m distance
5m depth (Slice 2)	~9m	~0.4°C	~0.1°C	<0.1C
60m depth (Slice 4)	~45m	~2.2°C	~0.9°C	~0.1°C

4.6 Fluvial sand and gravel aquifer

A GSHC system was simulated in a fluvial sand and gravel aquifer underlain by clay, to evaluate the long terms impacts posed by BHE operations on similar superficial aquifers. Model settings and results for these scenarios are described in the following sections.

The BHE system capacity, the array geometry and the yearly operational cyclicity are the same as for the baseline scenario, as outlined in Section 3.3.2, assuming maximum heat rejection rate of 45kW (equivalent to 1080 kWh/d), for 3 months/year (2160 FLEQ), delivering a net discharge of heat to the aquifer equals to 97.2MWh/year.

4.6.1 Model dimensions and hydraulic boundary conditions

Model dimensions and discretisation applied for this scenario are the same as for the baseline scenario (Section 3.3.1), however the vertical discretisation and the model layering was adjusted to reflect the hydrogeological settings relevant to this scenario. The conceptual model for this case assumes a 35 m thick sand and gravel aquifer, underlain by a clay aquiclude of 270m thickness as shown in the following figure.

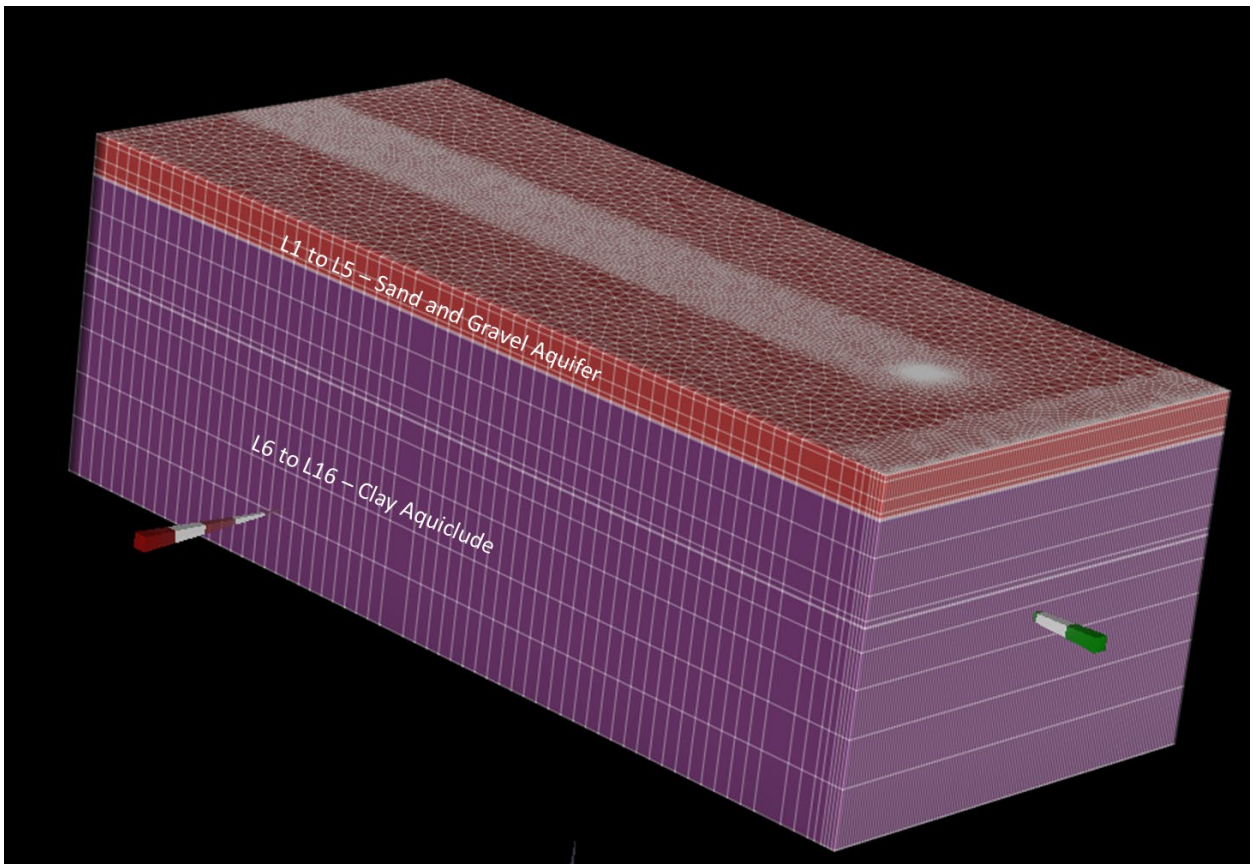

Figure 4-19: Model vertical discretisation and hydrogeological units reproduced in FEFLOW for a sand and gravel aquifer. Green arrow indicates upgradient (northern) boundary.

For cases of fluvial sand and gravel shallow aquifers, the water table would typically be close to the surface, following the hydraulic gradient imposed by nearby rivers. To reproduce a similar scenario, i.e. to represent saturated conditions to the aquifer and apply an effective hydraulic gradient across the model domain, regional groundwater flow was reproduced by assigning constant hydraulic head BC values of 80m AOD on the southern (upgradient) model edge and of 50m AOD on the northern (downgradient) edge.

4.6.2 Heat transport boundary conditions

The same heat transport boundary conditions/settings adopted in the baseline model were maintained in the current scenario:

- a constant temperature upper boundary condition of 10.5°C in Slice 1 to simulate annual average soil temperature, and
- a constant heat flux boundary condition of 0.06W/m^2 on the model bottom to simulate the geothermal heat flux.

4.6.3 Thermo-hydrogeological model parameters

The geothermal and hydraulic properties implemented in the model were selected following a literature review to confirm the range of values representative of similar lithologies.

The bulk saturated VHC applied in the model were selected from the EED database and Waples and Waples (2004), that suggested 2.5MJ/m³/K for sand and gravels and 2.3MJ/m³/K for clay/silt material. Bulk saturated thermal conductivities were set to 1.7W/m/K for silt/clay strata and 2.4W/m/K for the sand and gravel aquifer (MCS 2011, EED; Blomberg and others, 2019).

Hydraulic conductivity and effective porosity were selected from a (wide) range of values recorded in literature for similar materials, assigning hydraulic conductivity of 30m/d and 25% effective porosity for the sand and gravel aquifer, and a hydraulic conductivity of $1x10^{-5}$m/d and 5% effective porosity for clay/silt layers (Kruseman & de Ridder, 2000).

A summary of hydrogeological and geothermal parameters applied to the scenario, together with the relevant literature sources consulted, are listed in Table 4-10.

Table 4-10: Hydraulic and thermal properties used for the fluvial sand and gravel aquifer scenario.

Parameter	Model Value	Source of information
Bulk saturated thermal conductivity	Sand and gravel aquifer (L1 to L5) 2.4(W/m/K) Clay/silt aquiclude (L6 to L16) 1.7 (W/m/K)	EED, MCS (2011), Blomberg and others. (2019)
Bulk saturated VHC	Sand and gravel aquifer (L1 to L5) 2.5 (MJ/m³/K) Clay/silt aquiclude (L5 to L16) 2.3 (MJ/m³/K)	EED, Waples & Waples (2004), Blomberg and others. (2019)
Hydraulic conductivity	Sand and gravel aquifer (L1 to L5) Kh=30m/d, Kv=Kh/10 Clay/Silt aquiclude (L6 to L16) Kh=1E-5m/d, Kv=Kh/10	Kruseman & de Ridder (2000)
Effective porosity	Sand and gravel aquifer 25% Clay/silt aquiclude 2%	Kruseman & de Ridder (2000)
Thermal dispersivity	20m	De Marsily (1986)

4.6.4 Scenario Results

The length of the thermal plume were calculated after 50 years of BHE operation, at the end of the last cycle of heat rejection (17,975 days). Model outputs were extracted from slice 2 (5mbgl) and slice 3 (20mbgl), to evaluate the effect with the aquifer and interaction with the surface, and from slice 6 (65mbgl) to estimate the plume within the aquitard layer.

Thermal plume contour maps, extracted from slice view outputs for this scenario, are reported in Figure 4-20, and a cross section view with temperature distribution after 50 years is shown in Figures 4-21 and 4-22.

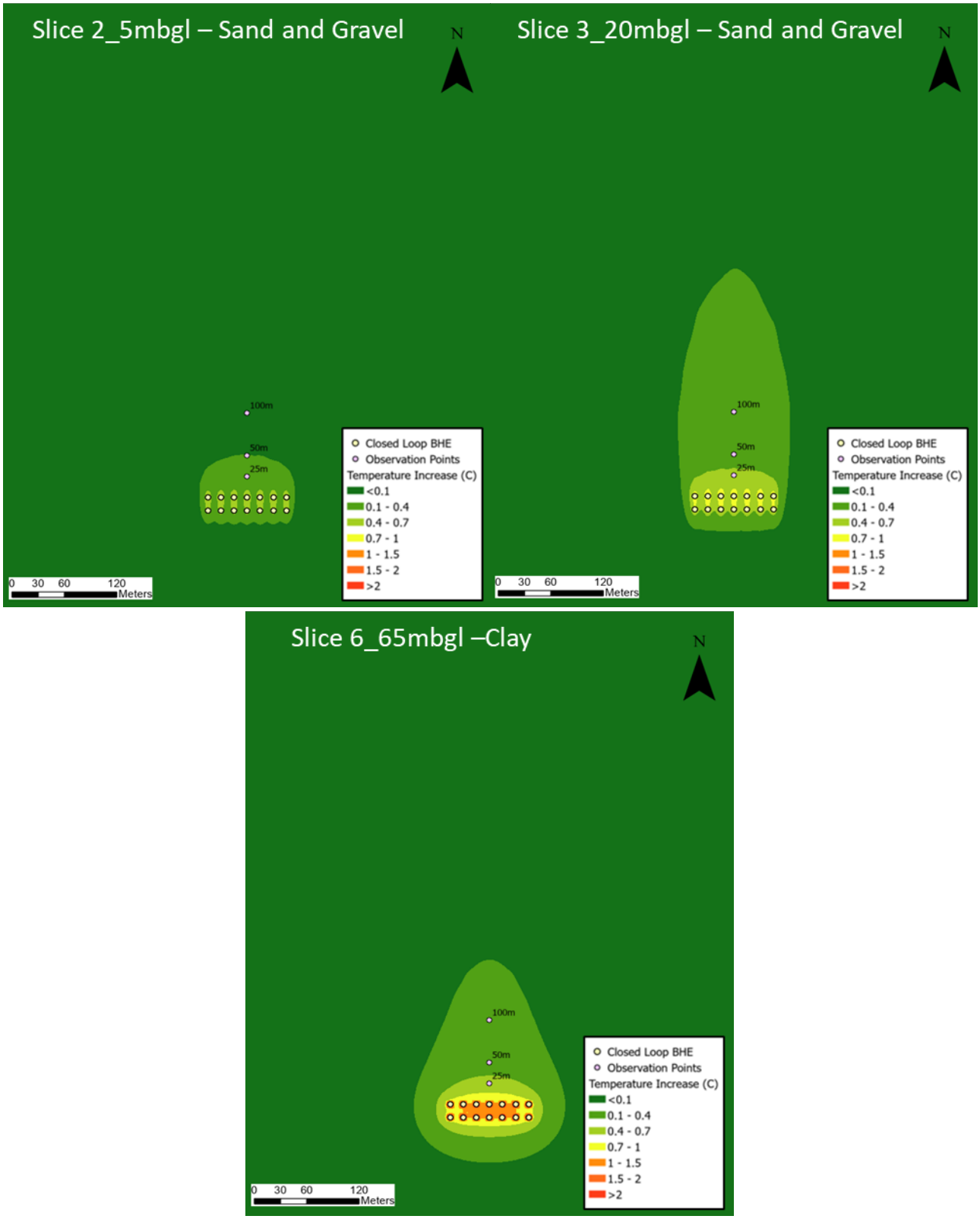

Figure 4-20: Extent and temperature change of the simulated thermal plume after 50 years for the sand and gravel aquifer scenario at 5, 20 and 65m bgl.

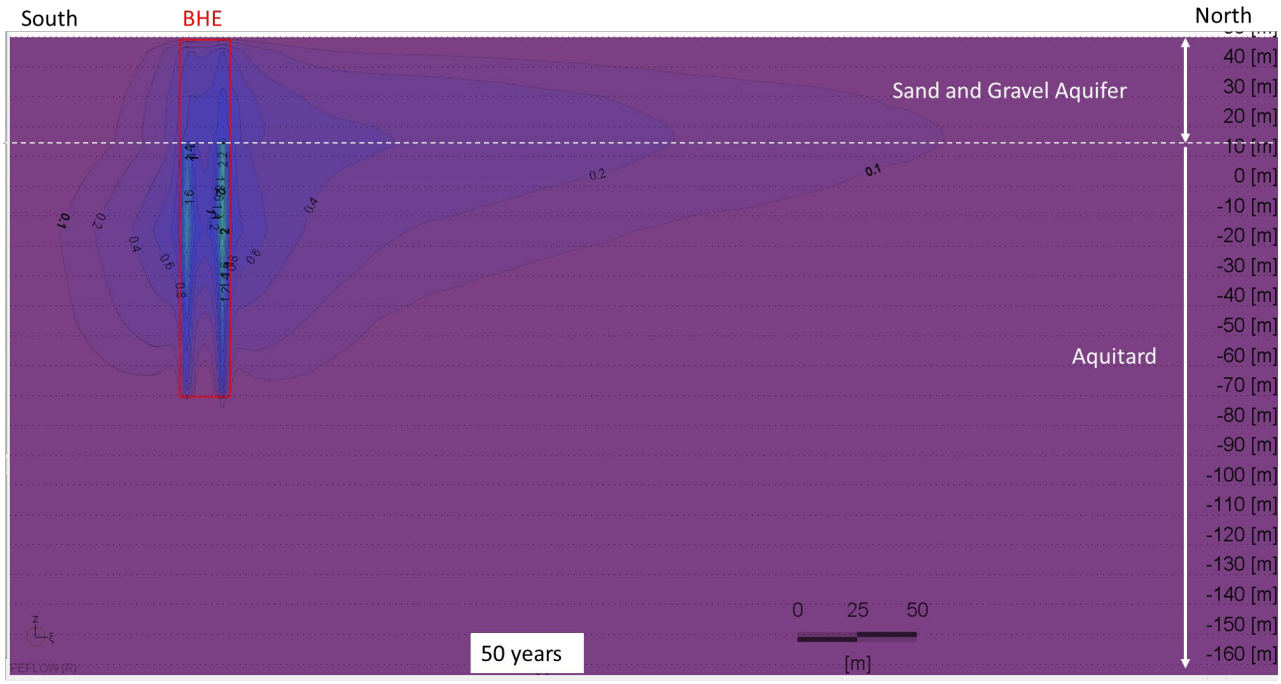

Figure 4-21: Cross section view through the sand and gravel aquifer scenario model showing vertical (z) and longitudinal (ξ) distribution of the thermal plume after 50 years, temperature change from background (∆T °C)shown as iso-contour lines. Scale along right side is m AOD.

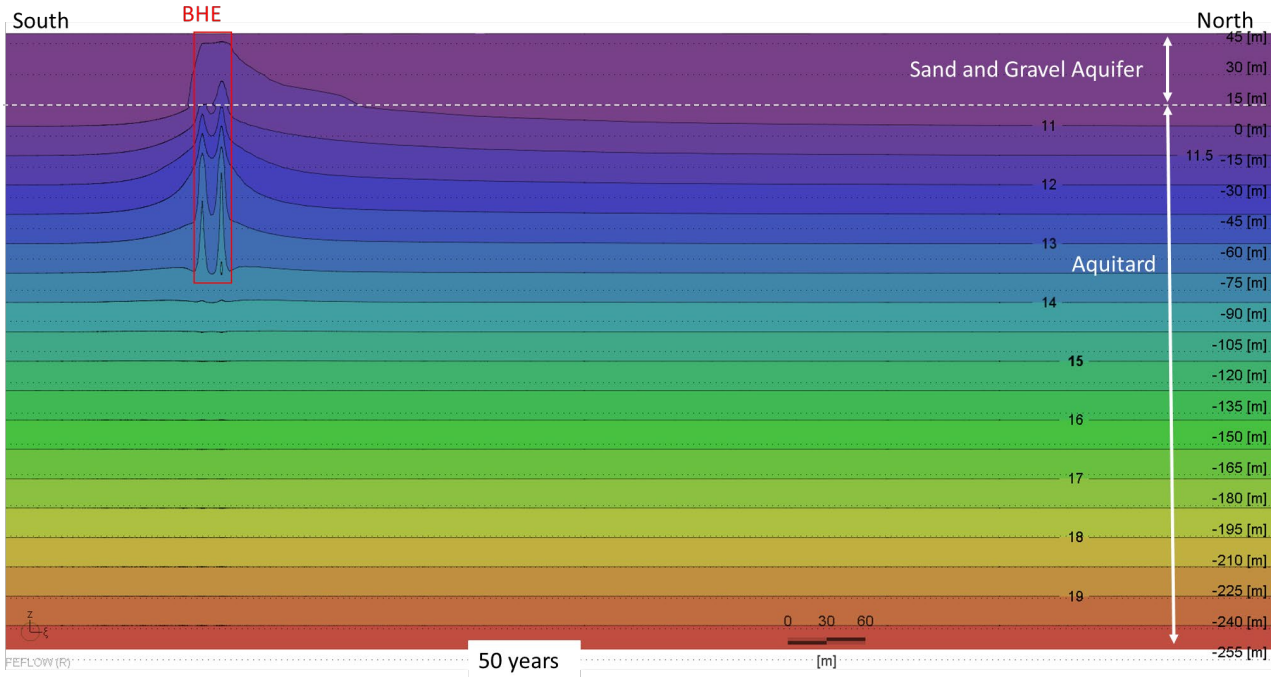

Figure 4-22: Cross section view through the sand and gravel aquifer scenario model showing vertical (z) and longitudinal (ξ) distribution of the thermal plume after 50

years, absolute temperatures (°C) shown as iso-contour lines. Scale along right side is m AOD.

Results illustrated in Figure 4-20 provide an overview of thermal plume propagation at different depths and through the different lithologies as a result of an active BHE system, rejecting heat to the aquifer for 50 years. Due to the high Darcy flux in the sand and gravel aquifer (~0.1m/d), dilution and dispersion along the flow direction strongly attenuate the temperature of the plume. Taking a 1°C temperature change to delineate the thermal plume, the potential thermal "impact" within the top 20 m of the aquifer is minimal.

Higher temperature gradients were simulated close to the BHE within the aquiclude layer (Slice 8, 65m bgl) where the negligible groundwater flow results in a wider thermal "halo" around the BHE array. However, the thermal plume (as defined by a 1°C temperature change), does not exceed 10 m along the flow direction after 50 years. A slightly elongated plume within the aquitard is apparent when considering the contours of 0.1°C temperature change; it seems likely that this may reflect downward conduction of heat from the plume in the overlying sand and gravel.

Temperature time series are shown in Figures 4-23, 4-24 and 4-25. These charts show the temperature time series, extracted from observation points located downstream the BHE at various distance (25m, 50m, 100m) in slice 2, slice 3 and slice 8, processed in terms of temperature increase (ΔT) from starting conditions. Note that on Figure 4-22 a comparison with available case study data has been made. This is discussed in Section 4.6.5.

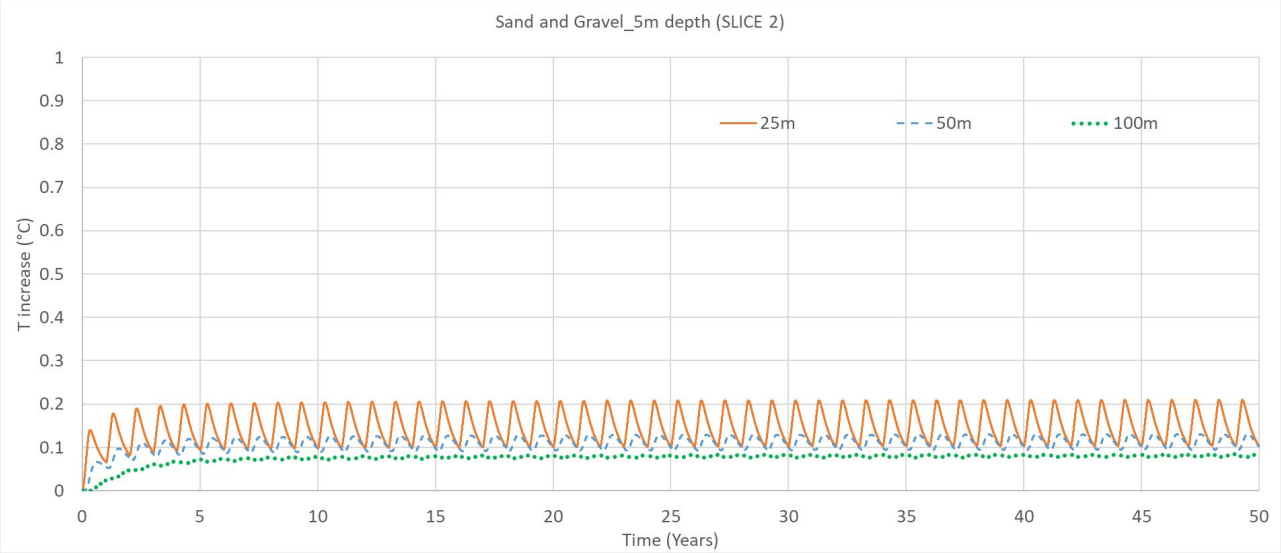

Figure 4-23: Change in temperature (ΔT) from initial conditions during the operational period (50 years) of the BHE array for the sand and gravel aquifer scenario at slice 2 (5m bgl).

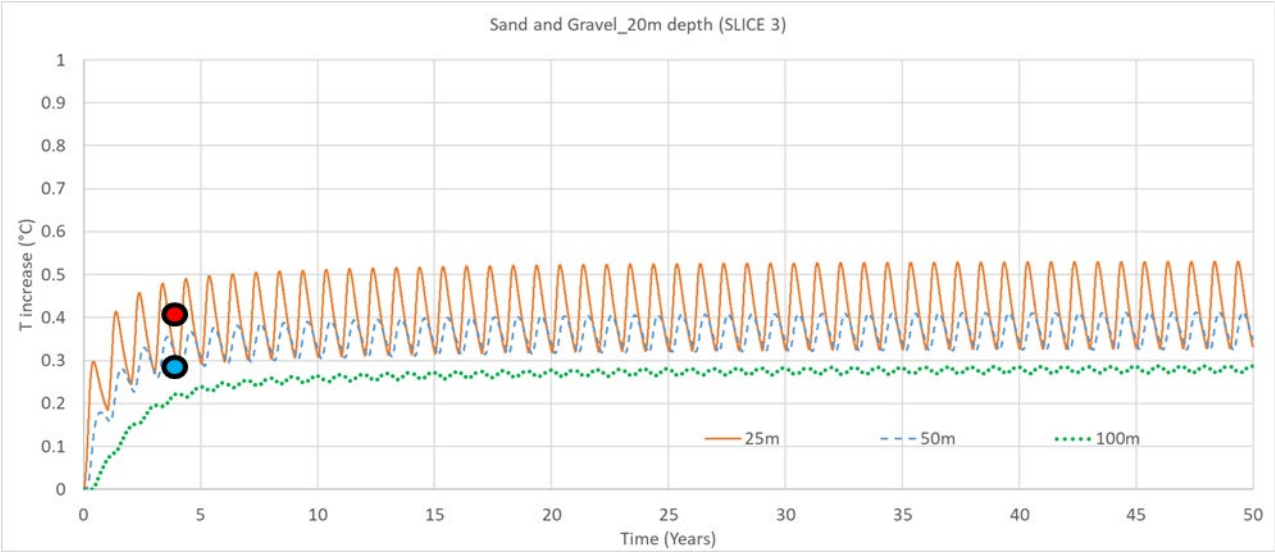

Figure 4-24: Change in temperature (ΔT) from initial conditions during the operational period (50 years) of the BHE array for the sand and gravel aquifer scenario at slice 3 (20m bgl). Red and blue circles discussed in Section 4.6.5.

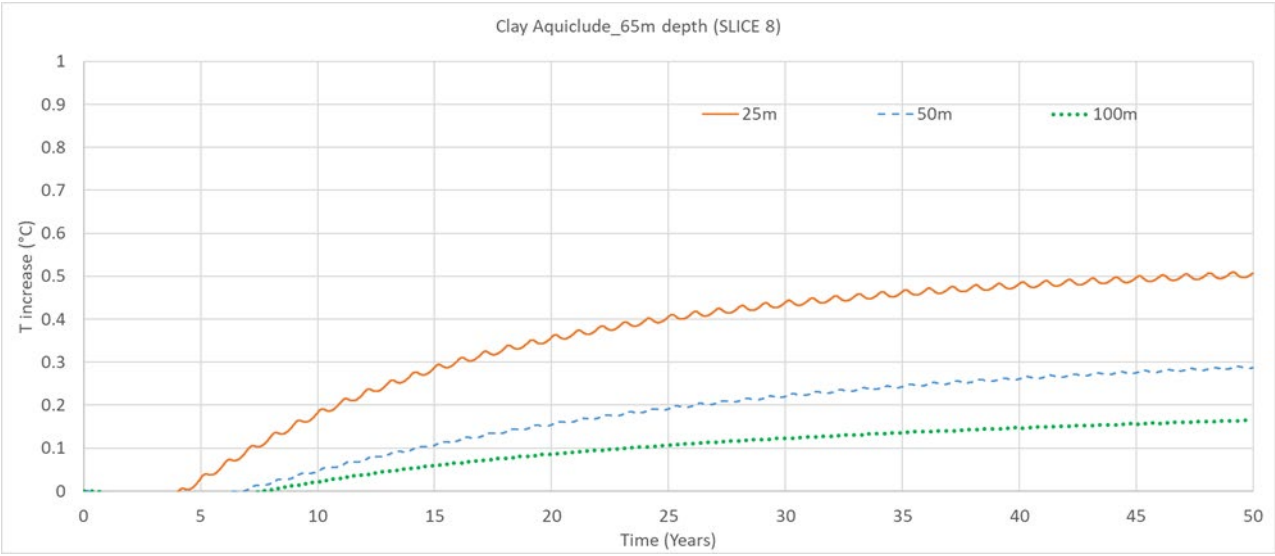

Figure 4-25: Change in temperature (ΔT) from initial conditions during the operational period (50 years) of the BHE array for the sand and gravel aquifer scenario at slice 8 (65m bgl).

The results show that temperature time series within the sand and gravel aquifer reach steady-state conditions quicker than the clay/silt aquiclude layer.

A summary of the results for the thermal plume length and temperature change from initial conditions after 50 years is given in Table 4-11.

Table 4-11: Thermal plume lengths and temperature changes for the sand and gravel aquifer scenario after 50 years of heat rejection.

50 years simulation time	Plume length, 1°C ΔT	ΔT observed at 25 m distance	ΔT observed at 50 m distance	ΔT observed at 100 m distance
5m depth (Slice 2)	<1m	~0.2°C	~0.1°C	<0.1°C
20m depth (Slice 3)	<1m	~0.5°C	~0.4°C	~0.3°C
65m depth (Slice 6)	~5m	~0.5°C	~0.3°C	~0.2°C

4.6.5 Comparison with case study data (Meng and others, 2018)

Meng and others (2018) is the only case study with available data suitable for comparison with the modelling reported here. Meng and others (2018) report a thermal plume temperature of 0.4°C after 4 years of operation at a distance of 75m downgradient of a series of 51 GSHCs (47 BHEs and 4 open loop systems) in a fluvial sand and gravel aquifer in the city of Cologne, Germany. This compares with a modelled value in the most similar scenario modelled for this study of 0.3°C at the same distance after the same period of time.

The main differences between the Meng and others (2018) case study and the model constructed for this report are that, in Cologne:

- There are more GSHC systems overall;
- Not all of them are closed loop (47 out of 51);
- The majority of BHEs are single well installations;
- Overall system capacity is ~1200 MWh/yr; and,
- GSHC are distributed over a larger area than modelled for the scenario run for this report.

So, in comparison to the model presented here, the Cologne study has a greater system capacity over a greater area. Whilst not strictly comparing like with like, the correlation in findings is nonetheless relatively close. This suggests that the modelling is relevant for drawing broader conclusions regarding the processes under consideration.

4.7 Conservative / worst case scenario

A final scenario implemented a combination of model parameters and operational settings to maximise thermal impacts from the BHE array.

Model parameter values and BHEs settings were informed by the sensitivity analysis, with a focus on those parameters having the strongest influence on thermal plume dimensions, namely a relatively low Darcy flux (but still capable of generating a thermal plume), poor thermal conductivity (high concentration of heat) and high heat injection rate (a large source term). Note that Darcy flux (i.e. groundwater flow) was intended to reduce dispersal of a plume (which has the effect of reducing temperature), whilst still allowing some flow to occur to allow heat to migrate downgradient to a potential receptor.

The groundwater model applied for this scenario uses the same model geometry used for the baseline model. The parameters for this scenario were applied equally to the all model layers, these are summarised in Table 4-12.

Table 4-12: Summary of model settings and parameters applied for conservative / worst case scenario.

Parameters	Value
Closed-loop BHE System peak heat rejection rate	200kW = 4800 kWh/day
Closed-loop BHE System operational cyclicity	Heat Injection, 4800 kWh/d for 4.5 months continuously, total 648MWh/year. This represents a protracted summer cooling load being rejected to the ground
BHE number, length and spacing	n.70 BHE installed to 90m depth (peak heat exchange rate of 32W/m) 15m spacing
Head boundary conditions (Head BC)	Head BC for inner southern model edge=80m Head BC for outer model northern edge =50m
Thermal boundary conditions	Constant temperature boundary (Slice1) =10.5°C Constant heat flux boundary (Slice14) =0.06W/m^2
Bulk saturated thermal conductivity (λ)	1.5W/m/K
Bulk saturated VHC (ρc)	1.9MJ/m^3/K
Matrix thermal conductivity (λ_s) which yields saturated thermal conductivity	1.51W/m/K
Matrix volumetric heat capacity ($\rho_s c_s$) which yields saturated volumetric heat capacity	1.88MJ/m^3/K
Hydraulic conductivity ($K_{x,y,z}$) in the x, y, z directions	K_h=1 (m/d) Layer 2 to 13, Kh=0.1 (m/d)

Hydraulic gradient (i)	0.0033
Darcy flux (vD)	0.003m/d
Effective porosity (ne)	1%
Longitudinal thermal dispersity (αL) and Transversal thermal dispersivity (αT)	10m, 1m

The length of the thermal plume was calculated after 50 years of BHE operation, at the end last cycle of heat rejection (17,975 days). Model outputs were extracted from slice 2 (5mbgl), and from slice 4 (60mbgl).

Thermal plume contour maps, extracted from slice view outputs for this scenario, are reported in Figure 4-26. Figures 4-27 and 4-28 show temperature time series extracted from slice 2 and slice 3 at different distance from BHE array (25m, 50m, 100m).

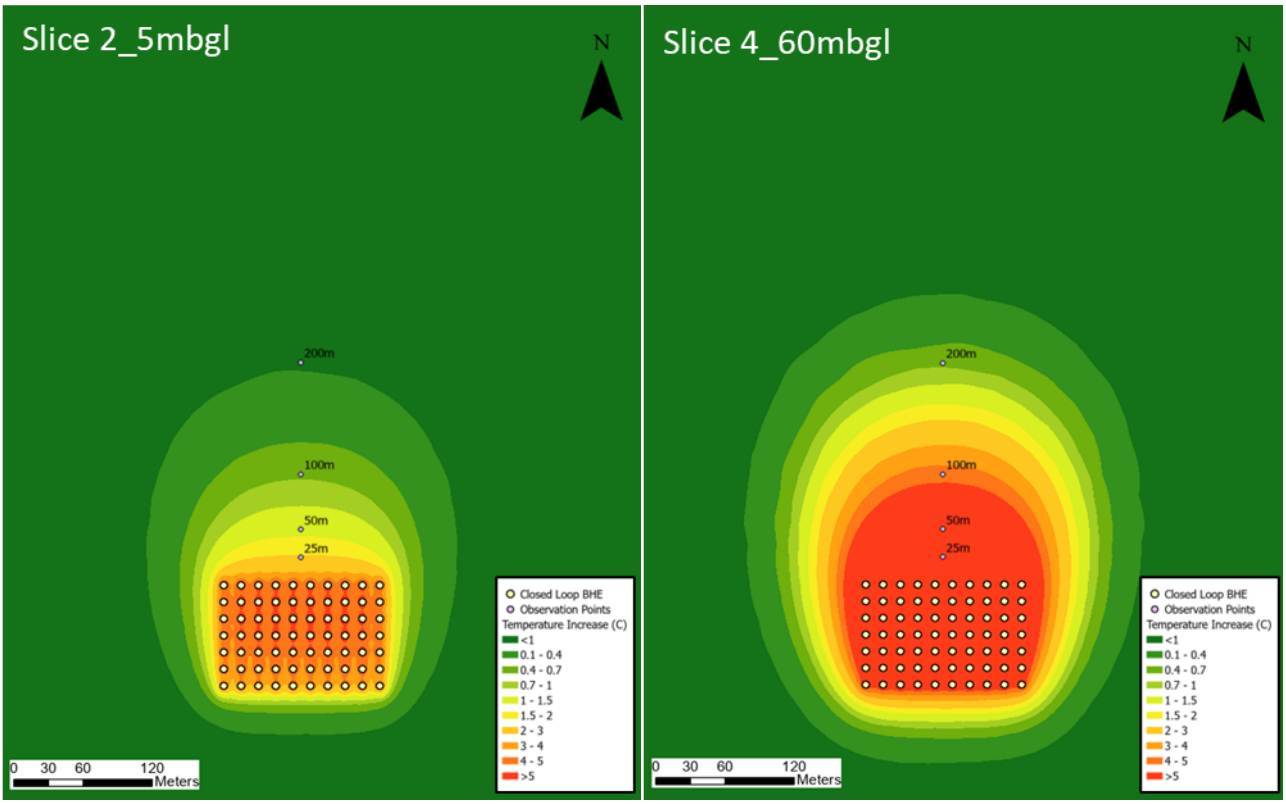

Figure 4-26: Extent and temperature change of the simulated thermal plume after 50 years for the conservative/worst case scenario at 5m bgl and 60mbgl.

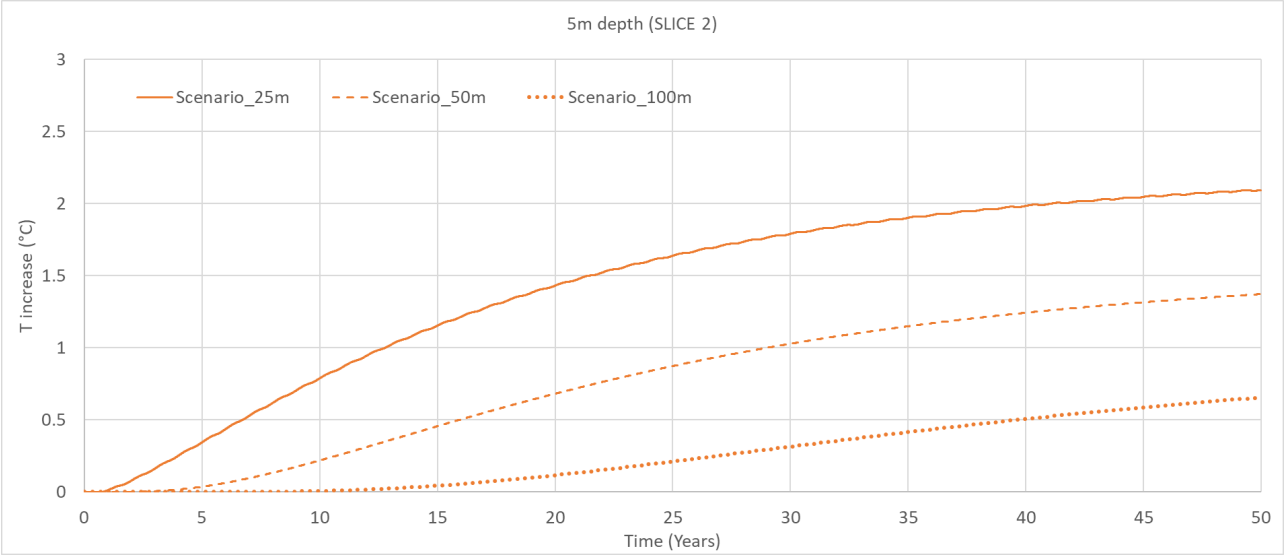

Figure 4-27: Change in temperature (ΔT) from initial conditions during the operational period (50 years) of the BHE array for the conservative/worst case scenario at slice 2 (5m bgl).

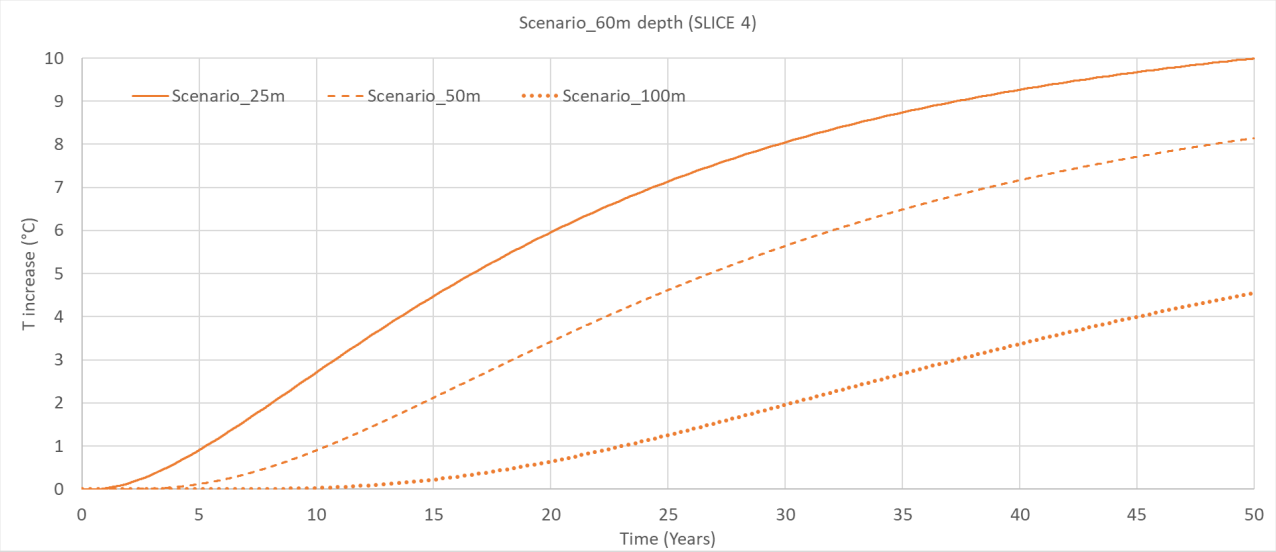

Figure 4-28: Change in temperature (∆T) from initial conditions during the operational period (50 years) of the BHE array for the conservative/worst case scenario at slice 4 (60m bgl).

The outputs simulated with the current model settings, show significant temperature gradients, both in slice 2 (5mbgl) and slice 4 (60mbgl), generated after 50 years of BHE closed-loop system operated for heat rejection.

In both slice 2 and slice 4 this results in a wide thermal plume, with an elongated pseudo-elliptical shape, extended along the groundwater flow direction due to advective transport. The plume simulated in the down-gradient direction is significantly shorter at 5m bgl than at 60m bgl, due to attenuation caused by heat loss to the surface. However, close to the BHE, the temperatures increase by approximately 2°C at 5m bgl and more by than 10°C at 60m bgl, without having reached equilibrium at 50 years.

Considering a thermal plume to be defined by the contour of 1°C temperature change, with the current model settings, this would be 70m at 5m depth and 180m at 60m depth. Final results for this scenario are summarised in the following table.

Table 4-13: Thermal plume lengths after 50 years of heat rejection.

50 years simulation time	Plume length, 1°C ΔT	ΔT observed at 25 m distance	ΔT observed at 50 m distance	ΔT observed at 100 m distance
5m depth (Slice 2)	~70m	~2°C	~1.5°C	~0.5°C
60m depth (Slice 4)	~180m	~10°C	~8°C	~5°C

4.8 Scenarios summary

Further to the sensitivity analysis, a series of scenarios were modelled to represent particular groundwater settings within England and GSHC setups. These included:

- Heat abstraction (rather than injection)
- Influence of the unsaturated zone
- Load balancing (phasing of heat injection/abstraction)
- The London Basin
- A mudrock aquitard
- A fluvial sand and gravel aquifer
- A conservative / worst case

Table 4-14 provides a summary of the typical plume lengths and temperatures resulting from the scenarios. In these tables, 1°C plume lengths that exceed 50 m[26] are highlighted in orange, and plume temperatures exceeding 1°C at the 25, 50 or 100 m observation points in the models, are highlighted in yellow.

[26] 50 m has been selected as it has some precedent with regards contaminant transport in terms of Source Protection Zones, with SPZ 1 set at a minimum 50 m radius from a public water supply and it is a pragmatic indication of distance given the numbers that the modelling exercise produced.

Table 4-14: Plume temperatures and lengths from model scenarios (orange cells indicate 1°C temperature change isocontour lengths that exceed 50 m; yellow cells indicate plume temperatures exceeding 1°C).

Heat abstraction scenario (50 years)	Plume length 1°C ΔT	ΔT observed at 25 m distance	ΔT observed at 50 m distance	ΔT observed at 100 m distance
5m depth (Slice 2)	~ - 9m	~ - 0.2 (°C)	~ -0.15 (°C)	~ - 0.1 (°C)
70m depth (Slice 4)	~ - 4m	~ -0.9 (°C)	~ - 0.9(°C)	~ - 0.75 (°C)
Partially saturated aquifer scenario (50 years)	**Plume length – 1°C ΔT**	**ΔT observed at 25m distance**	**ΔT observed at 50m distance**	**ΔT observed at 100m distance**
5m depth (Slice 2)	~4m	~0.35°C	~0.25°C	~0.15°C
60m depth (Slice 4)	~11m	~1.0°C	~0.9°C	~0.75°C
Alternate phasing (balanced load) scenario (50 years)	**Plume length– 1C ΔT**	**ΔT (°C) observed at 25 m distance**	**ΔT (°C) observed at 50 m distance**	**ΔT (°C) observed at 100 m distance**
5m depth (Slice 2)	NA	<0.1°C	<0.1°C	<0.1°C
70m depth (Slice 4)	NA	<0.1°C	<0.1°C	<0.1°C
London basin scenario (50 years)	**Plume length – 1°C ΔT**	**ΔT observed at 25 m distance**	**ΔT observed at 50 m distance**	**ΔT observed at 100 m distance**
5m depth (Slice 2)	~6m	~0.3°C	~0.1°C	<1°C
50m depth (Slice 4)	~42m	~1.6°C	~0.8°C	~0.4°C
95m depth (Slice 8)	~80m	~1.2°C	~1.1°C	~0.9°C
Mudrock aquitard scenario (50 years)	**Plume length (slice 4) – 1 C ΔT**	**ΔT (C) observed at 25 m distance**	**ΔT (C) observed at 50 m distance**	**ΔT (C) observed at 100 m distance**
5m depth (Slice 2)	~9m	~0.4°C	~0.1°C	<0.1°C
70m depth (Slice 4)	~45m	~2.2°C	~0.9°C	~0.1°C
Fluvial sand and gravel scenario (50 years)	**Plume length capped at 1°C ΔT**	**ΔT observed at 25 m distance**	**ΔT observed at 50 m distance**	**ΔT observed at 100 m distance**
5m depth (Slice 2)	<1m	~0.2°C	~0.1°C	<0.1°C
20m depth (Slice 3)	<1m	~0.5°C	~0.4°C	~0.3°C
65m depth (Slice 6)	~5m	~0.5°C	~0.3°C	~0.2°C
Conservative / worst case scenario (50 years)	**Plume length capped at 1°C ΔT**	**ΔT observed at 25 m distance**	**ΔT observed at 50 m distance**	**ΔT observed at 100 m distance**
5m depth (Slice 2)	~70m	~2°C	~1.5°C	~0.5°C
60m depth (Slice 4)	~180m	~10°C	~8°C	~5°C

5 Conclusions

The main findings from the modelling study are that thermal plumes, the boundary of which has been defined as a 1°C temperature change, only migrated beyond than 150 metres from BHE arrays when they are operated at over 200 MWh/year, and only migrate beyond 50 m from BHE arrays where either Darcy flux is low (below 0.002 m/d with a thermal load of ~100 MWh/year) and/or the applied thermal load is high (above 200 MWh/year), or alternatively where there is a high power requirement per metre (W/m) of BHE length (i.e. where BHEs are reduced in length for a given power requirement) .

The study demonstrated that enhanced groundwater flow and groundwater velocity, whilst it may serve to spread warmer or cooler water over larger distances, serves also to dissipate much more effectively any high temperatures. The highest observed temperatures always occur close to the BHE array in no-flow or very low-flow scenarios. Conversely, changes in temperatures were found to be small across the majority of modelled scenarios except in scenarios with the most conservative parameters, with plume temperatures at distances over 25 m from BHE arrays rarely exceeding 1°C.

On the other hand, where multiple BHEs or BHE arrays are situated in succession along a groundwater flowpath, the cumulative impacts downstream can be much more significant. Indeed, this may be more important than the characteristics of any individual closed-loop BHE array, unless either very large or situated in close proximity to a heat-sensitive receptor.

The findings from the modelling studies are broadly in line with findings from the literature, both in terms of the sensitivity of plume transport to specific parameters (notably, Darcy flux, thermal conductivity and dispersivity), and in terms of the dimensions of plumes reported both in other modelling studies and in field studies for which longer longer-term data were collected. Although this study did not model a series of BHEs in a downgradient sequence, such scenarios were identified in the literature where multiple BHEs/BHE arrays are aligned along a groundwater flowpath, leading to cumulative effects exceeding the impacts identified in this study.

An additional conclusion from the literature review is that other anthropogenic sources of ground heat (for example from landfills, sewers, underground car parks etc.) commonly exceed background ground/groundwater temperatures by several degrees and may present sources of ground heating or cooling of the same order of magnitude or greater as closed-loop BHE arrays.

6 References

ABESSER, C., SCHINCARIOL, R.A., RAYMOND, J., GARCÍA-GIL, A., DRYSDALE, R., PIATEK, A., GIORDANO, N., JAZIRI, N. AND MOLSON, J., 2023. Case Studies of Geothermal System Response to Perturbations in Groundwater Flow and Thermal Regimes. Groundwater, 61(2), 255–273. Doi: https://doi.org/10.1111/gwat.13086

ABESSER, C. AND SMEDLEY, P.L., 2008. Baseline groundwater chemistry of aquifers in England and Wales: the Carboniferous Limestone aquifer of the Derbyshire Dome. British Geological Survey Open Report. Available at: https://web.archive.org/web/20200321021055/http://nora.nerc.ac.uk/id/eprint/5671/1/DerbyshireCarbLimestoneOR08028.pdf

ALLEN DJ, BREWERTON LJ, COLEBY LM, GIBBS BR, LEWIS MA, MACDONALD AM, WAGSTAFF SJ & WILLIAMS AT., 1997. The physical properties of major aquifers in England and Wales. British Geological Survey, Hydrogeology Group, Technical Report WD/97/34. Environment Agency R&D Publication 8.

ANDERSON, M.P., 2005. Heat as a Ground Water Tracer. Ground Water, 43(6), 951–968. Doi: https://doi.org/10.1111/j.1745-6584.2005.00052.x.

ARMITAGE, P, J., WORDEN, R.H., FAULKNER, D.R., BUTCHER A.R. AND ESPIE, A.A. 2016. Permeability of the Mercia Mudstone: suitability as caprock to carbon capture and storage sites. Geofluids (2016) 16, 26-42. DOI 10.1111/gfl.121234.

BANKS, D., 2012. An Introduction to Thermogeology - Ground Source Heating and Cooling. Pub: Wiley. Pp526.

BANKS, D., 2015. A review of the importance of regional groundwater advection for ground heat exchange. Environmental Earth Sciences, 73(6), 2555–2565. Doi: https://doi.org/10.1007/s12665-014-3377-4.

BANKS, D., GANDY, C.J., YOUNGER, P.L., WITHERS, J. AND UNDERWOOD, C., 2009. Anthropogenic thermogeological ‘anomaly’ in Gateshead, Tyne and Wear, UK. Quarterly Journal of Engineering Geology and Hydrogeology, 42(3), 307–312. Doi: https://doi.org/10.1144/1470-9236/08-024.

BAYER, P., MUÑOZ, J.E., SCHWEIZER, D., SCHÄRLI, U., BLUM, P. AND RYBACH, L.,

2016. Extracting past atmospheric warming and urban heating effects from borehole temperature profiles. Geothermics, 64, 289–299. Doi: https://doi.org/10.1016/j.geothermics.2016.06.011.

BLOOMFIELD, J.P., JACKSON, C.R. AND STUART, M.E., 2013. Changes in groundwater levels, temperature and quality in the UK over the 20th century: an assessment of evidence of impacts from climate change. www.lwec.org.uk. Available at: https://nora.nerc.ac.uk/id/eprint/503271.

BLUM, P., MENBERG, K., KOCH, F., BENZ, S.A., TISSEN, C., HEMMERLE, H. AND BAYER, P., 2021. Is thermal use of groundwater a pollution? Journal of Contaminant Hydrology, 239, 103791. Doi: https://doi.org/10.1016/j.jconhyd.2021.103791.

BUSBY, J., 2010. Geothermal Prospects in the United Kingdom. Proceedings World Geothermal Congress 2010. Bali, Indonesia, 25-29 April 2020 (online). Available: Geothermal Prospects in the United Kingdom (nerc.ac.uk) [Accessed 16 June 2024].

BUSBY, J., 2015. UK shallow ground temperatures for ground coupled heat exchangers. Quarterly Journal of Engineering Geology and Hydrogeology, 48(3-4), 248–260. Doi: https://doi.org/10.1144/qjegh2015-077.

CARBON ZERO CONSULTING AND HOLYMOOR CONSULTANCY LTD, 2010. Summary Report: Analytical and Numerical Modelling of Thermal Plumes from Well Doublet Ground Source Cooling Schemes. Report from Carbon Zero Consulting, Draycott, and Holymoor Consultancy Ltd, Chesterfield, to Environment Agency (not published).

CHANGNON, S.A., 1999. A Rare Long Record of Deep Soil Temperatures Defines Temporal Temperature Changes and an Urban Heat Island. Climatic Change, 42(3), 531–538. Doi: https://doi.org/10.1023/a:1005453217967.

DAEMI, N. AND KROL, M.M., 2019. Impact of building thermal load on the developed thermal plumes of a multi-borehole GSHP system in different Canadian climates.

DARLING, G., 2019. Thermal groundwaters of the UK: geochemical indications of flow, vulnerability and possible threat to the shallow hydrosphere. Quarterly Journal of Engineering Geology and Hydrogeology 52(4). https://doi.org/10.1144/qjegh2018-199

DE MARSILY, G. 1986. Quantitative Hydrogeology; Academic Press: San Diego, CA, USA, 1986; p. 464.

DHI-WASY, 2023. FEFLOW finite element subsurface flow and transport simulation system—user's manual/reference manual/white papers. Recent release 8.1. Technical Report, DHI-WASY GmbH, Berlin, Germany

DIERSCH, H.J.G., D. BAUER, W. HEIDMANN, W. RUHAAK, and P. SCHATZL. 2010. Finite element formulation for borehole heat exchangers in modeling geothermal heating systems by FEFLOW. FEFLOW White Papers Vol. V, DHI-WASY GmbH, Berlin, Germany

DIERSCH, H.J.G., BAUER, D., HEIDEMANN, W., RUHAAK, W., SCHATZL, P., 2011a. Finite element modeling of borehole heat exchanger systems: Part 2. Numerical simulation. Computers & Geosciences 37, 1136–1147. https://doi.org/10.1016/j.cageo.2010.08.002

DIERSCH, H.J.G., BAUER, D., HEIDEMANN, W., RUHAAK, W., SCHATZL, P., 2011b. Finite element modeling of borehole heat exchanger systems: Part 1. Fundamentals. Computers & Geosciences 37, 1122–1135. https://doi.org/10.1016/j.cageo.2010.08.003

DOMENICO PA & SCHWARTZ FW, 1990. Physical and chemical hydrogeology. Wiley, 824 pp.

BLOMBERG, T., CLAESSON, J., ESKILSON, P., HELLSTRÖM, G. AND SANNER, B. (2019). Earth Energy Designer (EED) Version 4.20 (April 11th, 2019). BLOCON AB, Sweden.

EGIDIO, E., DE LUCA, D.A. AND LASAGNA, M., 2024. How groundwater temperature is affected by climate change: A systematic review. Heliyon, 10(6). Doi: https://doi.org/10.1016/j.heliyon.2024.e27762.

ELLISON, R.A., WOODS, M.A., ALLEN, D.J., FORSTER, A., PHARAOH, T.C. and KING, C., 2004. Geology of London. Memoir of the British Geological Survey, Sheets 256 (North London), 257 (Romford), 270 (South London, 271 (Dartford) (England and Wales).

ENERGY TECHNOLOGIES INSTITUTE, 2011. Feasibility of Geological Heat Storage Final Report (online). Available: https://ukerc.rl.ac.uk/ETI/PUBLICATIONS/ESD_EN2009_3.pdf [Accessed 16 June 2024].

ENVIRONMENT AGENCY, 2020. Mapping brackish aquifers and deep-sourced springs Chief Scientist's Group report. [online] Bristol: Environment Agency. Available at: https://assets.publishing.service.gov.uk/media/61a0f346e90e07043c35f3fa/Mapping_of_brackish_aquifers_and_deep_sourced_springs_-_report.pdf.

ENVIRONMENT AGENCY, 2023. Management of the London Basin Chalk Aquifer Status Report – 2022. Unpublished report. (Figure 11 Groundwater Level Contours for January 2022, page 18).

ENVIRONMENT AGENCY, 2024a. Identifying potential receptors to ground source heating and cooling (GSHC) systems. SC220017/R2. Chief Scientist's Group report, Bristol [online].

ENVIRONMENT AGENCY, 2024b. Ground source heating and cooling (GSHC): Status, policy and market review. SC220017/R3. Chief Scientist's Group report [online].

EPTING, J., 2017. Thermal management of urban subsurface resources - Delineation of boundary conditions. Procedia Engineering, 209, 83–91. Doi: https://doi.org/10.1016/j.proeng.2017.11.133.

EPTING, J., HÄNDEL, F. AND HUGGENBERGER, P., 2013. Thermal management of an unconsolidated shallow urban groundwater body. Hydrology and Earth System Sciences, 17(5), 1851–1869. Doi: https://doi.org/10.5194/hess-17-1851-2013.

EPTING, J. AND HUGGENBERGER, P., 2013. Unraveling the heat island effect observed in urban groundwater bodies – Definition of a potential natural state. Journal of Hydrology, 501, 193–204. Doi: https://doi.org/10.1016/j.jhydrol.2013.08.002.

EPTING, J., SCHEIDLER, S., AFFOLTER, A., BORER, P., EGLI, L., GARCÍA-GIL, A. AND HUGGENBERGER, P., 2017. The thermal impact of subsurface building structures on urban groundwater resources – A paradigmatic example. Science of The Total Environment, 596-597, 87–96. Doi: https://doi.org/10.1016/j.scitotenv.2017.03.296.

ESI, 2010. London Basin Aquifer: Conceptual Model. Report reference 60121R1, 51, 60, 61, 59, 157. Unpublished report for the Environment Agency.

ESI, 2011. Heat transport modelling of Central London – Final report (60352R1), 31- 32. Unpublished report for the Environment Agency.

FERGUSON, G. AND WOODBURY, A.D., 2004. Subsurface heat flow in an urban environment. Journal of Geophysical Research: Solid Earth, 109, Doi: https://doi.org/10.1029/2003jb002715.

FERGUSON, G. AND WOODBURY, A.D., 2007. Urban heat island in the subsurface.

Geophysical Research Letters, 34(23). Doi: https://doi.org/10.1029/2007gl032324.

FORD, D. AND WILLIAMS, P.D., 1989. Karst Hydrogeology and Geomorphology. 1st ed. Perlego. Wiley. Available at: https://www.perlego.com/book/1007282/karst-hydrogeology-and-geomorphology-pdf.

FRY, V., 2009. Lessons from London: regulation of open-loop ground source heat pumps in central London. Quarterly Journal of Engineering Geology and Hydrogeology (2009) 42 (3): 325–334. https://doi.org/10.1144/1470-9236/08-087

GARCÍA-GIL, A. AND MEJÍAS MORENO, M., 2019. Current Legal Framework on Shallow Geothermal Energy Use in Spain. Journal of Sustainability Research, 2(1). Doi: https://doi.org/10.20900/jsr20200005.

GARCÍA-GIL, A., MEJÍAS MORENO, M., GARRIDO SCHNEIDER, E., MARAZUELA, M.Á., ABESSER, C., MATEO LÁZARO, J. AND SÁNCHEZ NAVARRO, J.Á., 2020b. Nested Shallow Geothermal Systems. Sustainability, 12(12), 5152. Doi: https://doi.org/10.3390/su12125152.

GARCÍA-GIL, A., GOETZL, G., KŁONOWSKI, M.R., BOROVIC, S., BOON, D.P., ABESSER, C., JANZA, M., HERMS, I., PETITCLERC, E., ERLSTRÖM, M., HOLECEK, J., HUNTER, T., VANDEWEIJER, V.P., CERNAK, R., MEJÍAS MORENO, M. AND EPTING, J., 2020a. Governance of shallow geothermal energy resources. Energy Policy, 138, 111283. Doi: https://doi.org/10.1016/j.enpol.2020.111283.

GARCÍA-GIL, A., VÁZQUEZ-SUÑE, E., SCHNEIDER, E.G., SÁNCHEZ-NAVARRO, J.Á. AND MATEO-LÁZARO, J., 2014. The thermal consequences of river-level variations in an urban groundwater body highly affected by groundwater heat pumps. Science of the Total Environment, 485-486, 575-587. https://www.sciencedirect.com/science/article/abs/pii/S004896971400463X

GIZZI, M., TADDIA, G., ABDIN, E.C. AND RUSSO, S.L., 2020. Thermally Affected Zone (TAZ) Assessment in Open-Loop Low-Enthalpy Groundwater Heat Pump Systems (GWHPs): Potential of Analytical Solutions. Geofluids (Oxford. Print), 2020, 1–13. Doi: https://doi.org/10.1155/2020/2640917.

GUNN, J. 2014. Analysis of groundwater pathways by high temporal resolution water temperature logging in the Castleton Karst, Derbyshire, England. In B. Andreo and others

(eds.), Hydrogeological and Environmental Investigations in Karst Systems, Springer-Verlag, 227-235.

GUNN, J., FARRANT, A., HARDWICK, P. AND WORTHINGTON, S.W. 2015. Groundwater in Carboniferous carbonates - Field excursion to the Derbyshire "White Peak" District 26th June 2015. University of Birmingham unpublished field guide. https://core.ac.uk/download/pdf/33452922.pdf

HAEHNLEIN, S., BAYER, P., BLUM, P., 2010. International legal status of the use of shallow geothermal energy. Renewable and Sustainable Energy Reviews. 14, 2611–2625. https://doi.org/10.1016/j.rser.2010.07.069

HEADON, J., BANKS, D., WATERS, A. AND ROBINSON, V.K., 2009. Regional distribution of ground temperature in the Chalk aquifer of London, UK. Quarterly Journal of Engineering Geology and Hydrogeology, 42(3), 313–323. Doi: https://doi.org/10.1144/1470-9236/08-073.

HOUGH, E., SCHOFIELD, D., PHARAOH, T., HASLAM, R., LOVELESS, S., BLOOMFIELD, J. P.,LEE, J. R., BAPTIE, B., SHAW, R. P., BIDE T. AND MCEVOY, F.M.. 2018. National Geological Screening: Central England region. British Geological Survey Commissioned Report, CR/17/091. 77pp.

LOVERIDGE, F., HOLMES, G., POWRIE, W., ROBERTS, T., 2013. Thermal response testing trough the Chalk aquifer in London, UK. Institute of Civil Engineers, Volume 166 Issue G2. 203.

INTERGOVERNMENTAL PANEL ON CLIMATE CHANGE, 2021. Climate Change 2021: The Physical Science Basis. Contribution of Working Group I to the Sixth Assessment Report of the Intergovernmental Panel on Climate Change. Cambridge, United Kingdom and New York, NY, USA: Cambridge University Press. Doi: https://doi.org/10.1017/9781009157896.

INTERNATIONAL CIVIL AVIATION ORGANIZATION, 1923. Manual of the ICAO Standard Atmosphere - extended to 80 kilometres / 262,500 feet (Doc 7488). International Civil Aviation Organization. Available at: https://store.icao.int/en/manual-of-the-icao-standard-atmosphere-extended-to-80-kilometres-262500-feet-doc-7488

JOHNSON A.I., 1967. Specific yield: compilation of specific yields for various materials.

USGS Numbered Series, D1.

KRESIC, N. AND STEVANOVIC, Z., 2010. Groundwater Hydrology of Springs. Elsevier. Doi: https://doi.org/10.1016/c2009-0-19145-6.

KRUSEMAN, G.P. AND DE RIDDER, N.A., 2000. Analysis and Evaluation of Pumping Test Data. 2nd Edition, International Institute for Land Reclamation and Improvement, 24.

LANDSBERG, H., 1956. The climate of towns. Chicago: University of Chicago Press.

LEITERITZ, R., DAVIS, K., SCHULTE, M. and PFLUGER, D., 2022. A Deep Learning Approach for Thermal Plume Prediction of Groundwater Heat Pumps. Unpublished proceedings of the Tenth International Conference on Learning Representations, 2022.

LO RUSSO, S., GNAVI, E., ROCCI, G., TADDIA, G., VERDA, V. 2014. Groundwater Heat Pump (GWHP) system modeling and Thermal Affected Zone (TAZ) prediction reliability: Influence of temporal variations in flow discharge and injection temperature. Geothermics, 51, 103-112 https://doi.org/10.1016/j.geothermics.2013.10.008

LO RUSSO, S., TADDIA, G. AND VERDA, V., 2012. Development of the thermally affected zone (TAZ) around a groundwater heat pump (GWHP) system: A sensitivity analysis. Geothermics, 43, 66–74. Doi: https://doi.org/10.1016/j.geothermics.2012.02.001.

LUO, Z. AND ASPROUDI, C., 2015. Subsurface urban heat island and its effects on horizontal ground-source heat pump potential under climate change. Applied Thermal Engineering, 90, 530–537. Doi: https://doi.org/10.1016/j.applthermaleng.2015.07.025.

MCS, 2011. MCS 022: Ground Heat Exchanger Look-Up Tables. Supplementary material to MIS 3005. Issue 1.0. 1.2 Amended 3.4 Consumer Code of Practice wording Updated e-mail and website addresses 25/02/2008 1.2 Amended 3.4 Consumer Code of Practice wording Updated e-mail and website addresses 25/02/2008 Supplementary material to microgeneration installation standards 3005: Ground Heat Exchanger look-up tables (icax.co.uk)

MEINZER, O.E., 1923. Outline of ground-water hydrology, with definitions. U.S. Govt. Print. Off. Doi: https://doi.org/10.3133/wsp494.

MENBERG, K., BAYER, P., ZOSSEDER, K., RUMOHR, S. AND BLUM, P., 2013. Subsurface urban heat islands in German cities. Science of The Total Environment, 442,

123–133. Doi: https://doi.org/10.1016/j.scitotenv.2012.10.043.

MENG, B., VIENKEN, T., KOLDITZ, O. AND SHAO, H., 2018. Modeling the groundwater temperature response to extensive operation of ground source heat pump systems: A case study in Germany. Energy Procedia, 152, 971–977. Doi: https://doi.org/10.1016/j.egypro.2018.09.102.

MENG, B., VIENKEN, T., KOLDITZ, O. AND SHAO, H., 2019. Evaluating the thermal impacts and sustainability of intensive shallow geothermal utilization on a neighborhood scale: Lessons learned from a case study. Energy Conversion and Management 199 (2019) 111913. https://doi.org/10.1016/j.enconman.2019.111913

MET OFFICE, 2024. Soil 30 cm temperature Annual Average 1981-2010 (online). Available: https://www.metoffice.gov.uk/research/climate/maps-and-data/uk-climate-averages/gcwuvhmch [Last Accessed 18 June 2024].

NAVARRO, J.Á. AND MATEO-LÁZARO, J., 2014. The thermal consequences of river-level variations in an urban groundwater body highly affected by groundwater heat pumps. Science of The Total Environment, 485-486, 575–587. Doi: https://doi.org/10.1016/j.scitotenv.2014.03.123.

NOETHEN, M., HEMMERLE, H., MENBERG, K., EPTING, J., BENZ, S.A., BLUM, P. AND BAYER, P., 2023. Thermal impact of underground car parks on urban groundwater. Science of The Total Environment, 903, 166572–166572. Doi: https://doi.org/10.1016/j.scitotenv.2023.166572.

PARKES, D., BUSBY, J., KEMP, S., PETITCLERC, E., MOUNTENEY, I., 2021. The thermal properties of the Mercia Mudstone Group. Quarterly Journal of Engineering Geology and Hydrogeology. https://doi.org/10.1144/qjegh2020-098

PERRY, M. AND HOLLIS, D., 2005. The development of a new set of long-term climate averages for the UK. International Journal of Climatology, 25(8), 1023–1039. Doi: https://doi.org/10.1002/joc.1160.

PIGA, B., CASASSO, A., PACE, F., GODIO, A. AND SETHI, R., 2017. Thermal Impact Assessment of Groundwater Heat Pumps (GWHPs): Rigorous vs. Simplified Models. Energies (Basel), 10(9), 1385–1385. Doi: https://doi.org/10.3390/en10091385.

PIKE, D., BANKS, D., WATERS, A. AND ROBINSON, V.K., 2011. Regional distribution of

temperature in the Chalk of the western London Basin syncline. Quarterly Journal of Engineering Geology and Hydrogeology, 46(1), 117–125. Doi: https://doi.org/10.1144/qjegh2011-046.

POPHILLAT, W., BAYER, P., BLUM, P., ROSSIER, Y., EISENLOHR, L. AND ATTARD, G., 2019. How to assess the thermal plume of groundwater heat pump systems? EGU General Assembly. Available at: https://presentations.copernicus.org/EGU2019/EGU2019-287_presentation.pdf.

POPHILLAT, W., BAYER, P., TEYSSIER, E., BLUM, P. AND ATTARD, G., 2020. Impact of groundwater heat pump systems on subsurface temperature under variable advection, conduction and dispersion. https://doi.org/10.1016/j.geothermics.2019.101721

POST., 2022. POSTbrief 46: Geothermal energy. UK Parliamentary Office of Science and Technology (online). Available at: https://researchbriefings.files.parliament.uk/documents/POST-PB-0046/POST-PB-0046.pdf [Accessed 27/06/2023].

RIVERA, J.A., BLUM, P. AND BAYER, P., 2015. Ground energy balance for borehole heat exchangers: Vertical fluxes, groundwater and storage. Renewable Energy, 83, 1341–1351. Doi: https://doi.org/10.1016/j.renene.2015.05.051.

ROTTA LORIA, A.F., THOTA, A., THOMAS, A.M., FRIEDLE, N., LAUTENBERG, J.M. AND SONG, E.C., 2022. Subsurface heat island across the Chicago Loop district: Analysis of local drivers. Urban Climate, Volume 44, July 2022, 101211. https://doi.org/10.1016/j.uclim.2022.101211

RYBACH, L. AND SANNER, B., 2000. Ground-source heat pump systems the European experience. GHC Bulletin. Available at: https://www.sanner-geo.de/media/art4.pdf.

SCHELENZ, S., VIENCKEN, T. SHAO, H., FIRMBACH, L. AND DIETRICH, P. (2017). On the importance of a coordinated site characterization for the sustainable intensive thermal use of the shallow subsurface in urban areas: a case study. Environmental Earth Sciences (2017) 76:73.

STUART, M.E., JACKSON, C.R. AND BLOOMFIELD, J.P., 2010. Preliminary Analysis of Trends in UK Groundwater Temperature Measurements from England and Wales. British Geological Survey Internal Report IR/10/033.

TANIGUCHI, M., SHIMADA, J., FUKUDA, Y., YAMANO, M., ONODERA, S., KANEKO, S. AND YOSHIKOSHI, A., 2009. Anthropogenic effects on the subsurface thermal and groundwater environments in Osaka, Japan and Bangkok, Thailand. Science of The Total Environment, 407(9), 3153–3164. Doi: https://doi.org/10.1016/j.scitotenv.2008.06.064.

TANIGUCHI, M. AND UEMURA, T., 2005. Effects of urbanization and groundwater flow on the subsurface temperature in Osaka, Japan. Physics of the Earth and Planetary Interiors, 152(4), 305–313. Doi: https://doi.org/10.1016/j.pepi.2005.04.006.

TANIGUCHI, M., UEMURA, T. AND JAGO-ON, K., 2007. Combined Effects of Urbanization and Global Warming on Subsurface Temperature in Four Asian Cities. Vadose Zone Journal, 6(3), 591–596. Doi: https://doi.org/10.2136/vzj2006.0094.

TISSEN, C., BENZ, S.A., MENBERG, K., BAYER, P., BLUM, P., 2019. Groundwater temperature anomalies in Central Europe. Environmental Research Letters. 14, 104012. https://doi.org/10.1088/1748-9326/ab4240.

TSAGARAKIS, K.P., EFTHYMIOU, L., MICHOPOLOUS, A., MAVRAGANI, A., ANDELKOVIC, A.S., ANTOLINI, F., BACIC, M., BAJARE, D., BARALIS, M., BOGUSZ, W., BURLON, S., FIGUEIRA, J., GENC, M.S., JAVED, S., JURELIONIS, A., KOCA, K., RYZYNSKI, G., URCHUEGUIA, J.F., ZLENDER, B., 2018. A Review of the Legal Framework in Shallow Geothermal Energy in Selected European Countries: Need for Guidelines. Renewable Energy. https://doi.org/10.1016/j.renene.2018.10.007

VIENCKEN, T., KRECK, M. AND DIETRICH, P., 2019. Monitoring the impact of intensive shallow geothermal energy use on groundwater temperatures in a residential neighborhood. Geothermal Energy (2019) 7:8. https://doi.org/10.1186/s40517-019-0123-x

WAPLES AND WAPLES, 2004. A Review and Evaluation of Specific Heat Capacities of Rocks, Minerals, and Subsurface Fluids. Part 1: Minerals and Nonporous Rocks. Natural Resources Research, Vol. 13, No. 2, 97-122.

WORTHINGTON, S.R.H. AND FOLEY, A.E., 2021. Deriving celerity from monitoring data in carbonate aquifers. Journal of Hydrology, 598. Doi: https://doi.org/10.1016/j.jhydrol.2021.126451.

ZHU, K., BAYER, P., GRATHWOHL, P. AND BLUM, P., 2015. Groundwater temperature evolution in the subsurface urban heat island of Cologne, Germany. Hydrological

Processes, 29(6), 965–978. Doi: https://doi.org/10.1002/hyp.10209.

ZHU, K., BLUM, P., FERGUSON, G., BALKE, K.-D. AND BAYER, P., 2010. The geothermal potential of urban heat islands. Environmental Research Letters, 5(4), 044002. Doi: https://doi.org/10.1088/1748-9326/5/4/044002.

Would you like to find out more about us or your environment?

Then call us on

03708 506 506 (Monday to Friday, 8am to 6pm)

Email: enquiries@environment-agency.gov.uk

Or visit our website

www.gov.uk/environment-agency

Incident hotline

0800 807060 **(24 hours)**

Floodline

0345 988 1188 **(24 hours)**

Find out about call charges (https://www.gov.uk/call-charges)

Environment first

Are you viewing this onscreen? Please consider the environment and only print if absolutely necessary. If you are reading a paper copy, please don’t forget to reuse and recycle.

Appendix A.

Literature review summary table.

APPENDIX B.

Sensitivity analysis summary results

Temperature changes at observation points after 50 years of heat rejection for bulk saturated thermal conductivity sensitivity analysis.

Parameter	Depth	ΔT observed at 25m distance	ΔT observed at 50m distance	ΔT observed at 100m distance
Bulk Saturated Thermal Conductivity = 1 W/m/K	5m depth (Slice 2)	~0.55°C	~0.4°C	~0.3°C
	60m depth (Slice 4)	~1.0°C	~1.0°C	~0.9°C
Bulk Saturated Thermal Conductivity = 2 W/m/K	5m depth (Slice 2)	~0.4°C	~0.3°C	~0.2°C
	60m depth (Slice 4)	~0.95°C	~0.9°C	~0.8°C
Bulk Saturated Thermal Conductivity = 3 W/m/K	5m depth (Slice 2)	~0.3°C	~0.2°C	~0.15°C
	60m depth (Slice 4)	~0.9°C	~0.8°C	~0.65°C
Bulk Saturated Thermal Conductivity = 4 W/m/K	5m depth (Slice 2)	~0.25°C	~0.2°C	~0.1°C
	60m depth (Slice 4)	~0.8°C	~0.75°C	~0.6°C

Temperature changes at observation points after 50 years of heat rejection for bulk saturated volumetric heat capacity sensitivity analysis.

Parameter	Depth	ΔT observed at 25m distance	ΔT observed at 50m distance	ΔT observed at 100m distance
Bulk Saturated Volumetric Heat Capacity = 1.9MJ/m3/K	5m depth (Slice 2)	~0.35°C	~0.25°C	~0.15°C
	60m depth (Slice 4)	~0.9°C	~0.85°C	~0.7°C
Bulk Saturated Volumetric Heat Capacity = 2.05MJ/m3/K	5m depth (Slice 2)	~0.35°C	~0.25°C	~0.15°C
	60m depth (Slice 4)	~0.9°C	~0.85°C	~0.7°C
Bulk Saturated Volumetric Heat Capacity = 2.4MJ/m3/K	5m depth (Slice 2)	~0.35°C	~0.25°C	~0.15°C
	60m depth (Slice 4)	~0.9°C	~0.85°C	~0.7°C
Bulk Saturated Volumetric Heat Capacity = 2.3MJ/m3/K	5m depth (Slice 2)	~0.35°C	~0.25°C	~0.15°C
	60m depth (Slice 4)	~0.9°C	~0.85°C	~0.7°C

Temperature changes at observation points after 50 years of heat rejection for Porosity sensitivity analysis.

Parameter	Depth	ΔT observed at 25m distance	ΔT observed at 50m distance	ΔT observed at 100m distance
Porosity= 1%	5m depth (Slice 2)	~0.35°C	~0.25°C	~0.15°C
	60m depth (Slice 4)	~0.9°C	~0.85°C	~0.75°C
Porosity= 20%	5m depth (Slice 2)	~0.35°C	~0.25°C	~0.15°C
	60m depth (Slice 4)	~0.9°C	~0.85°C	~0.7°C
Porosity= 30%	5m depth (Slice 2)	~0.35°C	~0.25°C	~0.15°C
	60m depth (Slice 4)	~0.85°C	~0.8°C	~0.7°C

Temperature changes at observation points after 50 years of heat rejection for Darcy flux sensitivity analysis.

Parameter	Depth	ΔT observed at 25m distance	ΔT observed at 50m distance	ΔT observed at 100m distance
Darcy Flux#1=0m/d	5m depth (Slice 2)	~0.4°C	~0.15°C	~0.05°C
	60m depth (Slice 4)	~2°C	~0.9°C	~0.15°C
Darcy Flux#2=0.00017m/d	5m depth (Slice 2)	~0.4°C	~0.15°C	~0.05°C
	60m depth (Slice 4)	~2.1°C	~1.0°C	~0.2°C
Darcy Flux#3=0.0017m/d	5m depth (Slice 2)	~0.5°C	~0.25°C	~0.1°C
	60m depth (Slice 4)	~2.3°C	~1.5°C	~0.55°C
Darcy Flux#4=0.17m/d	5m depth (Slice 2)	~0.15°C	~0.1°C	~0.05°C
	60m depth (Slice 4)	~0.2°C	~0.1°C	~0.1°C

Temperature changes at observation points after 50 years of heat rejection for dispersivity sensitivity analysis.

Parameter	Depth	ΔT observed at 25m distance	ΔT observed at 50m distance	ΔT observed at 100m distance
Dispersivity=10m	5m depth (Slice 2)	~0.35°C	~0.25°C	~0.2°C
	60m depth (Slice 4)	~1.0°C	~0.95°C	~0.85°C
Dispersivity=40m	5m depth (Slice 2)	~0.3°C	~0.2°C	~0.15°C
	60m depth (Slice 4)	~0.75°C	~0.7°C	~0.55°C

Temperature changes at observation points after 50 years of heat rejection for operational cyclicity sensitivity analysis.

Parameter	Depth	ΔT observed at 25m distance	ΔT observed at 50m distance	ΔT observed at 100m distance
Cyclicity 531kWh/d for 183 days=97.2MWh/year	5m depth (Slice 2)	~0.35°C	~0.25°C	~0.15°C
	60m depth (Slice 4)	~0.9°C	~0.85°C	~0.7°C

Temperature changes at observation points after 50 years of heat rejection system power capacity sensitivity analysis.

Parameter	Depth	ΔT observed at 25m distance	ΔT observed at 50m distance	ΔT observed at 100m distance
BHE System Power Capacity#1 10kW - 240kWh/d	5m depth (Slice 2)	~0.2°C	~0.1°C	<0.1°C
	60m depth (Slice 4)	~0.45°C	~0.35°C	~0.25°C
BHE System Power Capacity#2 200kW-4800kWh/d	5m depth (Slice 2)	~0.7°C	~0.5°C	~0.4°C
	60m depth (Slice 4)	~2.3°C	~2.2°C	~2.0°C
BHE System Power Capacity#3 100kW-2400kWh/d	5m depth (Slice 2)	~0.45°C	~0.35°C	~0.25°C
	60m depth (Slice 4)	~1.4°C	~1.35°C	~1.2°C

Temperature changes at observation points after 50 years of heat rejection for BHE length sensitivity analysis.

Parameter	Depth	ΔT observed at 25m distance	ΔT observed at 50m distance	ΔT observed at 100m distance
BHE Length#1= 50m (~64W/m)	5m depth (Slice 2)	~0.5°C	~0.4°C	~0.2°C
	25m depth	~1.5°C	~1.2°C	~0.7°C
BHE Length#2= 90m (~36W/m)	5m depth (Slice 2)	~0.4°C	~0.3°C	~0.2°C
	45m depth	~1.1°C	~1.0°C	~0.8°C
BHE Length#3= 150m (~21W/m)	5m depth (Slice 2)	~0.3°C	~0.2°C	~0.15°C
	60m depth	~0.85°C	~0.8°C	~0.7°C